

# 000 001 002 003 004 005 006 007 008 009 010 011 012 013 014 015 016 017 018 019 020 021 022 023 024 025 026 027 028 029 030 031 032 033 034 035 036 037 038 039 040 041 042 043 044 045 046 047 048 049 050 051 052 053 LOCALIZING TASK RECOGNITION AND TASK LEARNING IN IN-CONTEXT LEARNING VIA ATTENTION HEAD ANALYSIS

Anonymous authors

Paper under double-blind review

## ABSTRACT

We investigate the mechanistic underpinnings of in-context learning (ICL) in large language models by reconciling two dominant perspectives: the component-level analysis of attention heads and the holistic decomposition of ICL into **Task Recognition** (TR) and **Task Learning** (TL). We propose a novel framework based on **Task Subspace Logit Attribution** (TSLA) to identify attention heads specialized in TR and TL, and demonstrate their distinct yet complementary roles. Through correlation analysis, ablation studies, and input perturbations, we show that the identified TR and TL heads independently and effectively capture the TR and TL components of ICL. Via steering experiments with geometric analysis of hidden states, we reveal that TR heads promote task recognition by aligning hidden states with the task subspace, while TL heads rotate hidden states within the subspace toward the correct label to facilitate prediction. We further show how previous findings on ICL’s mechanism—including induction heads, task vectors, and more—can be reconciled with our attention-head-level analysis of the TR–TL decomposition. Our framework thus provides a unified and interpretable account of how LLMs execute ICL across diverse tasks and settings<sup>1</sup>.

## 1 INTRODUCTION

A key property of Large Language Models (LLMs) is their ability to solve tasks from demonstrations embedded in the input—without further training. This phenomenon, known as **In-context Learning** (ICL) (Brown et al., 2020; Radford et al., 2019), has reduced the need for large datasets and finetuning, enabling fast adaptation of LLMs to new tasks (Dong et al., 2024; Sun et al., 2022). Since its success cannot be explained by traditional gradient-based paradigms (Ren et al., 2024b), deciphering the mechanism behind ICL has become a central research question of great academic interest.

Two research paradigms dominate this pursuit. (1) The introspective paradigm designates internal model components or representations as critical drivers of ICL functionality. Pioneering works (Elhage et al., 2021; Olsson et al., 2022) formulate the output logits of Transformers as the sum of individual component outputs and highlight the significance of **Induction Heads** (IHs) in toy models, with follow-ups confirming their importance in larger models via ablation (Crosbie & Shutova, 2024; Halawi et al., 2024; Cho et al., 2025a). These studies inspired the concept of **task vectors**—compact representations distilled from hidden states or attention head outputs that steer zero-shot prompts toward ICL-level predictions (Hendel et al., 2023; Todd et al., 2024; Liu et al., 2024), and spurred further inquiries into the properties, behaviors, and emergence of IHs (Ren et al., 2024b; Singh et al., 2024; Yin & Steinhardt, 2025). (2) The holistic paradigm instead treats the LLM as an entirety and investigates ICL’s properties by directly inspecting and probing how different demonstration configurations shape ICL performance. For instance, by perturbing the demonstration labels in context, Pan et al. (2023) factorize ICL into two core components: **Task Recognition (TR, recognizing the label space)** and **Task Learning (TL, learning the text–label mapping)**, each contributing to part of the ICL functionality (Figure 1 (A)). Min et al. (2022) also systematically explored the effect of the distribution of texts and labels in demonstrations individually, as well as the templates and number of demonstrations.

<sup>1</sup>The source code will be released upon acceptance of this paper.

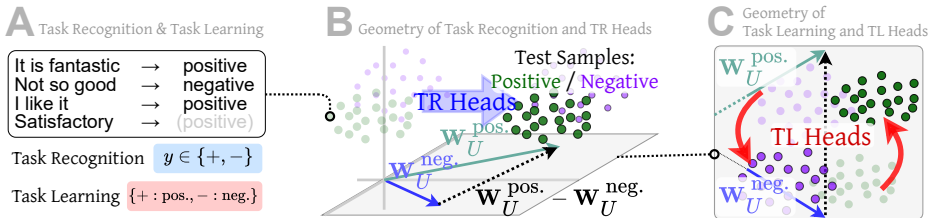


Figure 1: (A) Example of how LLMs deduce the label of a final query through ICL, which consists of two components: task recognition (identifying the label space) and task learning (mapping demonstration texts to labels). (B) The outputs of Task Recognition heads align with the task subspace spanned by candidate label unembeddings, thus they can steer the hidden states to align with the subspace by reducing the angle between the point clouds and the task subspace. (C) Task Learning heads act as rotations within the task subspace, aligning the query’s hidden state with the unembedding of the correct label and enabling the correct prediction.

The two research paradigms offer complementary insights but also limitations. The introspective paradigm localizes ICL to individual attention heads, yet its reliance on ablation only measures **how much** performance changes when heads are removed, without explaining **how** these heads realize ICL or behave under varied inputs. The holistic paradigm provides a broad functional view, separating ICL into TR and TL, but cannot trace these roles back to concrete components. A unified framework is needed to combine mechanistic precision with functional clarity.

Therefore, we propose a TR/TL decomposition via attention-head analysis (Figure 1). Task Subspace Logit Attribution (TSLA) quantifies each head’s effect on hidden states relative to task-label unembeddings, identifying **TR heads** and **TL heads** as ICL’s two drivers. Geometric analyses show that TR heads align hidden states to the task-label subspace, enabling label recognition and suppressing irrelevant tokens (Figure 1B), while TL heads rotate states within it toward the correct label, sharpening prediction (Figure 1C). Together they implement ICL functionality.

We validate the framework using correlation analyses, ablations, input perturbations, and steering across ICL settings, including corrupted demonstrations and free-form generation. These results reconcile prior findings: IHs emerge as a subset of TR heads for label-space recognition, and zero-shot performance is traced to poor task-subspace alignment, explaining why TR-head outputs (hence IHs) form effective task vectors that restore alignment (Todd et al., 2024).

The three core contributions of this paper are:

1. We derive TSLA to identify TR and TL heads, localizing the two ICL components from input-perturbation studies to concrete attention heads.
2. We use correlation/overlap analyses and TR/TL-channel ablations to show separable control of task recognition vs. task learning, unifying ICL observations (e.g., IHs) in the TR/TL framework.
3. We perform steering and geometric analyses to explain how TR heads drive task-subspace alignment and TL heads drive within-subspace rotation toward labels in classification and generation.

## 2 RELATED WORKS

**TR & TL decomposition of ICL** Early ICL work relied on input-perturbation experiments (Min et al., 2022; Pan et al., 2023; Wei et al., 2023). By removing semantic labels (e.g., “negative”  $\rightarrow$  “0”) or scrambling the text-label mapping while still observing non-trivial accuracy, these works concluded that ICL comprises two components: Task Recognition (TR) and Task Learning (TL). However, this approach cannot provide mechanistic explanations or tie ICL functionality to model components. We bridge this gap with our theoretically derived TSLA method based on task-subspace geometry, identifying critical TR and TL heads for the two ICL components (Subsection 3.2).

**Circuit formulation of Transformer** Our TSLA method builds upon the circuit formulation of Transformers (Elhage et al., 2021) by reframing head contributions in task-subspace geometry, which decomposes output logits into contributions from attention heads and MLPs. This formulation has enabled precise attribution of LLM behaviors to individual components (Crosbie & Shutova, 2024) and spotlighted the Induction Heads (IH) as crucial for ICL (Song et al., 2025). In toy copying tasks

([X][Y][X][Y]...[X] → [Y]), IHs attend to earlier occurrences of [Y], mimicking label copying. Their importance for ICL has been confirmed in large-scale models through ablation studies that replace or remove their outputs and observe changes in the final logits (Cho et al., 2025a). In this work, we demonstrate how the significance of IHs fits into the TR & TL decomposition of ICL via extensive correlation analyses and investigations of the heads’ distributional properties Subsection 4.1.

**Ablation of special attention heads** The circuit formulation motivates identifying special heads by ablating their outputs and inspecting prediction changes. Examples include Function Vector Heads (Yin & Steinhardt, 2025)—heads whose ablation most harms ground-truth label logits and are thus viewed as causes of ICL functionality (Sun et al., 2025). Similar approaches extend to retrieval-augmented generation (Jin et al., 2024; Kahardipraja et al., 2025) and chain-of-thought reasoning (Cabannes et al., 2024). Yet they reveal only **how much** a head contributes, not **how** or **which** ICL component it affects; heatmap-based explanations remain too shallow for causal claims (Kahardipraja et al., 2025; Ren et al., 2024a). We address this by new TR/TL-channel metrics and fine-grained ablations that expose component-specific effects Subsection 4.2.

**Task Vector steering and geometric analysis** An alternative to ablation is to aggregate head outputs into task vectors that steer zero-shot states to ICL-level accuracy (Hendel et al., 2023), with effective vectors viewed as ICL’s mechanistic origins (Todd et al., 2024). However, interpretability issues remain: **(1)** candidates are chosen via ablation, inheriting its limitations; **(2)** effects are measured only at outputs, leaving their role in computation unclear (Merullo et al., 2024). Geometric analyses of layer-wise hidden-state evolution, revealing how task vectors reshape geometry, offer a promising alternative (Kiryanov et al., 2025). Jiang et al. (2025) identify a compress–expand pattern in task representations during ICL, while Yang et al. (2025) link IH outputs to alignment between hidden states and unembedding vectors of task-relevant labels. This perspective elucidates their influence on outputs. We perform a comprehensive analysis of the distinct geometric effects that task vectors constructed from TL and TR heads have on the model’s hidden states Subsection 4.3.

### 3 METHODOLOGY

#### 3.1 BACKGROUND

**Circuit formulation of Transformer** In the circuit formulation of Transformer LLMs, an input query  $q$  with  $N$  tokens  $[x_1, \dots, x_N]$  (e.g., “I like this movie. Sentiment.” for a sentiment analysis task) is first transformed into layer-0 hidden states  $\mathbf{h}_1^0, \dots, \mathbf{h}_N^0$  via the embedding matrix  $\mathbf{W}_E \in \mathbb{R}^{|\mathbb{V}| \times d}$ , where  $d$  is the model dimension and  $\mathbb{V}$  the vocabulary. These hidden states then pass through  $L$  layers, where the update of the  $i$ -th token’s hidden state at layer  $l$  is:

$$\mathbf{h}_i^l = \mathbf{h}_i^{l-1} + \sum_{k=1}^K \mathbf{a}_{i,k}^l + \mathbf{m}_i^l,$$

with  $\mathbf{a}_{i,k}^l$  the output of the  $k$ -th attention head (denoted head  $(l, k)$ ) in the attention sublayer, and  $\mathbf{m}_i^l$  the MLP sublayer output.  $\mathbf{a}_{i,k}^l$  is the weighted sum of the layer- $(l-1)$  hidden states of the first  $i$  tokens,  $\mathbf{H}_{\leq i}^{l-1} = [\mathbf{h}_j^{l-1}]_{j=1}^i$ , transformed by the embedding matrices of head  $(l, k)$ . The final hidden state of the last token (“.” in the previous example) can thus be written as:

$$\mathbf{h}_N^L = \mathbf{h}_N^0 + \sum_{l=1}^L \left( \sum_{k=1}^K \mathbf{a}_{N,k}^l + \mathbf{m}_N^l \right). \quad (1)$$

$\mathbf{h}_N^L$  is multiplied by the unembedding matrix  $\mathbf{W}_U \in \mathbb{R}^{d \times |\mathbb{V}|}$  to form logits. Each head output thus contributes to the logits additively as  $\mathbf{a}_{N,k}^L \mathbf{W}_U$ , referred to as **Direct Logit Attribution (DLA)** (Olsson et al., 2022; Chughtai et al., 2024; Yu & Ananiadou, 2024; Lieberum et al., 2023).

**ICL and Induction Head** In ICL,  $m$  text-label demonstration pairs  $t_1, y_1, \dots, t_m, y_m$  are prepended to the query, forming the sequence  $t_1, y_1, \dots, t_m, y_m, q$  (e.g., “I hate this movie. Sentiment: negative. This movie is great. Sentiment: positive. I like this movie. Sentiment:.”). With these demonstrations, the attention head outputs  $\mathbf{a}_{N,k}^l$  to the final position, depending on all preceding tokens, producing logits that can lead the LLM to predict  $y^*$ , the correct label for  $q$ . An Induction Head (IH) is a special attention head that, at each position, searches for earlier occurrences of the current token, attends to

162 the immediately following tokens, and copies their information back to the current position. In the  
 163 example above, an IH at the final position places its attention on the “positive” and “negative” tokens  
 164 that follow previous “:” tokens and uses their hidden states to form its output.  
 165

### 166 3.2 IDENTIFYING TR AND TL HEADS USING TASK SUBSPACE LOGIT ATTRIBUTION 167

168 Pan et al. (2023) decomposes ICL into two components. Task Recognition (TR) means recognizing  
 169 the set of candidate task label tokens  $\mathbb{Y}$  from demonstration labels, with  $\{y_1, \dots, y_m\} \in \mathbb{Y}$ , without  
 170 using the text-label mapping information to deduce the correct token. Task Learning (TL), in contrast,  
 171 means learning the mapping from demonstration texts to task labels,  $f: \mathbb{X} \rightarrow \mathbb{Y}$ , to predict the only  
 172 correct label for query  $q$ . To identify heads contributing to TR and TL, Lieberum et al. (2023)  
 173 compute  $\mathbf{a}_{N,k}^l \mathbf{W}_U^{\mathbb{Y}}$  and  $\mathbf{a}_{N,k}^l \mathbf{W}_U^{y^*}$  for all heads  $(l, k)$ , where  $\mathbf{W}_U^{\mathbb{Y}} \in \mathbb{R}^{d \times |\mathbb{Y}|}$  and  $\mathbf{W}_U^{y^*} \in \mathbb{R}^d$  are the  
 174 unembedding matrix restricted to  $\mathbb{Y}$  and  $y^*$ . Heads with the highest element-wise sum  $\mathbf{1}^T \mathbf{a}_{N,k}^l \mathbf{W}_U^{\mathbb{Y}}$   
 175 are considered TR heads, and those with the highest  $\mathbf{a}_{N,k}^l \mathbf{W}_U^{y^*}$  are TL heads.  
 176

177 This approach has two problems. (1) For TR heads, Lieberum et al. (2023) study four-choice tasks  
 178 where the full label space is “A”, “B”, “C”, “D”. In general settings, demonstration labels are arbitrary  
 179 hyperparameters and may not capture full task semantics. Changing labels from positive/negative  
 180 to favourable/unfavourable does not alter the task, but heads amplifying logits for positive/negative  
 181 may not do so for favourable/unfavourable. (2) For TL heads, the method ignores competition among  
 182 label tokens: heads boosting  $y^*$  may also boost incorrect labels  $\mathbb{Y}/y^*$ , disqualifying them as true  
 183 task-mapping heads. A more precise approach must (a) capture task semantics beyond surface tokens  
 184 and (b) evaluate contributions relative to competing labels.  
 185

186 We therefore propose the **Task Subspace Logit Attribution (TSLA)** method. For TR heads, we  
 187 compute the TR score:  
 188

$$189 \|\text{Proj}_{\mathbf{W}_U^{\mathbb{Y}}} \mathbf{a}_{N,k}^l\|_2, \quad (2)$$

190 where  $\text{Proj}_{\mathbf{W}_U^{\mathbb{Y}}} = \mathbf{W}_U^{\mathbb{Y}} (\mathbf{W}_U^{\mathbb{Y}, \top} \mathbf{W}_U^{\mathbb{Y}})^{-1} \mathbf{W}_U^{\mathbb{Y}, \top}$  is the  $d \times d$  projection matrix onto  $\text{span}(\mathbf{W}_U^{\mathbb{Y}})$ , the  
 191 subspace spanned by unembedding vectors of demonstration labels. This subspace contains related-  
 192 token unembeddings, since LLMs encode semantics as subspaces (Saglam et al., 2025; Zhao et al.,  
 193 2025); we further verify this in Appendix F. The TR score—the projected norm of a head’s output  
 194 onto this subspace—captures logit contributions to task-related semantics regardless of demonstration-  
 195 label choice, alleviating DLA’s sensitivity to label choice. Intuitively, task-recognition heads should  
 196 output mainly within the task-label semantic subspace; the projected norm in Equation 2 tests this  
 197 property. We have the following theoretical guarantee for this metric’s effectiveness.  
 198

199 **Theorem 1** Let  $r = |\mathbb{Y}|$ . Assume  $n$  distinct  $r$ -dimensional subspaces drawn i.i.d. from the Grassmannian  
 200  $\text{Gr}(r, d)$  are spanned by columns of  $\mathbf{W}_U$ . If head  $(l, k)$  has TR score  $\gamma$ , then with probability  
 201 at least  $1 - (n-1)(1 - I_{(\frac{\gamma}{\|\mathbf{a}_{N,k}^l\|_2})^2}(\frac{r}{2}, \frac{d-r}{2}))$ ,  $\mathbf{a}_{N,k}^l$  has the largest projected  $l_2$  norm onto  $\text{span}(\mathbf{W}_U^{\mathbb{Y}})$   
 202 among all such subspaces,  
 203

204 where  $I_x(\alpha, \beta) = \frac{B(x; \alpha, \beta)}{B(\alpha, \beta)}$  is the regularized incomplete beta function, monotone in  $x$ . Thus, a large  
 205 TR score implies the head output lies in the subspace spanned by demonstration-label unembeddings,  
 206 qualifying it as a TR head. This formalizes the intuition above: high TR makes it unlikely that the  
 207 head output aligns better with an unrelated semantic subspace, so high-TR heads are likely the driving  
 208 force for Task Recognition. The proof is in Appendix B.  
 209

210 For TL heads, we compute:  
 211

$$212 \frac{\text{Ave}_{y' \in \mathbb{Y}/\{y^*\}} (\mathbf{a}_{N,k}^{l,\top} (\mathbf{W}_U^{y^*} - \mathbf{W}_U^{y'}))}{\|\text{Proj}_{\mathbf{W}_U^{\mathbb{Y}}} \mathbf{a}_{N,k}^l\|_2}. \quad (3)$$

213 The numerator is the average inner product of the head output with differences between the correct-  
 214 label unembedding and each incorrect label, measuring the logit gap a head creates; the denominator  
 215 is the TR score. Since  $\mathbf{W}_U^{y^*} - \mathbf{W}_U^{y'} \in \text{span}(\mathbf{W}_U^{\mathbb{Y}})$  for all  $y' \in \mathbb{Y}/\{y^*\}$ , the TL score ranges in  
 216  $[-1, 1]$ . Geometrically, it is the fraction of projected head output aligned with the correct–incorrect

unembedding difference. Thus, the TL score isolates the contrastive within-subspace direction that favors  $y^*$  over its competitors. Heads with high TL scores enlarge the correct–incorrect logit gap, effectively rotating hidden states within the task subspace toward the correct label and away from others (see Figure 1 (C)). This conforms to task learning, which identifies the correct label and excludes incorrect ones for an input. We provide further clues on this mechanism in Subsection 4.1: TL heads allocate more attention to query tokens, suggesting they absorb query semantics to select the correct in-context mapping. Moreover, this TL score mitigates the DLA issue of interference from incorrect labels by disregarding heads that fail to differentiate and instead raise both logits. To verify this, we provide the detailed comparison between TSLA and DLA in Appendix C by demonstrating that TSLA solves the practical limitations of DLA as the theory predicts. For each dataset, we use ICL prompts from the first 50 queries to compute TR and TL scores for each head with TSLA, summing across prompts. Heads are ranked by these scores to identify TR and TL heads.

Having identified TR and TL heads with TSLA, we next ask whether these heads behave in the mechanistic ways TSLA claims. In particular, TSLA predicts (i) TR and TL heads should affect different ICL components in a separable manner, and (ii) their outputs should drive qualitatively different geometric changes in hidden states. Accordingly, Subsection 4.1 examines TR/TL specialization and their relation to IHs, Subsection 4.2 tests separability causally via TR/TL-channel ablations, and Subsection 4.3 probes the predicted geometric mechanisms through steering and layerwise analysis.

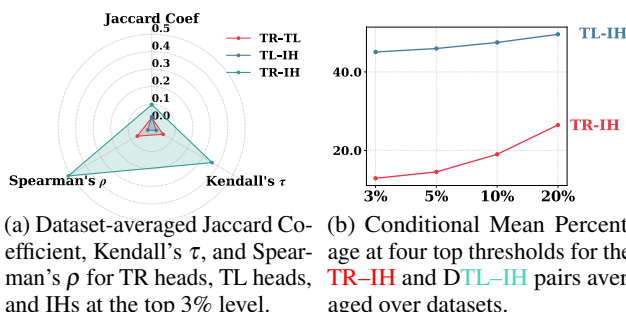
## 4 EXPERIMENTS

**Models** We experiment on models with diverse architectures and sizes, including Llama3-8B, Llama3.1-8B, Llama3.2-3B (Grattafiori et al., 2024), Qwen2-7B, Qwen2.5-32B (Yang et al., 2024), and Yi-34B (01. AI et al., 2024). Unless otherwise noted, results are reported on Llama3-8B.

**Datasets** We evaluate on the following datasets: SUBJ (Wang & Manning, 2012), SST-2 (Socher et al., 2013), TREC (Li & Roth, 2002), MR (Pang & Lee, 2005), SNLI (MacCartney & Manning, 2008), RTE (Dagan et al., 2005), and CB (De Marneffe et al., 2019). We further include an LLM-generated dataset introduced in Subsection 4.3, with curation details in Appendix D and Appendix K. We also experiment with the SubjQA dataset (Bjerva et al., 2020) in Appendix I.3.

**ICL setting** We use 8-shot demonstrations for ICL. For implementation details (models, datasets, prompt templates, etc.), see Appendix D.

### 4.1 VALIDATING TR/TL HEAD SPECIALIZATION AND THE ROLE OF INDUCTION HEADS



(a) Dataset-averaged Jaccard Coefficient, Kendall’s  $\tau$ , and Spearman’s  $\rho$  for TR heads, TL heads, and IHs at the top 3% level.

(b) Conditional Mean Percentage at four top thresholds for the TR-IH and TL-IH pairs averaged over datasets.

Figure 2: Overlap, correlation, and consistency of three attention head types averaged across datasets. (A) TR heads

exhibit substantially greater overlap and correlation with IHs compared to TR-TL or TL-IH pairs. (B) Top IHs consistently rank higher in the TR ranking than in the TL ranking. Results for other models are in Appendix G.2.

Guided by TSLA, we first test whether the identified TR and TL heads exhibit the predicted specialization and how they relate to previously studied induction heads. Specifically, we analyze the overlap, rank correlation, and consistency between TR and TL head rankings, and include IHs as a reference point. Given the significance of IHs in mechanistic accounts of ICL (Zheng et al., 2024), we also ask whether IHs contribute primarily through TR, TL, or both. Following Todd et al. (2024) and Yang et al. (2025), we compute IH scores (i.e., the degree to which a head’s attention pattern resembles that of IHs) as described in Appendix E.

Adopting the methodology of Yin & Steinhardt (2025), we report Jaccard Coefficients<sup>2</sup> among the top 3% (further ablation studies for the choice of the threshold percentage are in Appendix G.1) of

<sup>2</sup>For two subsets  $\mathbb{A}_1, \mathbb{A}_2 \subseteq \mathbb{A}$ , the Jaccard Coefficient is  $\frac{|\mathbb{A}_1 \cap \mathbb{A}_2|}{|\mathbb{A}_1 \cup \mathbb{A}_2|}$ .

each head type to measure overlap at the top level. We also compute Kendall’s  $\tau$  and Spearman’s  $\rho$  among the three rankings to evaluate the global correlations levels among the head types. Finally, we introduce **Conditional Mean Percentage**, which measures the average rank percentile of the top 3%, 5%, 10%, and 20% IHs within the TR and TL rankings. This metric bridges the local and global perspectives and answers the question of how significantly on average does the top IHs exhibit the TR and TL functionality, which is important in subsequent ablation-based experiments in [Subsection 4.2](#).

### Strong association between IHs and TR heads

[Figure 2a](#) shows that TR heads and IHs are highly similar: (1) their overlap at the top 3% is much larger than either TR-TL or TL-IH pairs, and significantly above random baseline<sup>3</sup>; (2) their rank correlations are consistently higher. By contrast, TR-TL and TL-IH pairs show weaker overlap and correlation. This reveals how IHs, the magnitude of whose influence on ICL has been widely recorded, affect ICL: they influence ICL mainly by enabling recognition of the label space, rather than selectively amplifying the correct label. It reconciles conflicting previous findings with some reporting IHs as recognizing correct labels ([Olsson et al., 2022](#); [Cho et al., 2025b](#)), others mentioning “false induction heads” that mislead ([Halawi et al., 2024](#); [Yu & Ananiadou, 2024](#)). It also echoes [Yin & Steinhardt \(2025\)](#), who observed IHs overlap strongly with “function vector heads”<sup>4</sup>, reinforcing the centrality of TR heads in ICL.

[Figure 2b](#) further shows that top IHs consistently rank higher within TR rankings than TL rankings.

For example, the top 10% IHs correspond to roughly the top 20% TR heads but only the top 50% TL heads. This further justifies the large accuracy implications of ablating top IHs, which would imply ablating fairly high-ranking TR heads and the failure of task recognition.

### Layer-wise distribution of special heads

[Figure 3](#) shows the per-layer distribution of the top 10% TR, TL, and IH heads for SST-2. We observe: (1) TR heads appear significantly deeper than both TL heads and IHs, while the layer distributions of TL heads and IHs are more similar (see [Appendix G.3](#) for significance tests) (We provide further explanations and experimental validations of why TR heads occur in deeper layers than TL heads in [Appendix G.7](#)). This partly echoes but also challenges [Yin & Steinhardt \(2025\)](#), who reported function vector heads as only “slightly deeper” than IHs. (2) The TR-IH overlaps are much greater than TL-IH or TR-TL overlaps, and occur primarily in deeper layers. This indicates that the correlation between TR heads and IHs is systematic rather than haphazard: the overlaps conform to the general trend of TR heads being concentrated in deeper layers, instead of reflecting coincidental matches with scattered TR heads that occasionally appear in early layers.

**Attention distribution of TL and TR heads** A second property of the identified heads is their attention distribution, which reveals how they operationalize TL and TR. We quantify this using two metrics: (1) the total attention weight assigned to demonstration-label tokens, reflecting how much a head incorporates information about the task label space (supporting TR); and (2) the total attention weight assigned to query tokens, reflecting how much a head integrates the semantic content of the query (supporting TL). As shown in [Figure 4](#), the top 3% TR heads allocate substantially more attention to demonstration labels than TL or random heads (the small magnitude is expected

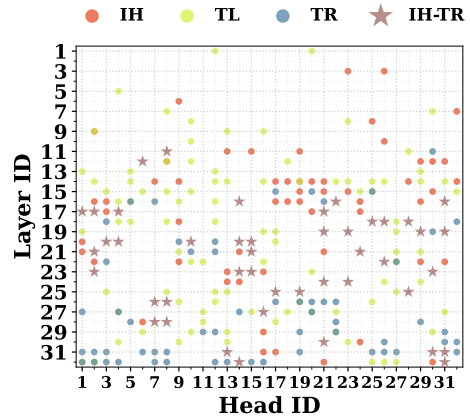


Figure 3: Distribution of the top 10% TR heads, TL heads, and IHs on SST-2. TR heads occur significantly deeper than TL heads and IHs. Overlaps between TR heads and IHs are also more frequent in deeper layers. Results for other models are in [Appendix G.3](#).

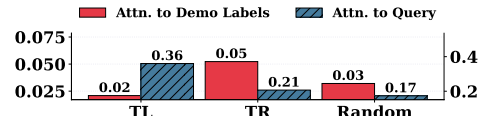


Figure 4: Average attention-weight distribution of top TL and TR heads. TR heads attend more to demonstration labels—supporting task recognition—whereas TL heads focus more on the query to extract semantics for correct prediction. Results for other models are in [Appendix G.5](#).

<sup>3</sup>For random subsets of size  $k\%$ , the expected Jaccard Coefficient is  $\frac{k}{200-k}$ , which is 0.0152 for  $k = 3$ .

<sup>4</sup>Heads revealed to have greatest impact on correct label logits through ablations.

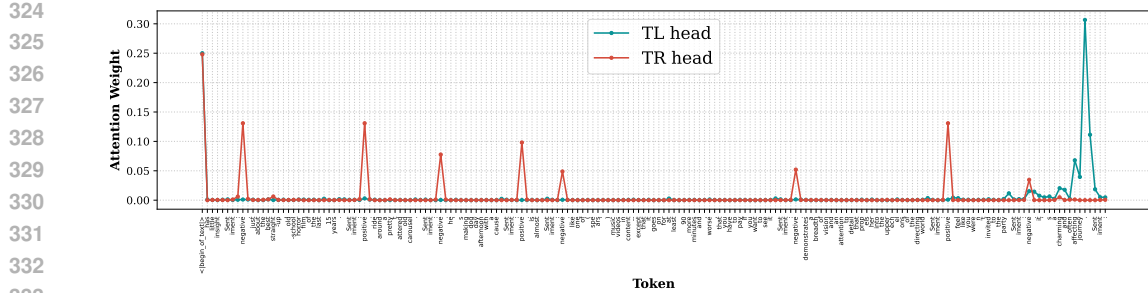


Figure 5: Attention distribution of the top 1 TL and TR head identified on SST-2 over an ICL prompt.

given the scarcity of label tokens in long ICL contexts), indicating that TR heads broadly summarize task-label information. In contrast, TL heads exhibit a far more local attention pattern, attending strongly to the query tokens to extract their semantic meaning and support correct label inference. Direct visualization (Figure 5) of the top SST-2 TL and TR heads on an SST-2 ICL prompt using the first query in the test set further highlight this contrast: TR heads focus on demonstration labels, whereas TL heads primarily attend to the queries. See Appendix G.6 for results using more queries.

**Cross-dataset correlation** To examine whether TR, TL, and IH heads generalize across tasks, we measure Jaccard, Kendall’s  $\tau$ , and Spearman’s  $\rho$  among the top 3% heads on seven datasets, averaged across  $\binom{7}{2} = 21$  dataset pairs. As shown in Figure 6, TR heads and IHs exhibit higher cross-task overlap and correlation than TL heads. *This underscores TR heads (and IHs) as task-invariant mechanistic foundations for label-space recognition, upon which TL heads specialize to learn dataset-specific mappings.* We further explore this discovery in Appendix H.4.

#### 4.2 FINE-GRAINED ABLATION TESTS OF TR/TL SEPARABILITY

Having established behavioral specialization in Subsection 4.1, we now provide causal, fine-grained validation. If TR and TL heads realize distinct ICL components, selectively ablating them should yield different signatures for task recognition versus task learning. Accordingly, we ablate TSLA-identified TR and TL heads to test separable contributions. Prior work mainly evaluated ablations by overall ICL-accuracy drop (Crosbie & Shutova, 2024), which indicates performance change but obscures which ICL component is disrupted. To disentangle these effects, we introduce the **Task Recognition Ratio (TR ratio)**, defined as the proportion of predictions within the in-context label set. Formally, for  $m$  ICL prompts with predicted labels  $\hat{y}_1, \dots, \hat{y}_m$ ,

$$\text{TR ratio} = \frac{1}{m} \sum_{i=1}^m \mathbf{1}_{\hat{y}_i \in \mathbb{Y}}.$$

Since accuracy is upper-bounded by the TR ratio, the two metrics together let us separately evaluate contributions of TR and TL heads. We conjecture: (1) ablating TR heads should reduce both accuracy and TR ratio, while (2) ablating TL heads should reduce accuracy but leave TR ratio largely intact—causing performance to approximate random guessing over all candidate labels with expected accuracy  $\frac{1}{|\mathbb{Y}|}$ <sup>5</sup>. As a control, we also ablate 3% of randomly chosen heads disjoint from the identified TR/TL sets. We report the results averaged over the seven datasets.

**Separability of TR and TL functionality** Figure 7 confirms our conjecture. Removing top TR heads collapses the TR ratio from nearly 100% to  $\sim 20\%$ , leading to a drastic accuracy drop. In contrast, removing top TL heads

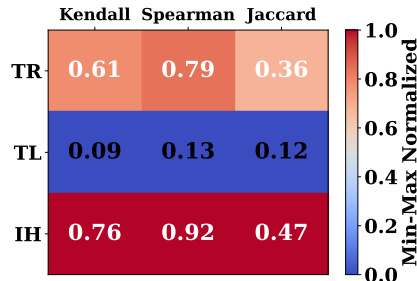
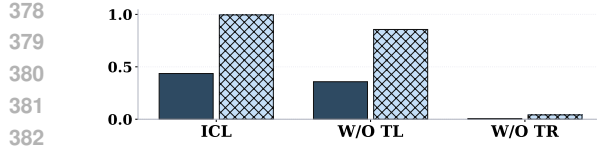
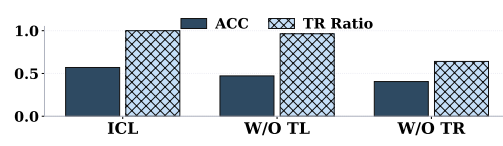


Figure 6: Pairwise overlap/correlation of TR/TL heads and IHs across datasets. TR heads and IHs are task-consistent, whereas TL heads vary widely. See Appendix G.4 for other models.

<sup>5</sup>For the seven datasets with 4 having 2 labels, 2 having 3 labels, 1 having 6 labels, the average random guessing level is 40.48%



383 (a) Ablating with shuffled demonstration texts.



383 (b) Ablating with relabeled demonstrations.

384 Figure 8: Dataset-average effects of ablating TR and TL heads under input perturbations. **(A)**  
 385 Shuffling character order of demonstration texts destroys TL, making TL ablation negligible while TR  
 386 ablation still matters. **(B)** Relabeling demonstrations alters the label space, thereby greatly reducing  
 387 the impact of TR head ablation.

389 lowers accuracy by  $\sim 30\%$  but only slightly reduces the TR ratio (by  $\sim 10\%$ ). This highlights a  
 390 key property: *separability*, i.e., TR and TL can be independently controlled and intervened upon,  
 391 consistent with the conclusions in Pan et al. (2023) achieved through input perturbations. (see  
 392 Appendix H.1 for other models).

393 **TR heads, IHs, and implications for zero-shot** Ablating IHs produces a pattern closely resembling  
 394 TR head ablation: large accuracy losses primarily due to failed task recognition. This supports the  
 395 conclusion that IHs influence ICL mainly by strengthening TR. Likewise, the root cause of poor  
 396 zero-shot performance is insufficient task recognition. Thus, restoring ICL-level accuracy in zero-shot  
 397 settings hinges on activating the TR functionality—a question we revisit in Subsection 4.3.

#### 398 Testing independence via input perturbations

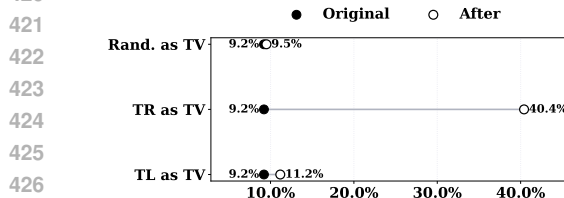
399 To complement head ablations with an orthogonal causal test, we perturb ICL inputs to se-  
 400 lectively disrupt TR or TL. Following Wei et al.  
 401 (2023); Pan et al. (2023), we consider two cases:  
 402 Case 1: Keep labels unchanged but randomize  
 403 the character order of demonstration texts (e.g.,  
 404 “I like it: positive”  $\rightarrow$  “tkl iieI : positive”). This  
 405 destroys TL, since no meaningful mapping from  
 406 such nonsensical texts to labels remains. Case  
 407 2: Keep texts unchanged but replace demonstra-  
 408 tion labels with arbitrary tokens (e.g., “negative”  $\rightarrow$   
 409 “0”, “positive”  $\rightarrow$  “1”), thereby altering the label space recognized by TR heads.

410 We hypothesize that: if the TR heads and TL heads maintain sufficient independence, then in Case  
 411 1, ablating TL heads should have little effect (TL is already disabled), while in Case 2, ablating TR  
 412 heads should matter less (the original TR functionality is nullified).

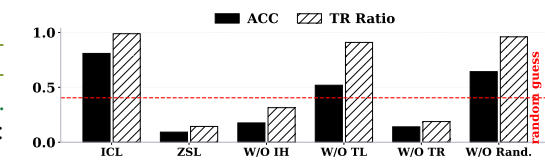
413 As shown in Figure 8a, when texts are shuffled, TL ablation barely matters while TR ablation remains  
 414 devastating. Conversely, in Figure 8b, TR ablation has little effect, compared to the significant impact  
 415 shown in Figure 7, since the recognized label space has shifted, while TL ablation behaves as in  
 416 the standard case. These results confirm the robustness of TR/TL independence across diverse ICL  
 417 settings (see Appendix H.2 for other models).

418

### 419 4.3 STEERING WITH TR/TL HEADS: FUNCTIONAL AND GEOMETRIC INSIGHTS



420  
 421 Figure 9: Zero-shot accuracy gains from steering  
 422 with task vectors constructed from TR,  
 423 TL, or random heads. TR-based task vec-  
 424 tors consistently recover ICL-level accuracy,  
 425 while TL-based vectors have weaker effects.  
 426  
 427



428 Figure 7: Effects of ablating the top 3% of different  
 429 heads, averaged across datasets. TR head ablation  
 430 severely reduces both accuracy and TR ratio, while  
 431 TL head ablation primarily reduces accuracy.

432 With fine-grained ablations establishing that TR and  
 433 TL heads are necessary for their respective channels,  
 434 we now test their sufficiency and TSLA-predicted  
 435 geometric roles by injecting their outputs. Ablations  
 436 show what happens when heads are removed, but not  
 437 what happens when they are added. We therefore  
 438 complement them with steering experiments that ex-  
 439 amine how TR and TL head outputs affect zero-shot  
 440 behavior and hidden-state updates. Specifically, we  
 441 test their suitability as task vectors (TVs) (Todd et al.,  
 442 2024; Hendel et al., 2023) by extracting their outputs  
 443 at the final token position from ICL prompts, sum-  
 444 ming them across prompts, and injecting them into the residual stream of zero-shot inputs to evaluate

recovery toward ICL-level performance. We use the top 3% TR/TL heads, compare against 3% random heads, and follow [Appendix J.1](#) to construct task vectors.

**Task recognition as the key to zero-shot failure** [Figure 9](#) mirror our ablation findings ([Figure 7](#)): poor zero-shot performance stems primarily from weak task recognition. Injecting TR-based TVs restores this functionality and improves performance. TL-based vectors are less effective, reinforcing that TL operates based on TR (see [Appendix I.1](#) for other models).

**Task-type dependence of steering effectiveness** Note that the relative ineffectiveness of TL heads as task vectors can be partly attributed to the classification datasets we use, where performance is tightly linked to task recognition and effectively upper-bounded by the TR ratio. In contrast, generation tasks differ fundamentally in that no fixed label space exists—the label space is indefinite and, in principle, infinite. As a result, model success in such tasks is less constrained by recognizing a closed set of labels, and instead depends more on learning and applying the correct input–output mapping. To examine this scenario, we consider a sentiment-controlled review generation task with prompts such as: “*Write a positive/negative review of a movie within 30 words.*” Labels are coherent reviews with the desired sentiment<sup>6</sup>. We identify TR and TL heads on ICL-styled prompts from this task following [Appendix J.2](#), and use their outputs as task vectors to influence the zero-shot generations. An LLM evaluator is then used to rate generations from 0 to 10 based on sentiment adherence and language coherence. As shown in [Figure 10](#), TL-based vectors significantly outperform TR-based and random vectors, consistent with TL heads capturing mappings from demonstrations to the sentiment values and semantic coherence of the labels (see [Appendix I.2](#) for other models). Nevertheless, given the relative simple and structured nature of this task and the fact that the label reviews are generated by GPT (OpenAI et al., 2024), we extend our investigation regarding the TV effectiveness using the SubjQA dataset (Bjerva et al., 2020), which we detail in [Appendix I.3](#).

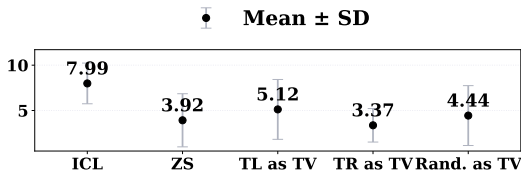


Figure 10: Ratings in the review generation task when steering with TR, TL, or random TVs. TL vectors yield the largest improvements, reflecting their strength in capturing in-context mappings.

head outputs are added to the residual stream during layer progression inside the model. We measure two geometric metrics before and after steering: (1) **Logit Difference**: inner product of the hidden state with the mean unembedding difference between correct and incorrect labels, reflecting label discrimination. (2) **Subspace Alignment**: cosine similarity between the hidden state and the subspace spanned by label unembeddings, reflecting alignment with task-related semantics<sup>7</sup>.

The results in [Figure 11](#) demonstrate the specialized geometric effects TR and TL heads have in the evolution of hidden states (for other models, see [Appendix I.4](#)). Steering with TR outputs causes hidden states to align significantly more with the task subspace. In contrast, TL outputs adjust the hidden state to align better with the unembedding direction of the correct label in the task space but not with the task subspace overall. This leads us to conjecture that TR outputs are *well-aligned with the task subspace*, thus increase hidden-state alignment with the subspace after addition by decreasing the angle in between. By contrast, TL heads create *pure rotation toward the*

**Geometric effects of TR and TL outputs** To understand the significance of TR/TL heads in ICL at a finer level than task vector experiments, we invoke the geometric analysis of hidden states (Kirsanov et al., 2025; Yang et al., 2025), which analyzes the evolution of ICL hidden states and the role of different components. Concretely, given an ICL prompt, we extract the summed outputs of the top 3% TR or TL heads, revert to the hidden state at an earlier layer, and steer it with these outputs. This mimics how

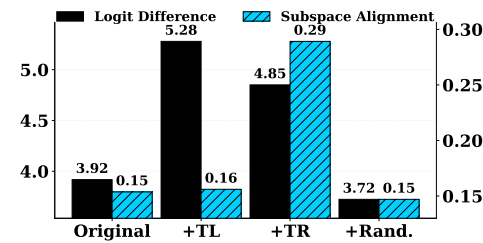
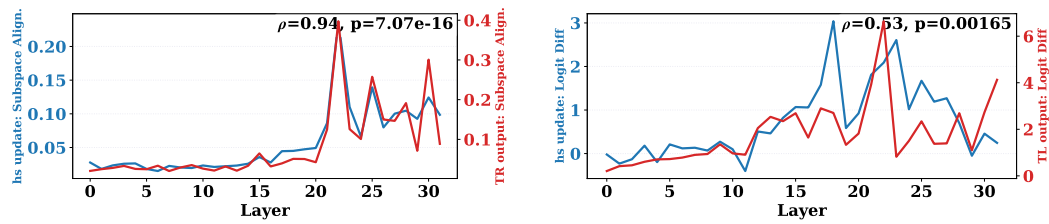


Figure 11: Geometric effects of TR and TL steering. TR outputs enhance alignment with the task subspace, while TL outputs rotate hidden states toward the correct label unembedding within the subspace.

<sup>6</sup>Example positive review: “Bold experimental narrative structure defies genre conventions delightfully. Socioeconomic themes challenge viewers’ perceptions thoughtfully and respectfully.”

<sup>7</sup>See [Appendix J.3](#) for full definitions.



(a) Correlation between hidden state updates and TR head outputs in subspace alignment. Strong correlation confirms TR heads as main drivers of alignment.  
(b) Correlation between hidden state updates and TL head outputs in logit difference. TL heads consistently drive discrimination toward correct labels.  
Figure 12: Layerwise verification of TR and TL geometric effects. TR heads enforce alignment with the task subspace, while TL heads enforce rotations toward correct label directions.

*correct label unembedding direction*, fine-tuning hidden-state orientation toward the correct label without boosting subspace alignment. See [Appendix I.4](#) for other models.

**Layerwise verification of geometric influence** To validate that TR and TL heads indeed primarily drive these geometric dynamics, we examine hidden state updates under ICL across layers. At each layer, we compute the mean subspace alignment of top-3 TR heads (i.e. heads with top-3 TR scores at the layer) outputs and the mean logit difference of top-3 TL heads outputs, then correlate them with the same metrics computed on the full hidden state updates. Since head outputs contribute directly to layer updates, their correlations with hidden-state geometry across layers indicate how strongly TR and TL heads drive the dynamics. As shown in [Figure 12](#), the correlations are strong, confirming that TR and TL heads dominate layerwise geometric shaping of hidden states. For other models see [Appendix I.5](#). Additional ablation-based verification is provided in [Appendix I.6](#).

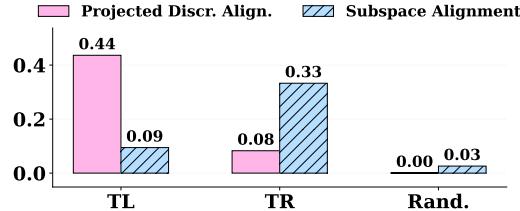


Figure 13: Decomposed geometric effects of TR and TL outputs. TR heads align hidden states to the task subspace; TL heads rotate states within the subspace toward correct label directions.

*ing towards the task space and steering within the task space*, enabling more fine-grained verification of the heads’ distinct effects ([Figure 1 \(B\), \(C\)](#)). [Figure 13](#) shows that TL head outputs have high cosine similarity with the mean unembedding difference after projection, confirming that TL heads, when restricted to the task subspace, propel rotation from wrong-label to correct-label unembedding directions. The high cosine similarity between TR heads and the task subspace itself strongly evidences their capability to steer hidden states towards the task subspace and support prediction of task-related labels (see [Appendix I.7](#) for more models).

**TR heads align to task space, TL heads rotate within it** To support our geometric intuition from [Figure 11](#) that TR heads foster alignment while TL heads perform rotation, we consider two geometric measures of TR and TL head outputs. **(1) Subspace Alignment** — cosine similarity with the task subspace, and **(2) Projected Discriminant Alignment** — cosine similarity with the mean unembedding difference between the correct and incorrect labels after projection onto the task subspace. These measures dissect the geometric effects of head outputs into *steer-*

## 5 CONCLUSION

We presented a unified framework reconciling component and holistic views of in-context learning (ICL) by identifying attention heads specialized for Task Recognition (TR) and Task Learning (TL). Using TSLA, we showed that TR heads align hidden states with the task subspace to recognize labels, while TL heads rotate states within it toward the correct label. Ablation experiments confirmed separable roles: removing TR heads collapses task recognition, whereas removing TL heads mainly reduces accuracy. Steering experiments showed task dependence: TR-based vectors are crucial for classification with fixed labels, while TL-based vectors dominate in open-ended generation. Geometric analyses supported these findings, attributing alignment to TR heads and discriminative rotations to TL heads. Our results also clarify induction heads and task vectors as TR manifestations. Together, this work establishes TR and TL heads as mechanistic foundations of ICL.

540 REFERENCES  
541

- 542 01. AI, Alex Young, Bei Chen, Chao Li, Chengen Huang, Ge Zhang, Guanwei Zhang, Heng Li,  
543 Jiangcheng Zhu, Jianqun Chen, Jing Chang, Kaidong Yu, Peng Liu, Qiang Liu, Shawn Yue, Senbin  
544 Yang, Shiming Yang, Tao Yu, Wen Xie, Wenhao Huang, Xiaohui Hu, Xiaoyi Ren, Xinyao Niu,  
545 Pengcheng Nie, Yuchi Xu, Yudong Liu, Yue Wang, Yuxuan Cai, Zhenyu Gu, Zhiyuan Liu, and  
546 Zonghong Dai. Yi: Open foundation models by 01.ai, 2024.
- 547 Johannes Bjerva, Nikita Bhutani, Behzad Golshan, Wang-Chiew Tan, and Isabelle Augenstein.  
548 Subjqa: A dataset for subjectivity and review comprehension, 2020. URL <https://arxiv.org/abs/2004.14283>.
- 549
- 550 Tom B. Brown, Benjamin Mann, Nick Ryder, Melanie Subbiah, Jared Kaplan, Prafulla Dhariwal,  
551 Arvind Neelakantan, Pranav Shyam, Girish Sastry, Amanda Askell, Sandhini Agarwal, Ariel  
552 Herbert-Voss, Gretchen Krueger, Tom Henighan, Rewon Child, Aditya Ramesh, Daniel M. Ziegler,  
553 Jeffrey Wu, Clemens Winter, Christopher Hesse, et al. Language models are few-shot learners. In  
554 *Proceedings of the 34th International Conference on Neural Information Processing Systems*, pp.  
555 1877–1901, Online and Vancouver, Canada, 2020. URL <https://dl.acm.org/doi/abs/10.5555/3495724.3495883>.
- 556
- 557 Vivien Cabannes, Charles Arnal, Wassim Bouaziz, Xingyu Yang, Francois Charton, and Julia  
558 Kempe. Iteration head: A mechanistic study of chain-of-thought. *Advances in Neural Information  
559 Processing Systems*, 37:109101–109122, 2024.
- 560
- 561 Hakaze Cho, Mariko Kato, Yoshihiro Sakai, and Naoya Inoue. Revisiting in-context learning  
562 inference circuit in large language models. In *The Thirteenth International Conference on Learning  
563 Representations*, 2025a. URL <https://openreview.net/forum?id=xizpnYNvQq>.
- 564
- 565 Hakaze Cho, Yoshihiro Sakai, Mariko Kato, Kenshiro Tanaka, Akira Ishii, and Naoya Inoue. Token-  
566 based decision criteria are suboptimal in in-context learning. In Luis Chiruzzo, Alan Ritter, and  
567 Lu Wang (eds.), *Proceedings of the 2025 Conference of the Nations of the Americas Chapter  
568 of the Association for Computational Linguistics: Human Language Technologies (Volume 1:  
569 Long Papers)*, pp. 5378–5401, Albuquerque, New Mexico, April 2025b. Association for Computational  
570 Linguistics. ISBN 979-8-89176-189-6. URL <https://aclanthology.org/2025.nacl-long.278/>.
- 571
- 572 Bilal Chughtai, Alan Cooney, and Neel Nanda. Summing up the facts: Additive mechanisms behind  
573 factual recall in llms. *arXiv preprint arXiv:2402.07321*, 2024.
- 574
- 575 Joy Crosbie and Ekaterina Shutova. Induction heads as an essential mechanism for pattern matching  
576 in in-context learning. *arXiv preprint arXiv:2407.07011*, 2024.
- 577
- 578 Ido Dagan, Oren Glickman, and Bernardo Magnini. The pascal recognising textual entailment  
579 challenge. In *Machine learning challenges workshop*, pp. 177–190. Springer, 2005. URL [https://link.springer.com/chapter/10.1007/11736790\\_9](https://link.springer.com/chapter/10.1007/11736790_9).
- 580
- 581 Marie-Catherine De Marneffe, Mandy Simons, and Judith Tonhauser. The commitmentbank: In-  
582 vestigating projection in naturally occurring discourse. In *proceedings of Sinn und Bedeutung*,  
583 volume 23, pp. 107–124, 2019. URL <https://ojs.ub.uni-konstanz.de/sub/index.php/sub/article/view/601>.
- 584
- 585 Qingxiu Dong, Lei Li, Damai Dai, Ce Zheng, Jingyuan Ma, Rui Li, Heming Xia, Jingjing Xu,  
586 Zhiyong Wu, Tianyu Liu, Baobao Chang, Xu Sun, Lei Li, and Zhifang Sui. A survey on in-context  
587 learning, 2024. URL <https://arxiv.org/abs/2301.00234>.
- 588
- 589 Nelson Elhage, Neel Nanda, Catherine Olsson, Tom Henighan, Nicholas Joseph, Ben Mann,  
590 Amanda Askell, Yuntao Bai, Anna Chen, Tom Conerly, et al. A mathematical framework  
591 for transformer circuits. *Transformer Circuits Thread*, 1(1):12, 2021. URL <https://transformer-circuits.pub/2021/framework/index.html>.
- 592
- 593 Aaron Grattafiori, Abhimanyu Dubey, Abhinav Jauhri, and Abhinav Pandey et al. The llama 3 herd  
of models, 2024. URL <https://arxiv.org/abs/2407.21783>.

- 594 Danny Halawi, Jean-Stanislas Denain, and Jacob Steinhardt. Overthinking the truth: Understanding  
 595 how language models process false demonstrations, 2024. URL <https://arxiv.org/abs/2307.09476>.
- 597 Roe Hendel, Mor Geva, and Amir Globerson. In-context learning creates task vectors. In  
 598 Houda Bouamor, Juan Pino, and Kalika Bali (eds.), *Findings of the Association for Computational Linguistics: EMNLP 2023*, pp. 9318–9333, Singapore, December 2023. Association  
 600 for Computational Linguistics. doi: 10.18653/v1/2023.findings-emnlp.624. URL <https://aclanthology.org/2023.findings-emnlp.624/>.
- 602 Jiachen Jiang, Yuxin Dong, Jinxin Zhou, and Zhihui Zhu. From compression to expansion: A  
 603 layerwise analysis of in-context learning, 2025. URL <https://arxiv.org/abs/2505.17322>.
- 605 Zhuoran Jin, Pengfei Cao, Hongbang Yuan, Yubo Chen, Jie Xin Xu, Huaijun Li, Xiaojian Jiang, Kang  
 607 Liu, and Jun Zhao. Cutting off the head ends the conflict: A mechanism for interpreting and  
 608 mitigating knowledge conflicts in language models, 2024. URL <https://arxiv.org/abs/2402.18154>.
- 610 Patrick Kahardipraja, Reduan Achitbat, Thomas Wiegand, Wojciech Samek, and Sebastian La-  
 611 puschkin. The atlas of in-context learning: How attention heads shape in-context retrieval augmen-  
 612 tation. *arXiv preprint arXiv:2505.15807*, 2025.
- 613 Artem Kirsanov, Chi-Ning Chou, Kyunghyun Cho, and SueYeon Chung. The geometry of prompt-  
 614 ing: Unveiling distinct mechanisms of task adaptation in language models. In Luis Chiruzzo,  
 615 Alan Ritter, and Lu Wang (eds.), *Findings of the Association for Computational Linguistics: NAACL 2025*, pp. 1855–1888, Albuquerque, New Mexico, April 2025. Association for Computational Linguistics. ISBN 979-8-89176-195-7. URL <https://aclanthology.org/2025.findings-naacl.100/>.
- 614 Xin Li and Dan Roth. Learning question classifiers. In *COLING 2002: The 19th International Conference on Computational Linguistics*, 2002. URL <https://www.aclweb.org/anthology/C02-1150>.
- 615 Yuxuan Li, Declan Campbell, Stephanie CY Chan, and Andrew Kyle Lampinen. Just-in-time and  
 616 distributed task representations in language models. *arXiv preprint arXiv:2509.04466*, 2025.
- 617 Tom Lieberum, Matthew Rahtz, János Kramár, Neel Nanda, Geoffrey Irving, Rohin Shah, and  
 618 Vladimir Mikulik. Does circuit analysis interpretability scale? evidence from multiple choice  
 619 capabilities in chinchilla, 2023. URL <https://arxiv.org/abs/2307.09458>.
- 620 Sheng Liu, Haotian Ye, Lei Xing, and James Zou. In-context vectors: Making in context learning  
 621 more effective and controllable through latent space steering, 2024. URL <https://arxiv.org/abs/2311.06668>.
- 622 Bill MacCartney and Christopher D. Manning. Modeling semantic containment and exclusion in  
 623 natural language inference. In Donia Scott and Hans Uszkoreit (eds.), *Proceedings of the 22nd International Conference on Computational Linguistics (Coling 2008)*, pp. 521–528, Manchester, UK, August 2008. Coling 2008 Organizing Committee. URL <https://aclanthology.org/C08-1066/>.
- 624 Jack Merullo, Carsten Eickhoff, and Ellie Pavlick. Language models implement simple word2vec-  
 625 style vector arithmetic, 2024. URL <https://arxiv.org/abs/2305.16130>.
- 626 Sewon Min, Xinxi Lyu, Ari Holtzman, Mikel Artetxe, Mike Lewis, Hannaneh Hajishirzi, and Luke  
 627 Zettlemoyer. Rethinking the role of demonstrations: What makes in-context learning work? *arXiv preprint arXiv:2202.12837*, 2022.
- 628 Catherine Olsson, Nelson Elhage, Neel Nanda, Nicholas Joseph, Nova DasSarma, Tom Henighan,  
 629 Ben Mann, Amanda Askell, Yuntao Bai, Anna Chen, Tom Conerly, Dawn Drain, Deep Ganguli,  
 630 Zac Hatfield-Dodds, Danny Hernandez, Scott Johnston, Andy Jones, Jackson Kernion, Liane  
 631 Lovitt, Kamal Ndousse, Dario Amodei, Tom Brown, Jack Clark, Jared Kaplan, Sam McCandlish,  
 632 and Chris Olah. In-context learning and induction heads, 2022. URL <https://arxiv.org/abs/2209.11895>.

- 648 OpenAI, Josh Achiam, Steven Adler, Sandhini Agarwal, Lama Ahmad, Ilge Akkaya, Florencia Leoni  
 649 Aleman, Diogo Almeida, Janko Altenschmidt, Sam Altman, Shyamal Anadkat, Red Avila, Igor  
 650 Babuschkin, Suchir Balaji, Valerie Balcom, Paul Baltescu, Haiming Bao, Mohammad Bavarian,  
 651 Jeff Belgum, Irwan Bello, et al. Gpt-4 technical report, 2024. URL <https://arxiv.org/abs/2303.08774>.
- 653 Jane Pan, Tianyu Gao, Howard Chen, and Danqi Chen. What in-context learning “learns” in-context:  
 654 Disentangling task recognition and task learning. In Anna Rogers, Jordan Boyd-Graber, and Naoaki  
 655 Okazaki (eds.), *Findings of the Association for Computational Linguistics: ACL 2023*, pp. 8298–  
 656 8319, Toronto, Canada, July 2023. Association for Computational Linguistics. doi: 10.18653/  
 657 v1/2023.findings-acl.527. URL <https://aclanthology.org/2023.findings-acl.527>.
- 659 Bo Pang and Lillian Lee. Seeing stars: Exploiting class relationships for sentiment categorization  
 660 with respect to rating scales. *arXiv preprint cs/0506075*, 2005.
- 662 Alec Radford, Jeffrey Wu, Rewon Child, David Luan, Dario Amodei, and Ilya Sutskever.  
 663 Language models are unsupervised multitask learners. *OpenAI blog*, 2019. URL  
 664 <https://d4mucfpksywv.cloudfront.net/better-language-models/language-models.pdf>.
- 666 Jie Ren, Qipeng Guo, Hang Yan, Dongrui Liu, Quanshi Zhang, Xipeng Qiu, and Dahua Lin. Identifying  
 667 semantic induction heads to understand in-context learning. *arXiv preprint arXiv:2402.13055*,  
 668 2024a.
- 670 Jie Ren, Qipeng Guo, Hang Yan, Dongrui Liu, Quanshi Zhang, Xipeng Qiu, and Dahua Lin.  
 671 Identifying semantic induction heads to understand in-context learning, 2024b. URL <https://arxiv.org/abs/2402.13055>.
- 673 Baturay Saglam, Paul Kassianik, Blaine Nelson, Sajana Weerawardhena, Yaron Singer, and Amin  
 674 Karbasi. Large language models encode semantics in low-dimensional linear subspaces, 2025.  
 675 URL <https://arxiv.org/abs/2507.09709>.
- 677 Aaditya K Singh, Ted Moskovitz, Felix Hill, Stephanie CY Chan, and Andrew M Saxe. What  
 678 needs to go right for an induction head? a mechanistic study of in-context learning circuits  
 679 and their formation. In *Forty-first International Conference on Machine Learning*, 2024. URL  
 680 <https://arxiv.org/abs/2404.07129>.
- 681 Richard Socher, Alex Perelygin, Jean Wu, Jason Chuang, Christopher D. Manning, Andrew Ng, and  
 682 Christopher Potts. Recursive deep models for semantic compositionality over a sentiment treebank.  
 683 In David Yarowsky, Timothy Baldwin, Anna Korhonen, Karen Livescu, and Steven Bethard (eds.),  
 684 *Proceedings of the 2013 Conference on Empirical Methods in Natural Language Processing*, pp.  
 685 1631–1642, Seattle, Washington, USA, October 2013. Association for Computational Linguistics.  
 686 URL <https://aclanthology.org/D13-1170/>.
- 687 Jiajun Song, Zhuoyan Xu, and Yiqiao Zhong. Out-of-distribution generalization via composition: a  
 688 lens through induction heads in transformers. *Proceedings of the National Academy of Sciences*,  
 689 122(6):e2417182122, 2025. URL <https://arxiv.org/abs/2408.09503>.
- 691 Chenghao Sun, Zhen Huang, Yonggang Zhang, Le Lu, Houqiang Li, Xinmei Tian, Xu Shen, and  
 692 Jieping Ye. Interpret and improve in-context learning via the lens of input-label mappings. In  
 693 *Proceedings of the 63rd Annual Meeting of the Association for Computational Linguistics (Volume  
 694 1: Long Papers)*, pp. 3873–3895, 2025.
- 695 JTianxiang Sun, Yunfan Shao, Hong Qian, Xuanjing Huang, and Xipeng Qiu. Black-box tun-  
 696 ing for language-model-as-a-service. In *Proceedings of the 39th International Conference  
 697 on Machine Learning*, pp. 20841–20855, Baltimore, Maryland, USA, 2022. ACM. URL  
 698 <https://proceedings.mlr.press/v162/sun22e/sun22e.pdf>.
- 699 Eric Todd, Millicent L. Li, Arnab Sen Sharma, Aaron Mueller, Byron C. Wallace, and David Bau.  
 700 Function vectors in large language models, 2024. URL <https://arxiv.org/abs/2310.15213>.

- 702 Sida Wang and Christopher Manning. Baselines and bigrams: Simple, good sentiment and topic  
 703 classification. In Haizhou Li, Chin-Yew Lin, Miles Osborne, Gary Geunbae Lee, and Jong C. Park  
 704 (eds.), *Proceedings of the 50th Annual Meeting of the Association for Computational Linguistics*  
 705 (*Volume 2: Short Papers*), pp. 90–94, Jeju Island, Korea, July 2012. Association for Computational  
 706 Linguistics. URL <https://aclanthology.org/P12-2018/>.
- 707 Jerry Wei, Jason Wei, Yi Tay, Dustin Tran, Albert Webson, Yifeng Lu, Xinyun Chen, Hanxiao  
 708 Liu, Da Huang, Denny Zhou, and Tengyu Ma. Larger language models do in-context learning  
 709 differently, 2023. URL <https://arxiv.org/abs/2303.03846>.
- 710 An Yang, Baosong Yang, Binyuan Hui, Bo Zheng, Bowen Yu, Chang Zhou, Chengpeng Li,  
 711 Chengyuan Li, Dayiheng Liu, Fei Huang, Guanting Dong, Haoran Wei, Huan Lin, Jialong Tang,  
 712 Jialin Wang, Jian Yang, Jianhong Tu, Jianwei Zhang, Jianxin Ma, Jin Xu, Jingren Zhou, Jinze Bai,  
 713 Jinzheng He, Junyang Lin, Kai Dang, Keming Lu, Keqin Chen, Kexin Yang, Mei Li, Mingfeng  
 714 Xue, Na Ni, Pei Zhang, Peng Wang, Ru Peng, Rui Men, Ruize Gao, Runji Lin, Shijie Wang, Shuai  
 715 Bai, Sinan Tan, Tianhang Zhu, Tianhao Li, Tianyu Liu, Wenbin Ge, Xiaodong Deng, Xiaohuan  
 716 Zhou, Xingzhang Ren, Xinyu Zhang, Xipin Wei, Xuancheng Ren, Yang Fan, Yang Yao, Yichang  
 717 Zhang, Yu Wan, Yunfei Chu, Yuqiong Liu, Zeyu Cui, Zhenru Zhang, and Zhihao Fan. Qwen2  
 718 technical report. *arXiv preprint arXiv:2407.10671*, 2024.
- 719 Haolin Yang, Hakaze Cho, Yiqiao Zhong, and Naoya Inoue. Unifying attention heads and task  
 720 vectors via hidden state geometry in in-context learning, 2025. URL <https://arxiv.org/abs/2505.18752>.
- 721 Kayo Yin and Jacob Steinhardt. Which attention heads matter for in-context learning? *arXiv preprint*  
 722 *arXiv:2502.14010*, 2025.
- 723 Zeping Yu and Sophia Ananiadou. How do large language models learn in-context? query and key  
 724 matrices of in-context heads are two towers for metric learning. *arXiv preprint arXiv:2402.02872*,  
 725 2024.
- 726 Haiyan Zhao, Heng Zhao, Bo Shen, Ali Payani, Fan Yang, and Mengnan Du. Beyond single  
 727 concept vector: Modeling concept subspace in llms with gaussian distribution, 2025. URL  
 728 <https://arxiv.org/abs/2410.00153>.
- 729 Zifan Zheng, Yezhaohui Wang, Yuxin Huang, Shichao Song, Mingchuan Yang, Bo Tang, Feiyu  
 730 Xiong, and Zhiyu Li. Attention heads of large language models: A survey. *arXiv preprint*  
 731 *arXiv:2409.03752*, 2024.
- 732
- 733
- 734
- 735
- 736
- 737
- 738
- 739
- 740
- 741
- 742
- 743
- 744
- 745
- 746
- 747
- 748
- 749
- 750
- 751
- 752
- 753
- 754
- 755

# 756 Appendices

## 759 A STATEMENT OF LLM USAGE

760 In this work, LLMs are used to help with writing, experiment coding, and visualization of the results.  
 761 LLMs are also used to produce results in one of the experiments, as explained in [Subsection 4.3](#) and  
 762 [Appendix K](#).

## 765 B PROOF OF [THEOREM 1](#)

766 Let  $S \in \mathbb{R}^{d \times r}$  be one of the  $n$  distinct  $r$ -dimensional subspaces in  $\text{span}(W_U)$  drawn uniformly i.i.d.  
 767 from the Grassmannian  $Gr(r, d)$ . Denote  $P_S$  as the projection matrix of  $S$ . Let  $c = \frac{\|P_S a_{N,k}^l\|_2}{\|a_{N,k}^l\|_2}$  be  
 768 the projected norm of the normalized head output  $\frac{a_{N,k}^l}{\|a_{N,k}^l\|_2}$  onto  $S$ . Since the uniform distribution  
 769 over  $Gr(r, d)$  is induced by the Haar measure over the orthogonal group  $O(d)$ , the distribution  
 770 is rotation-invariant; i.e., multiplying  $S$  by an orthogonal matrix  $U \in \mathbb{R}^{d \times d}$  does not change its  
 771 distribution. Because orthogonal transformations preserve angles, we also have

$$\frac{\|P_U S U a_{N,k}^l\|_2}{\|a_{N,k}^l\|_2} = \frac{\|P_S a_{N,k}^l\|_2}{\|a_{N,k}^l\|_2}.$$

772 Hence, without loss of generality, we pick an  $U$  such that  $U \frac{a_{N,k}^l}{\|a_{N,k}^l\|_2} = e_1$ , the unit vector in the first  
 773 coordinate, with  $c' = \|P_U S e_1\|_2$  having the same distribution as  $c$ .

774 Since  $U S = \text{span}(v_1, \dots, v_r)$ , where  $v_1, \dots, v_r$  are the first  $r$  columns of a Haar orthogonal matrix  $V$ ,  
 775 let  $V_r = [v_1, \dots, v_r]$ . Then  $P_U S = V_r V_r^\top$ , and we have

$$c'^2 = e_1^\top V_r V_r^\top e_1 = \|V_r^\top e_1\|_2^2 = \sum_{i=1}^r \langle e_1, v_i \rangle^2 = \sum_{i=1}^r V_{1,i}^2,$$

776 where  $V_{1,:}$  denotes the first row of  $V_r$ . Since  $V_r$  is Haar orthogonal,  $V_{1,:}$  is uniformly distributed on  
 777  $\mathbb{S}^{d-1}$  and has the same distribution as  $\frac{g}{\|g\|_2}$  with  $g \sim \mathcal{N}(0, I)$ . Therefore,  $\sum_{i=1}^r V_{1,i}^2$  has the same  
 778 distribution as

$$\frac{\sum_{i=1}^r g_i^2}{\|g\|_2^2} = \frac{\sum_{i=1}^r g_i^2}{\sum_{i=1}^d g_i^2} = \frac{\chi_r^2}{\chi_r^2 + \chi_{d-r}^2},$$

779 since  $g_i \sim \mathcal{N}(0, 1)$  for all  $i$ . Because  $\chi_r^2 \perp\!\!\!\perp \chi_{d-r}^2$ , we have

$$\frac{\chi_r^2}{\chi_r^2 + \chi_{d-r}^2} \sim \text{Beta}\left(\frac{r}{2}, \frac{d-r}{2}\right).$$

780 If  $c^2 \sim \text{Beta}\left(\frac{r}{2}, \frac{d-r}{2}\right)$ , then the tail probability is

$$\Pr(c \geq x) = 1 - I_{x^2}\left(\frac{r}{2}, \frac{d-r}{2}\right) = 1 - \frac{B(x^2; \frac{r}{2}, \frac{d-r}{2})}{B(\frac{r}{2}, \frac{d-r}{2})},$$

781 where  $B$  is the Beta function. Since the TR score of the head is  $\gamma$ , the probability that  $\|P_S a_{N,k}^l\|_2 \geq \gamma$   
 782 is

$$1 - I\left(\frac{\gamma}{\|a_{N,k}^l\|_2}\right)^2\left(\frac{r}{2}, \frac{d-r}{2}\right).$$

783 Because there are  $n - 1$  subspaces alongside  $W_U^Y$ , the probability that the head output has the largest  
 784 projected norm on  $W_U^Y$  is

$$1 - (n-1) \left( 1 - I\left(\frac{\gamma}{\|a_{N,k}^l\|_2}\right)^2\left(\frac{r}{2}, \frac{d-r}{2}\right) \right)$$

785 via the union bound.

810  
 811 **C ABLATION EXPERIMENTS REGARDING THE IDENTIFICATION OF TR AND**  
 812 **TL HEADS**

813  
 814 In this section, we demonstrate the advantage of our Task Subspace Logit Attribution (TSLA) method  
 815 over the naive approach of selecting TR and TL heads based on  $a_{N,k}^l W_U^{\mathbb{Y}}$  and  $a_{N,k}^l W_U^{y^*}$ , i.e., Direct  
 816 Logit Attribution (DLA) to the demonstration labels and the correct label. Specifically, [Figure 14](#)  
 817 shows the consequences of ablating the top 3% TR and TL heads identified via DLA, averaged  
 818 across datasets on Llama3-8B. While ablating the identified TR heads achieves the intended effect of  
 819 disabling task recognition by reducing the TR ratio, ablating the identified TL heads fails to induce  
 820 the expected outcome of driving ICL toward random guessing over the label space. This indicates  
 821 that the DLA approach cannot isolate distinct mechanistic causes for the TR and TL components of  
 822 ICL, and reflects its inability to correctly identify the real TL heads. Instead, it largely identifies heads  
 823 that broadly amplify the logits of all demonstration label tokens, which may also increase the correct  
 824 label logits but still primarily function through task recognition rather than true label differentiation.  
 825

826 To validate this statement, and following the setup of [Figure 2](#), we report the dataset-averaged Jaccard  
 827 Coefficient, Kendall’s  $\tau$ , and Spearman’s  $\rho$  values between TR/TL heads identified by DLA and those  
 828 identified by TSLA, as well as their relationship with IHs. As shown in [Figure 15](#), both TL and TR  
 829 heads selected via DLA strongly overlap with the TR heads identified by TSLA at the 3% level. This  
 830 corroborates our conclusion that DLA fails to effectively recover genuine TL heads. Furthermore, the  
 831 weak correlation between the TR/TL sets obtained from the two methods is reinforced by [Figure 16](#),  
 832 which displays overlap, correlation, and consistency analyses between DLA TR/TL heads and IHs.  
 833 The strikingly high consistency between DLA TR and TL heads across all three metrics demonstrates  
 834 the lack of a meaningful distinction between them. Meanwhile, the low correlation between DLA  
 835 heads and IHs highlights another limitation of DLA: it cannot provide mechanistic explanations for  
 836 the well-documented importance of IHs in ICL.  
 837

838 Finally, to justify our second critique of the DLA approach in [Subsection 3.1](#) regarding its sensitivity  
 839 to the concrete set of demonstration labels as a hyperparameter and its inability to comprehensively  
 840 capture the task semantics, we consider the following experiment on SST-2. We replace “positive”  
 841 and “negative”, i.e. the default demonstration labels used to create ICL prompts from the dataset,  
 842 with “unfavourable” and “favourable”, which do not alter the essence of the task. Then we test how  
 843 the ablation of TR heads identified with DLA and our TSLA using the ICL prompts with the original  
 844 labels will impact the ICL accuracy and TR ratio with the new labels. The results in Figures 25–30  
 845 confirm the robustness of our TSLA method against demonstration label shifts in identifying TR  
 846 heads. On all models except Qwen2.5-32B, ablating the TR heads selected using our TSLA approach  
 847 causes a significantly larger impact on ICL performance and TR ratio with the new demonstration  
 848 labels on the SST-2 dataset, with the gap being most prominent for the three Llama family models.  
 849

850 **D IMPLEMENTATION DETAILS**

851 **Models** We use the official HuggingFace implementations of all models. Models with more than  
 852 10B parameters are quantized to 4-bit for efficiency.  
 853

854 **Datasets** We use the official HuggingFace implementations of all datasets, except for the Review  
 855 dataset, which we curated ourselves. The Review dataset was generated using ChatGPT-4o ([OpenAI](#)  
 856 et al., 2024) and contains 200 datapoints. Each datapoint consists of a prompt instructing the  
 857 model to generate a movie review in the format: ‘‘Write a positive review for a  
 858 movie. The positive review should be within 30 words.’’ The 30-word  
 859 limit was chosen to set the `max_new_tokens` parameter (set to 45) when calling the generation  
 860 function. Labels are ChatGPT-4o-generated reviews that comprehensively assess a movie from  
 861 multiple aspects in the requested positive/negative tone. For example: *“Bold experimental narrative  
 862 structure defies genre conventions delightfully. Rich orchestral score enhances every pivotal moment.  
 863 Progressive messages inspire reflection on equality and justice. Raw vulnerability on screen fosters  
 864 sincere emotional investment.”* as a positive review. Details of dataset curation are provided in  
 865 [Appendix K](#). The dataset is balanced, with 100 positive and 100 negative reviews.  
 866

867 **ICL setting** For each dataset (except the Review dataset), we select demonstrations from the training  
 868 set and queries from the test set, or the validation set if ground-truth test labels are unavailable. For  
 869

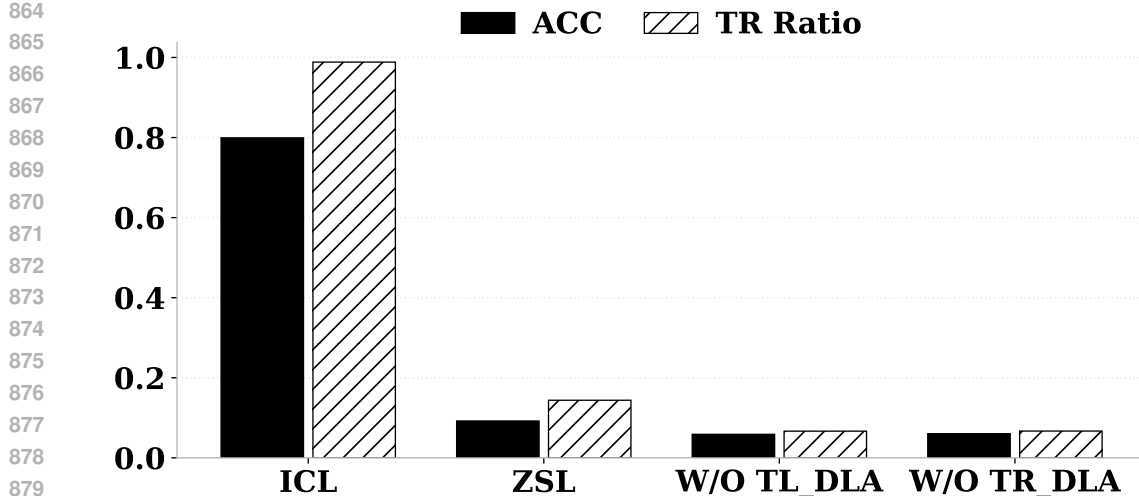


Figure 14: Effects of ablating the top 3% TR and TL heads identified using DLA, averaged across datasets on Llama3-8B. While TR heads reduce task recognition as expected, TL heads do not replicate the behavior predicted for task-learning components.

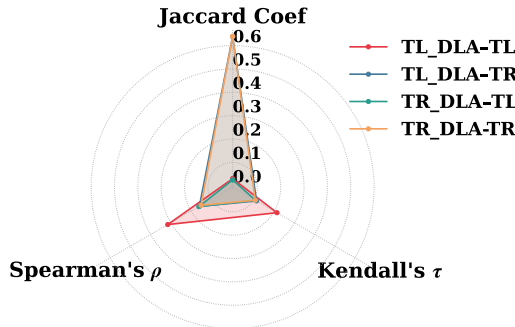


Figure 15: Dataset-averaged Jaccard Coefficient, Kendall's  $\tau$ , and Spearman's  $\rho$  between TR and TL heads identified using DLA and TSLA at the top 3% level. DLA heads overlap substantially with TR heads, confirming their inability to recover distinct TL heads.

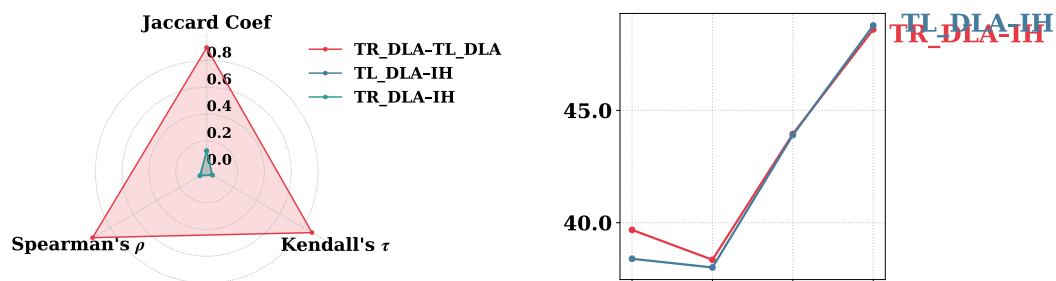


Figure 16: Dataset-averaged overlap, correlation, and consistency analyses of TR and TL heads identified using DLA and their relationship with IHs. Results show high redundancy between DLA TR and TL heads and weak association with IHs, underscoring the limitations of DLA in separating TR and TL mechanisms or explaining IH significance.

918 demonstration selection, we retain at most the first 10,000 training examples. For evaluation, we use  
 919 the first 1,000 test or validation examples. For the Review dataset, we use the first 50 examples for  
 920 demonstration selection and the remaining 150 for testing. Prompt templates used to construct ICL  
 921 prompts are listed in [Table 1](#).

922 **Devices** All experiments were conducted on an H200 GPU.  
 923

924 **Random label mappings** For the experiment in [Appendix G](#), where demonstration labels are  
 925 replaced with numbers, we use the mappings in [Table 2](#).

926 When demonstration labels are replaced with numeric symbols, we also modify the prompt templates  
 927 in [Table 1](#). Specifically, for SNLI and CB, “True or maybe or false” is replaced with “0 or 1 or 2,”  
 928 and for RTE, “True or false” is replaced with “0 or 1.”

929 **Flipped label mappings** For the experiment in [Subsection 4.2](#), where demonstration labels are  
 930 flipped, we use the mappings in [Table 3](#).  
 931

## E EXPERIMENT DETAILS CONCERNING THE IDENTIFICATION OF IHs

935 For each dataset, we use the first 50 queries to identify the top IHs. Let the queries be  
 936  $q_1, \dots, q_{50}$ , where  $q_i$  has token length  $s(q_i)$ . For each  $q_i$ , the LLM outputs an attention tensor  
 937  $\text{Attn}_i \in \mathbb{R}^{L \times N_h \times s(q_i) \times s(q_i)}$ , with  $L$  being the number of layers and  $N_h$  the number of attention heads  
 938 per layer. The  $n_h$ -th head in layer  $l$  has an attention matrix  $\text{Attn}(l, n_h)_i \in \mathbb{R}^{s(q_i) \times s(q_i)}$ , where  
 939  $\text{Attn}(l, n_h)_{i,j,k}$  denotes the attention from the  $k$ -th token to the  $j$ -th token in  $x_i$ .

940 **Identification of IHs** For each  $q_i$ , we randomly sample 8 demonstrations and prepend them to  $q_i$ .  
 941 The resulting ICL prompt,  $Q_i$  (length  $s(Q_i)$ ), follows the format  $\langle t_{i,1} \rangle : \langle y_{i,1} \rangle, \dots, \langle t_{i,8} \rangle : \langle y_{i,8} \rangle, \langle q_i \rangle$  :  
 942 where  $\langle t_{i,k} \rangle$  is the sentence part of demonstration  $k$  (e.g., “I like this movie. Sentiment”), and  $\langle y_{i,k} \rangle$  is  
 943 the label (e.g., “positive”), separated by a colon.  $\langle q_i \rangle$  is the sentence for the query. At the position of  
 944 the final colon, an IH is expected to attend to tokens after previous colons—that is, the label tokens  
 945  $\langle y_{i,1} \rangle, \dots, \langle y_{i,8} \rangle$ . Let  $\mathbb{I}_i$  be the set of label token indices in  $Q_i$ . The IH score for head  $(l, n_h)$  over the  
 946 50 queries is defined as  $\sum_{i=1}^{50} \sum_{k \in \mathbb{I}_i} \text{Attn}(l, n_h)_{i,k,s(Q_i)}$ , i.e., the total attention a head assigns at the final  
 947 “:” position to the positions of all the label tokens, summed over all 50 queries. We calculate the IH  
 948 scores for all  $(l, n_h)$  pairs and choose the top 3% attention heads as the identified IHs.  
 949

## F VERIFYING WHETHER THE UNEMBEDDINGS OF SEMANTICALLY RELATED 950 LABELS EXIST IN COMMON SUBSPACES

953 The theoretical and practical validity of our TSLA method relies on the assumption that LLM unem-  
 954 beddings of semantically related tokens lie in common low-dimensional subspaces, an observation  
 955 supported by prior work (Zhao et al., 2025; Saglam et al., 2025). To further verify this assumption,  
 956 we conduct the following experiment. We consider a set  $\mathbb{T}$  of semantically related sentiment tokens,  
 957 with  $\mathbb{T} = \{\text{positive, negative, favourable, unfavourable, pleasing, disappointing, enjoyable, unpleasant,}\$   
 958  $\text{satisfying, dissatisfying, delightful, distasteful, uplifting, depressing, enjoyable, regrettable, excellent,}\$   
 959  $\text{terrible}\}$ . For each token  $t \in \mathbb{T}$ , we measure the norm of its unembedding projected onto the subspace  
 960 spanned by the unembeddings of the remaining tokens in  $\mathbb{T}$ , i.e.,

$$\|\text{Proj}_{\mathbf{W}_U^{\mathbb{T}/\{t\}}} \mathbf{W}_U^t\|_2.$$

963 Then we randomly draw a token set  $\mathbb{T}'$  of the same size as  $\mathbb{T} \setminus \{t\}$  from the full vocabulary (i.e.,  
 964  $|\mathbb{T}'| = |\mathbb{T} \setminus \{t\}|$ ), and compute

$$\|\text{Proj}_{\mathbf{W}_U^{\mathbb{T}'} \mathbf{W}_U^t}\|_2.$$

966 If unembeddings of semantically related tokens indeed concentrate in common subspaces, we should  
 967 observe

$$\|\text{Proj}_{\mathbf{W}_U^{\mathbb{T}/\{t\}}} \mathbf{W}_U^t\|_2 > \|\text{Proj}_{\mathbf{W}_U^{\mathbb{T}'} \mathbf{W}_U^t}\|_2,$$

970 meaning that the unembedding of  $t$  aligns more strongly with the subspace spanned by its semantic  
 971 peers than with a randomly selected subspace. We compute both norms for every  $t \in \mathbb{T}$  across all  
 972 models and report the results in Figures 19–24. The results show that projection norms are indeed

972 substantially larger when  $t$  is projected onto the subspace spanned by its semantic correlates, thereby  
 973 validating the core assumption behind our TSLA approach. To further support these visual findings,  
 974 we conduct a Wilcoxon signed-rank test on the paired norm values. The results in Table 5 show that  
 975 the differences are highly statistically significant.  
 976

## 977 G SUPPLEMENTARY MATERIALS FOR SUBSECTION 4.1

### 981 G.1 ABLATION STUDIES FOR THE PERCENTAGE THRESHOLD OF SELECTING TOP TL AND TR 982 HEADS

984 Throughout the paper, we select the top 3% TL and TR heads based on their respective scores and  
 985 use them in subsequent analysis, ablation studies, and steering-based experiments. To assess whether  
 986 this particular threshold influences our conclusions, we sweep the percentage from 1% to 10% in  
 987 increments of 1%. For Llama3-8B, which has 1024 heads, each 1% corresponds to 10 heads. For  
 988 ablation experiments, we remove different percentages of top TL or TR heads and evaluate the effect  
 989 on accuracy and TR ratio. For task-vector steering experiments, we construct task vectors from the  
 990 outputs of TL or TR heads selected at each percentage level. The results in Figure 52 and Figure 53  
 991 show that our findings are robust to the choice of threshold. Specifically, ablating different percentages  
 992 of TL heads impacts accuracy but leaves the TR ratio largely unchanged, whereas ablating TR heads  
 993 affects both accuracy and the TR ratio. Moreover, using more top TR heads when constructing task  
 994 vectors increases accuracy (with saturation around 7%), whereas including more TL heads does not  
 995 yield accuracy gains.

996 These observations not only reinforce our main conclusions but also shed light on how attention  
 997 heads collectively realize TL and TR functionality: heads at different top-percentage levels make  
 998 additive contributions—albeit with varying strengths—rather than the behavior being dominated by  
 999 only a few exceptional heads. This further justifies selecting heads based on a percentage threshold  
 1000 rather than attempting to isolate only a handful of specific heads.

### 1001 G.2 REPLICATION OF FIGURE 2 FOR OTHER MODELS

1003 Figures 31–35 replicate the experiments from Figure 2, demonstrating the robustness of our findings  
 1004 across different models. In every case, TR heads show markedly stronger overlap, correlation, and  
 1005 consistency with IHs than the other head pairs. The consistently higher values of the TR–IH pair in  
 1006 terms of Jaccard Coefficient, Kendall’s  $\tau$ , Spearman’s  $\rho$ , and Conditional Average Percentage across  
 1007 all levels and architectures confirm our conclusion.

### 1008 G.3 REPLICATION OF FIGURE 3 FOR OTHER MODELS

1010 Figures 36–40 replicate the experiments from Figure 3 on additional models. These visualizations  
 1011 support our claims in Subsection 4.1 that: 1) TR heads generally reside in deeper layers than TL  
 1012 heads and IHs; 2) The overlap between TR heads and IHs is larger and predominantly occurs in  
 1013 deeper layers.

1014 To complement these figures, Tables 6–11 report the mean layer indices of the top 3%, 5%, and 10%  
 1015 TR heads, TL heads, and IHs averaged across datasets. We also conduct Mann–Whitney U tests to  
 1016 assess whether the differences in layer distributions between TR heads and IHs, and between IHs and  
 1017 TL heads, are statistically significant. The results show that the distributional differences between  
 1018 IHs and TL heads are often not significant ( $p \geq 0.05$ ). Even when significant, the  $p$ -values are much  
 1019 larger than those observed between TR heads and IHs, indicating that the TR–IH distinction is far  
 1020 more robust.

### 1022 G.4 REPLICATION OF FIGURE 6 FOR OTHER MODELS

1024 Figures 41–45 extend the analysis of Figure 6 to the remaining models. The results reinforce our  
 1025 conclusion that TR heads and IHs identified across datasets or tasks are largely consistent, whereas  
 TL heads vary substantially.

1026 To further test this, we evaluate the cross-dataset transferability of TR heads. Specifically, we ablate  
 1027 top 3% TR heads identified using SST-2 prompts and measure their impact on accuracy and TR  
 1028 ratio for the six remaining datasets. The results for all models in Figures 73-78 in general confirm  
 1029 the transferrability of TR heads across datasets, but some interesting variations among datasets  
 1030 and models are also worth noting. First, on the three Llama family models, ablating the TR heads  
 1031 identified on the SST-2 dataset can effectively drive both the accuracy and TR ratio on RTE, CB,  
 1032 and MR datasets to near zero, and to a lesser extent impact the two metrics on TREC and SNLI. On  
 1033 Yi-34B, the ablation instead significantly impact the model performance on SNLI rather than MR.  
 1034 For the remaining two Qwen family models the consequence of the ablation over datasets is similar  
 1035 to the case of Llama models but to a lesser degree overall.

1036  
 1037

### 1038 G.5 REPLICATION OF FIGURE 4 FOR OTHER MODELS

1040 In Figures 54-58 we report the results of quantifying the attention weight distributions of top TL and  
 1041 TR heads on other models, which are largely similar to Figure 4. TR heads assign larger weights to  
 1042 demonstration labels to collect information about the task label space, whilst TL heads attend to the  
 1043 query to leverage its specific semantics to facilitate its matching to the proper label token.

1044  
 1045

### 1046 G.6 REPLICATION OF FIGURE 5 FOR OTHER MODELS

1048 In Figure 5, we visualize the distinct attention patterns of TL and TR heads by showing the attention  
 1049 distributions of the top-1 TL and TR heads over an ICL prompt formed using the first test query  
 1050 of SST-2. In Figures 59-67, we report the corresponding attention distributions over ICL prompts  
 1051 formed using the second through tenth test queries of SST-2; these largely resemble Figure 5 and  
 1052 thus support its validity.

1053  
 1054

### 1055 G.7 DEMYSTIFYING THE LAYER ORDER OF TL AND TR FROM THE PERSPECTIVE OF THE 1056 LAYERWISE EVOLUTION OF ICL HIDDEN STATES

1058 Our results in Figure 3 suggest that attention heads responsible for TL emerge in earlier layers than  
 1059 those responsible for TR. This raises a question: how can the model perform task learning before  
 1060 it has recognized the task? The key to resolving this lies in our definition of TL and TR (and their  
 1061 corresponding heads) based on how they are carried out in the actual forward computation process  
 1062 of the model, which ultimately results in the promotion of certain tokens’ logits at the output layer  
 1063 and their prediction. From a logit-centric viewpoint, TL corresponds to the process by which the  
 1064 model increases the logit margin between the correct label and the incorrect candidate labels *within*  
 1065 the task’s label set. In contrast, TR corresponds to increasing the logit margin between the task’s  
 1066 label set as a whole and all other non-task-related tokens, enabling the model to detect which task it  
 1067 should perform. Under this interpretation, TL and TR are fundamentally distinct and need not occur  
 1068 simultaneously, which explains the low overlap and weak correlation between TL and TR heads  
 1069 observed in Figure 2a.

1070

1071 To further validate our claim that TL heads precede their TR counterparts, we analyze the layerwise  
 1072 logit dynamics of correct labels, incorrect candidate labels, and non-task-related tokens using  
 1073 the ICL hidden-state evolution. Specifically, we use the Logit Difference metric introduced in  
 1074 Subsection 4.3 to measure (i) the logit difference between the correct and incorrect candidate labels  
 1075 by projecting intermediate hidden states onto the corresponding unembedding differences, and (ii) the  
 1076 logit difference between the maximum logit among task-label tokens and the maximum logit among  
 1077 irrelevant tokens, which reflects task recognition capability. The results, averaged across datasets  
 1078 and models and shown in Figures 46-51, reveal a striking contrast between these two margins. The  
 1079 margin between correct and incorrect task labels starts around 0 and becomes positive after only  
 a few layers—indicating that the model quickly performs task learning and distinguishes between  
 the candidate labels. In contrast, the margin between task labels and non-task labels is strongly  
 negative in early layers and only becomes positive much later, indicating that the model initially

fails to identify the task but begins to perform task recognition in deeper layers. This pattern aligns precisely with our observed ordering of TL and TR heads.

## H SUPPLEMENTARY MATERIALS FOR SUBSECTION 4.2

### H.1 REPLICATION OF FIGURE 7 FOR OTHER MODELS

In Figures 68–72, we replicate the ablation experiments on additional models and examine their effects on dataset-average accuracy and TR ratio. The results echo our observations in Subsection 4.2: 1) Ablation of TR heads and TL heads impacts the TR and TL components of ICL separately. 2) Ablating IHs produces effects similar to ablating TR heads. 3) The primary cause of low accuracy in the zero-shot case—as well as in cases where TR heads or IHs are ablated—is the failure to adequately activate the TR functionality.

### H.2 REPLICATION OF FIGURE 8 FOR OTHER MODELS

In Figures 79–83, we repeat the experiments from Figure 8 on other models, focusing on the ablation of TR and TL heads when ICL inputs are subjected to perturbations. The results closely mirror those in Figure 8: when the in-context text–label mapping is destroyed or reversed, ablating TL heads has no effect—or even a positive effect—on accuracy. By contrast, since these perturbations do not alter the demonstration label space, the TR component of ICL remains unaffected.

### H.3 ASSESSING THE INDEPENDENCE OF TR AND TL WITH FLIPPED DEMONSTRATION LABELS

To further validate the independence of TR and TL and the mechanisms of their associated heads, we analyze the effect of ablating TR/TL heads under flipped demonstration labels. Specifically, we apply a mapping  $g : \mathbb{Y} \rightarrow \mathbb{Y}'$  that reverses the demonstration labels (e.g., “negative”  $\rightarrow$  “positive,” “positive”  $\rightarrow$  “negative”), as listed in Table 3. Since label flipping invalidates the original text–label mapping captured by TL heads, we conjecture that ablating top TL heads will *increase* accuracy, while the effect of ablating TR heads will remain unchanged because the label space itself is preserved.

The dataset-average results in Figures 84–89 confirm this conjecture: ablating top TL heads indeed raises accuracy, whereas ablating top TR heads still drives accuracy close to zero, as observed in the standard setting of Figure 7.

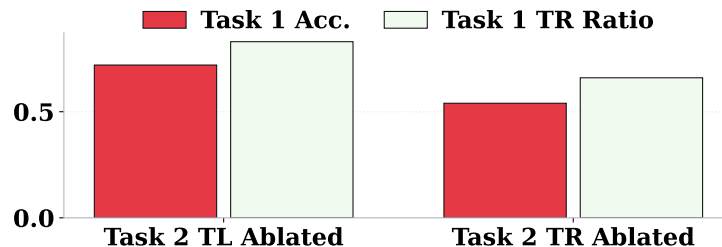
### H.4 COMPOSITE TASK LEARNING AND RECOGNITION IN ICL

In this section, we discuss how the findings in Li et al. (2025) relate to our framework of Task Learning (TL) and Task Recognition (TR), together with the corresponding experimental results. The main findings of Li et al. (2025) are threefold:

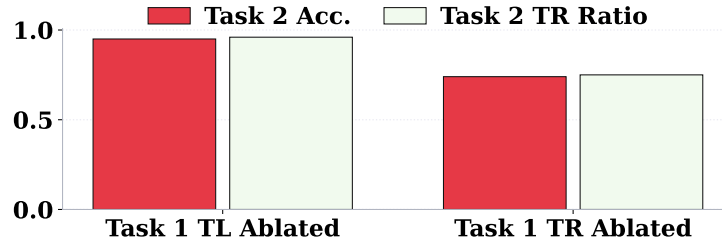
1. For an ICL prompt, only the hidden states or head outputs at certain specific token positions serve as effective TVs. For instance, in the prompt “I like this movie: positive, I don’t like it: negative, I love it:”, only the hidden states or head outputs at the two “:” positions can serve as TVs because they encode the information needed to predict “positive” and “negative” as the next tokens. This suggests that a TV encodes only the information needed for next-token prediction.
2. Consequently, in settings involving multiple or composite tasks, a TV only supports predicting the label of the first task, but not subsequent ones. For example, in the prompt “France, big  $\rightarrow$  Paris, small”, which combines a Country–Capital task and an Antonym task, a TV can correctly produce “Paris” for the first task but not “small” for the second.
3. Nevertheless, hidden states from prompts corresponding to different composite tasks that share the same initial task remain well-separated and linearly classifiable.

The limitation of task vectors to single-token prediction is directly relevant to our work, since we identify TL and TR heads based on their outputs at a single token position, and similarly construct TVs from those outputs to inject at a single position. Moreover, the effectiveness of TVs only for the

1134 first task, together with the linear separability of hidden states from different composite tasks, suggests  
 1135 that under composite tasks the model must repeatedly perform task learning for each constituent task  
 1136 while simultaneously maintaining a recognition mechanism that tracks the full scope of the composite  
 1137 structure. This unusual composite setting therefore provides an opportunity to extend our TL & TR  
 1138 framework to more complex scenarios. To investigate TL and TR in composite task learning, we  
 1139 conduct the following experiment. We consider the Country–Capital + Antonym composite task  
 1140 with ICL prompts of the form “France, big → Paris, small. China, high → Beijing, low ... Germany,  
 1141 quick →”. Using 8-shot ICL prompts, we obtain two sets of top 3% TR and TL heads, one for each  
 1142 constituent task. For Task 1 (Country–Capital), we identify the heads whose outputs at the final “→”  
 1143 position promote the logits of different capital names, as well as those whose outputs increase the  
 1144 logit margin between the correct capital label “Berlin” and the remaining capital names (the Task 1  
 1145 TR and TL heads). Then, we supplement the query with the first task’s label, yielding the prompt  
 1146 “France, big → Paris, small. China, high → Beijing, low ... Germany, quick → Berlin,”, and repeat  
 1147 the procedure to identify the TR and TL heads for Task 2 (Antonym), whose label space consists  
 1148 of all adjectives used in the Antonym task. After identifying the relevant heads, we ablate the top  
 1149 10% **Task 2** TR and TL heads to measure their impact on the accuracy and TR ratio of **Task 1** (for  
 1150 prompts such as “Germany, quick →”). Likewise, we ablate the top 3% **Task 1** TR and TL heads to  
 1151 evaluate the performance of **Task 2** (for prompts such as “Germany, quick → Berlin,”). The results  
 1152 in [Figure 17](#) and [Figure 18](#) reveal a striking pattern: ablating TL heads across tasks has minimal  
 1153 effect on accuracy and TR ratio, whereas ablating TR heads across tasks significantly affects both,  
 1154 even though the TR heads are identified from entirely different task label spaces. We also report the  
 1155 Jaccard coefficient between the two TR (and TL) sets, as well as the Spearman’s  $\rho$  between the Task 1  
 1156 and Task 2 TL (and TR) scores across all heads, in [Table 4](#). These statistics show that TR heads  
 1157 across tasks have substantially higher overlap and much stronger correlation than TL heads, further  
 1158 confirming the cross-task similarity of TR heads and the cross-task dissimilarity of TL heads. Based  
 1159 on these findings, we provide the following mechanistic explanation for ICL under composite tasks.  
 1160 To correctly infer each task’s label, a distinct set of TL heads specialized for that specific task (see  
 1161 [\(Yin & Steinhardt, 2025\)](#) for discussion of such specialization in pretraining) activates to promote  
 1162 the correct task-specific label using the task labels learned from the demonstrations. In contrast,  
 1163 at the broader level of solving the entire composite task, a unified set of TR heads tracks the label  
 1164 spaces of all constituent tasks. These heads provide the task-recognition foundation that enables each  
 1165 task-specific TL set to selectively promote its respective labels as the prompt progresses through the  
 1166 subtasks. This interpretation closely aligns with our findings in [Figure 6](#), where TR heads—but not  
 1167 TL heads—identified across datasets exhibit a high degree of overlap and correlation.  
 1168  
 1169



1175 Figure 17: Effects of ablating the Task 2 TR and TL heads on the accuracy and TR ratio of Task 1.  
 1176



1187 Figure 18: Effects of ablating the Task 1 TR and TL heads on the accuracy and TR ratio of Task 2.

1188 I SUPPLEMENTARY MATERIALS FOR [SUBSECTION 4.3](#)  
1189  
11901191 I.1 REPLICATION OF [FIGURE 9](#) FOR OTHER MODELS  
1192  
1193

Figures 90–94 replicate the steering experiments from [Figure 9](#), evaluating the effectiveness of task vectors constructed from special attention head outputs in other models. For all models except the two Qwen-family models, the results are consistent with [Subsection 4.2](#): task vectors built from TR heads are substantially more effective than those from TL heads. In the Qwen models, however, TL heads match TR heads as task vectors. This deviation can be explained by the high zero-shot accuracy of the Qwen models ([Figure 93](#), [Figure 92](#)), which exceeds 20%—considerably higher than the other models. Because these models already achieve strong task recognition in the zero-shot setting, injecting TR-head-based task vectors (which primarily encode recognition) provides less additional benefit.

1204 I.2 REPLICATION OF [FIGURE 10](#) FOR OTHER MODELS  
1205  
1206

Figures 95–99 evaluate how task vectors built from different types of heads affect the quality of generated reviews across models. Consistently, TL heads outperform TR heads and random heads as task vectors. An exception is Yi-34B, where steering reduces the average rating below the original zero-shot level. For Qwen2-7B and Qwen2.5-32B, TL-head task vectors even push ratings above the ICL-level baseline. Interestingly, the zero-shot reviews of these models score higher than their ICL reviews. Closer inspection reveals why: ICL reviews, though coherent and stylistically faithful, sometimes contradict the sentiment required in the query. TL heads appear to filter out such inconsistencies by correctly capturing the text–label mapping and discarding misleading signals, thereby boosting zero-shot review quality beyond ICL.

In addition to cross-model replication, [Table 12](#) presents sampled outputs under ICL, zero-shot, and steering with different task vectors. These examples highlight the TL heads’ ability to extract the correct text–label mapping and use it for generation. In contrast, zero-shot or TR-head steering often yields generic, off-topic sentences loosely related to the concept of “review.”

1223 I.3 EVALUATING TASK VECTOR PERFORMANCE ON A MORE COMPLEX  
1224 REVIEW-GENERATION TASK  
1225

Because the movie review generation task in the main text has a relatively simple structure and a synthetic two-way label space, we further evaluate task vectors constructed from TL and TR head outputs on a more complex setting: the SubjQA dataset (Bjerva et al., 2020). We use the “book” split, where each datapoint contains a sentiment label and a human-written book review. Unlike the movie task—whose labels are limited to “positive” and “negative”—this dataset features a much richer and more diverse sentiment label space, including labels such as “captivating,” “anticlimactic,” and “wrenching,” among many others. The human-written reviews also introduce greater linguistic complexity and semantic variability. Following the same TSLA-based procedure used to identify TL and TR heads in the main text, we compute TL and TR scores under this enlarged sentiment label space. We then construct task vectors from the outputs of the top TL or TR heads and use them to steer book-review generation in a zero-shot setting. GPT is subsequently asked to rate each generated review on a 10-point scale based on coherence and how well it reflects the intended sentiment label. The average ratings across models, shown in Figures 100–105, mirror the patterns observed in the movie-review task: TL-based task vectors consistently outperform TR-based vectors and random baselines. This demonstrates that TL heads capture abstract associations between demonstration/query texts and sentiment labels strongly enough to yield effective task vectors even in substantially more complex, real-world generation scenarios, thereby validating the robustness of our TSLA-based identification of TL heads.

1242 I.4 REPLICATION OF FIGURE 11 FOR OTHER MODELS  
12431244 Figures 106–110 extend the geometric analysis of Figure 11 to other models. The results largely  
1245 confirm our earlier observation: TL heads tend to align hidden states with label-unembedding  
1246 difference directions, while TR heads align hidden states with the broader task subspace.  
12471248 I.5 REPLICATION OF FIGURE 12 FOR OTHER MODELS  
12491250 Figures 116–120 report layer-wise correlations between mean TR/TL head outputs and full layer  
1251 updates, measured by logit difference and subspace alignment. Across models, we observe clear  
1252 and consistent correlation patterns, reinforcing that TR and TL heads are the primary drivers of the  
1253 geometric shaping of hidden states in layer updates.  
12541255 I.6 ABLATING TOP TR AND TL HEADS PER LAYER TO VERIFY THEIR GEOMETRIC  
1256 SIGNIFICANCE1257 In Figure 12, we validated the geometric importance of TR/TL heads by correlating their outputs  
1258 with full layer updates. Here, we provide an alternative perspective. Specifically, we ablate the top  
1259 three TR/TL heads per layer and then remeasure layer-wise hidden state updates under the same two  
1260 metrics. Figures 121–126 show that TR and TL heads are indeed crucial: without top TR heads,  
1261 hidden states fail to gradually align with the task subspace, crippling task recognition; without top TL  
1262 heads, logit differences collapse, preventing hidden states from rotating toward the correct label’s  
1263 unembedding direction. By contrast, ablating three random heads per layer has negligible impact.  
12641265 I.7 REPLICATION OF FIGURE 13 FOR OTHER MODELS  
12661267 Figures 111–115 replicate the analysis of Figure 13 across models. The results are consistent: TL  
1268 heads excel in projected discriminant alignment, rotating hidden states toward the correct label  
1269 unembedding and away from incorrect ones. TR heads, conversely, excel in subspace alignment,  
1270 keeping hidden states well-positioned within the task subspace. Both substantially outperform  
1271 randomly chosen heads on their respective strengths.  
12721273 J EXPERIMENT DETAILS RELATED TO TASK VECTORS  
1274

## 1275 J.1 CONSTRUCTION AND APPLICATION OF TASK VECTORS

1276 For each dataset, we first construct 8-shot ICL prompts using the last 50 queries. The demonstrations  
1277 are identical to those used when evaluating the 8-shot ICL accuracy for each dataset. Following the  
1278 procedure of Todd et al. (2024), we compute the average output (across the 50 prompts) of each  
1279 identified top 3% TR, TL, or random head at the final token position. We then sum these average  
1280 outputs across heads to form the task vector.  
12811282 In the steering experiment, the task vector is added to the hidden state of the final token of each  
1283 zero-shot query at the midpoint layer (e.g., layer 16 for the 32-layer Llama3-8B). The modified  
1284 hidden states are then propagated through the subsequent layers, and accuracy as well as TR ratio are  
1285 measured at the final layer.  
12861287 J.2 IDENTIFYING TR AND TL HEADS ON THE MOVIE REVIEW DATASET  
12881289 A key difficulty in identifying TR and TL heads for free-form generation tasks is the unbounded label  
1290 space, since labels are not restricted to a finite set of tokens. To address this, we define the relevant  
1291 label tokens as “positive” and “negative,” reflecting the sentiment nature of the review-generation  
1292 task. Specifically, the TR score of a head is defined as the projection norm of its output onto the  
1293 span of the unembedding vectors of “positive” and “negative” when processing ICL prompts from  
1294 the review dataset. The TL score is defined as the inner product between the head output and the  
1295 difference between the unembeddings of “positive” and “negative,” normalized by its TR score. After  
1296 identifying TR and TL heads, we construct task vectors from their outputs following the procedure in  
1297 Appendix J.1.  
1298

1296 J.3 MATHEMATICAL DETAILS OF THE MEASURES IN [SUBSECTION 4.3](#) AND CALCULATION  
 1297 PROCEDURE  
 1298

1299 1. **Logit Difference** Given a hidden state  $\mathbf{h}$ , we compute  $\text{Ave}_{y' \in \mathbb{Y} \setminus \{y^*\}} (\mathbf{h}^\top (\mathbf{W}_U^{y^*} - \mathbf{W}_U^{y'}))$ , where  
 1300  $\mathbf{W}_U$  is the unembedding matrix,  $y^*$  is the correct label, and  $\mathbb{Y}$  is the demonstration label space.

1301 2. **Subspace Alignment** We compute  $\frac{\mathbf{h}^\top \text{Proj}_{\mathbf{W}_U^{\mathbb{Y}}}^\top \mathbf{h}}{\|\text{Proj}_{\mathbf{W}_U^{\mathbb{Y}}}^\top \mathbf{h}\|_2 \|\mathbf{h}\|_2}$ , which is the cosine similarity between  
 1302  $\text{Proj}_{\mathbf{W}_U^{\mathbb{Y}}}^\top \mathbf{h}$  and  $\mathbf{h}$ .  
 1303

1304 For evaluation, we take the hidden state of the final position at the layer corresponding to 75% of the  
 1305 model depth (e.g., layer 24 in Llama3-8B). Reported metric values are averaged across the first 30  
 1306 ICL prompts of each dataset.  
 1307

1309 K CURATION DETAILS OF THE REVIEW DATASET  
 1310

1312 We use the following template, adapted from [Zhao et al. \(2025\)](#), to prompt ChatGPT-4o to generate  
 1313 movie reviews.

<b>Prompt</b> Compose a concise 30-word movie review that addresses the following four aspects: plot, sound and music, cultural impact, and emotional resonance. Use a positive tone throughout the review. For the plot, comment on its structure or originality. For sound and music, describe how they enhance the storytelling. For cultural impact, mention any relevant social commentary. Finally, highlight how the film resonates emotionally. Ensure the positive tone is consistent throughout and include positive descriptions of the movie.
<b>Samples</b> <i>Inventive non-linear storyline weaves intrigue with clever twists. Soaring vocal melodies heighten the film's emotional arcs. Relevant socioeconomic themes challenge viewers' perceptions thoughtfully and respectfully. Joyful humor interwoven with drama creates comforting resonance.</i>

1326 We use the following template to ask ChatGPT-4o to rate the movie reviews.  
 1327

<b>Prompt</b> Rate the following movie review on a scale of 10. Your rating should be based on two criteria: (1) whether the text is indeed a movie review, and (2) whether it conveys the positive or negative sentiment indicated by the label. Review: Inventive non-linear storyline weaves intrigue with clever twists. Soaring vocal melodies heighten the film's emotional arcs. Relevant socioeconomic themes challenge viewers' perceptions thoughtfully and respectfully. Joyful humor interwoven with drama creates comforting resonance. Sentiment: Positive
<b>Response</b> <i>10</i>

1340  
 1341  
 1342  
 1343  
 1344  
 1345  
 1346  
 1347  
 1348  
 1349

1350  
1351

Table 1: Prompt templates and labels for different datasets.

Dataset	Template	Labels
SST-2	{Sentence} Sentiment: {Label}	positive / negative
SUBJ	{Sentence} Type: {Label}	subjective / objective
TREC	Question: {Sentence} Type: {Label}	abbreviation / entity / description / human / location / number
MR	{Sentence} Sentiment: {Label}	positive / negative
SNLI	The question is: {Premise}? True or maybe or false? The answer is: {Hypothesis} {Label}	true / maybe / false
RTE	The question is: {Premise}? True or false? The answer is: {Hypothesis} {Label}	true / false
CB	The question is: {Premise}? True or maybe or false? The answer is: {Hypothesis} {Label}	true / maybe / false

1361

1362  
1363

Table 2: Mappings used to replace ground-truth labels with numeric symbols.

Dataset	Label Mapping
SST-2	negative/positive → 0/1
SUBJ	objective/subjective → 0/1
MR	negative/positive → 0/1
TREC	abbreviation/entity/description/person/number/location → 0/1/2/3/4/5
SNLI	true/maybe/false → 0/1/2
RTE	true/false → 0/1
CB	true/maybe/false → 0/1/2

1370

1371

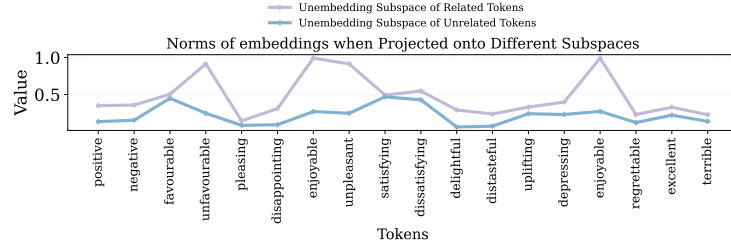
Table 3: Mappings used to flip the demonstration labels for each dataset.

Dataset	Label Mapping
SST-2	negative/positive → positive/negative
SUBJ	objective/subjective → subjective/objective
TREC	abbreviation/entity/description/person/number/location → entity/description/person/number/location/abbreviation
MR	negative/positive → positive/negative
SNLI	true/maybe/false → maybe/false/true
RTE	true/false → false/true
CB	true/maybe/false → maybe/false/true

1379

1380

1381



1382

1383

1384

1385

1386

1387

1388

1389

1390

1391

Figure 19: Norms of Llama3-8B token unembeddings when projected onto the unembedding subspace spanned by semantically related tokens vs semantically unrelated tokens.

1392

1393

1394

1395

1396

1397

1398

1399

1400

1401

1402

1403

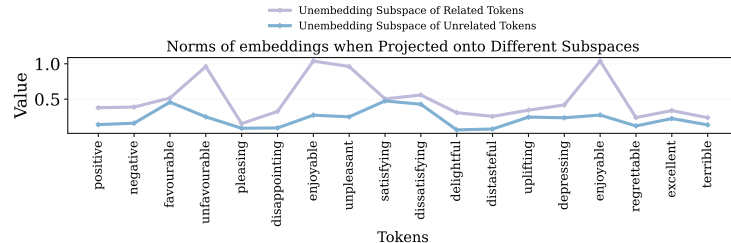
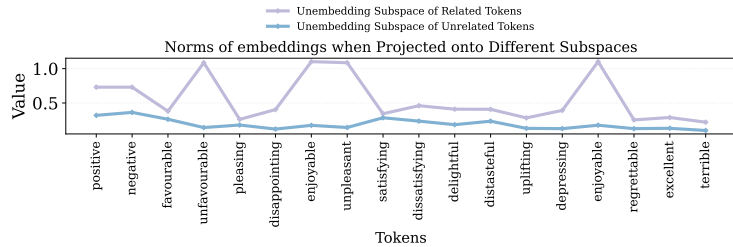


Figure 20: Norms of Llama3.1-8B token unembeddings when projected onto the unembedding subspace spanned by semantically related tokens vs semantically unrelated tokens.

1404  
1405  
1406  
1407  
1408  
1409  
1410  
1411  
1412  
1413



1414  
1415  
Figure 21: Norms of Llama3.2-3B token unembeddings when projected onto the unembedding  
1416  
1417  
1418  
1419  
1420  
1421  
1422  
1423  
1424  
1425  
1426  
1427  
1428  
1429  
1430  
1431  
1432  
1433  
1434  
1435  
1436  
1437  
1438  
1439  
1440  
1441  
1442  
1443  
1444  
1445  
1446  
1447  
1448  
1449  
1450  
1451  
1452  
1453  
1454  
1455  
1456  
1457

Figure 21: Norms of Llama3.2-3B token unembeddings when projected onto the unembedding subspace spanned by semantically related tokens vs semantically unrelated tokens.

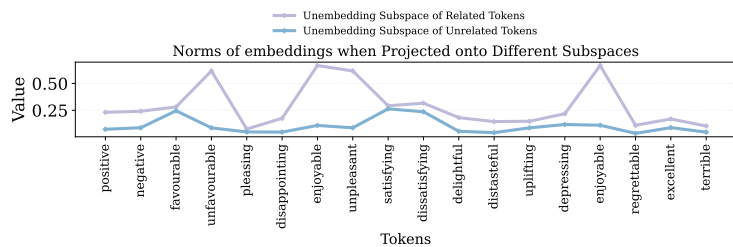


Figure 22: Norms of Qwen2-7B token unembeddings when projected onto the unembedding subspace spanned by semantically related tokens vs semantically unrelated tokens.

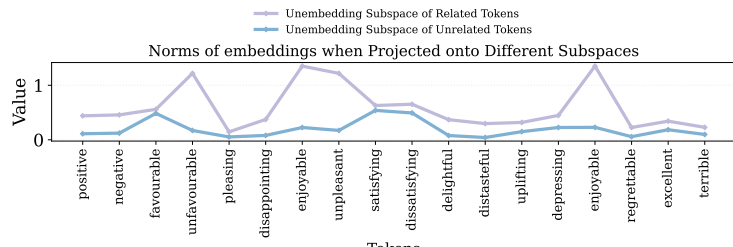


Figure 23: Norms of Qwen2.5-32B token unembeddings when projected onto the unembedding subspace spanned by semantically related tokens vs semantically unrelated tokens.

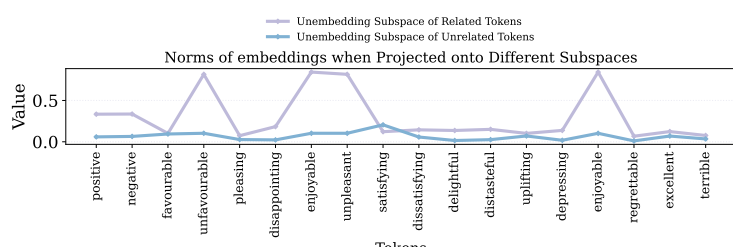
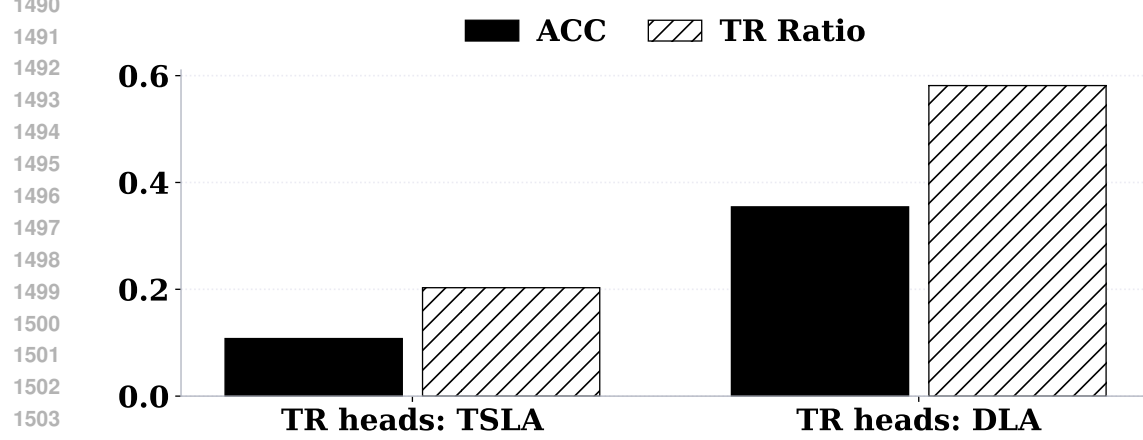
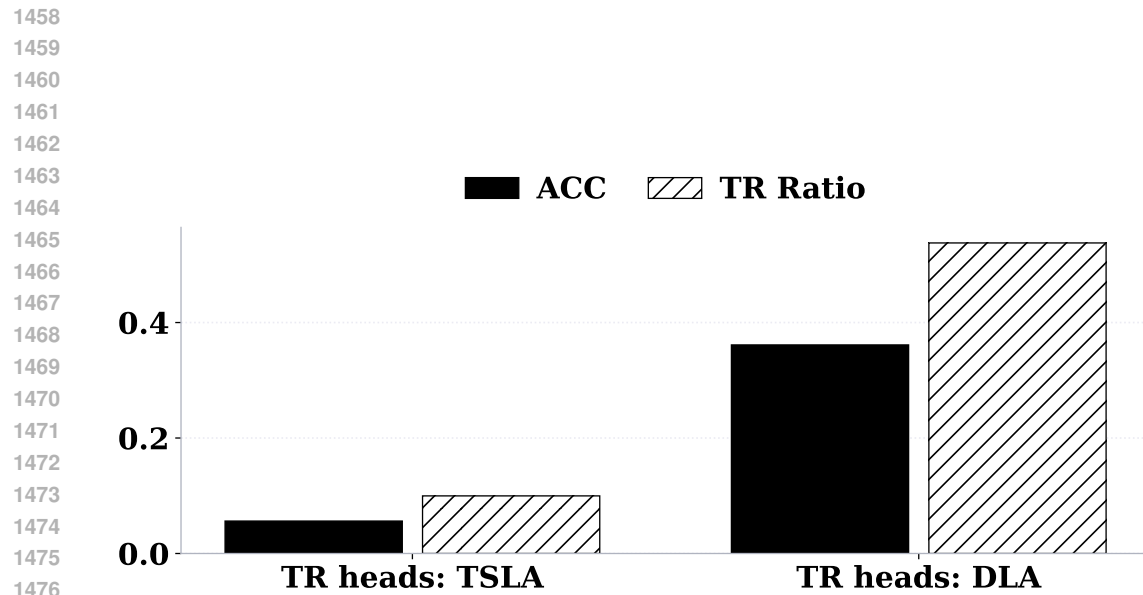


Figure 24: Norms of Yi-34B token unembeddings when projected onto the unembedding subspace spanned by semantically related tokens vs semantically unrelated tokens.



1505      Figure 26: Results on Llama3.1-8B: Effects of ablating top 10% TR heads identified using TSLA  
 1506      or DLA when the SST-2 demonstration labels are shifted from positive/negative to favourable/un-  
 1507      favourable.

1508  
 1509  
 1510  
 1511

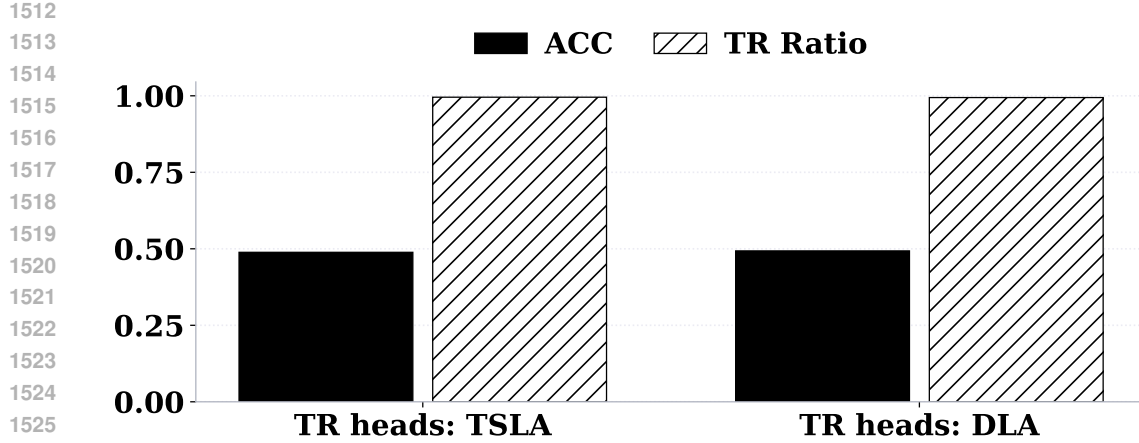


Figure 27: Results on Llama3.2-3B: Effects of ablating top 10% TR heads identified using TSLA or DLA when the SST-2 demonstration labels are shifted from positive/negative to favourable/unfavourable.

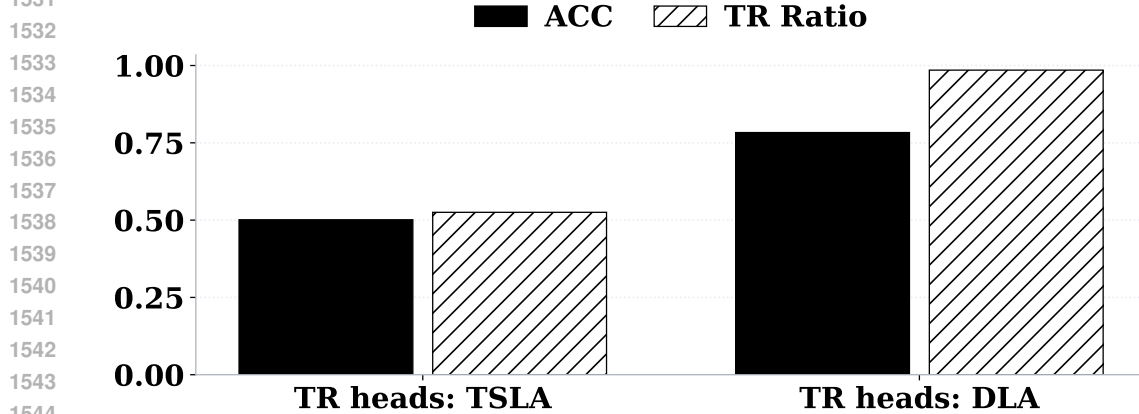


Figure 28: Results on Qwen2-7B: Effects of ablating top 10% TR heads identified using TSLA or DLA when the SST-2 demonstration labels are shifted from positive/negative to favourable/unfavourable.

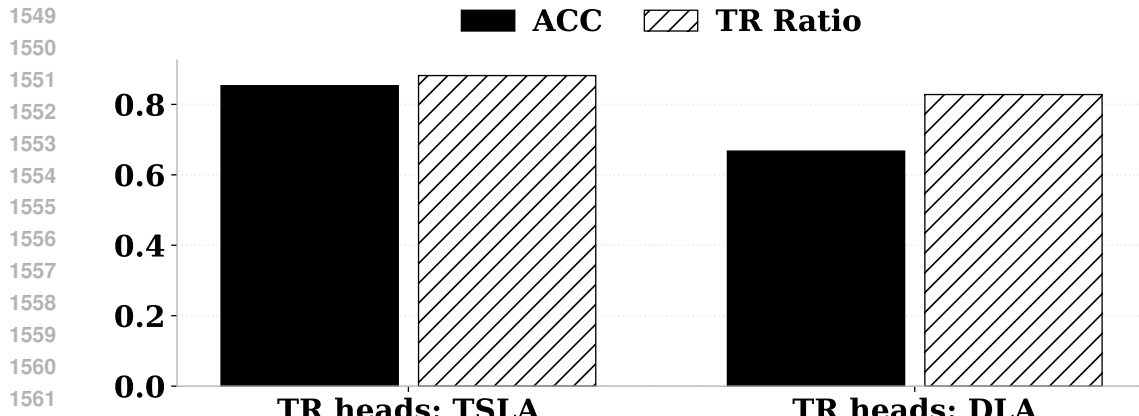


Figure 29: Results on Qwen2.5-32B: Effects of ablating top 10% TR heads identified using TSLA or DLA when the SST-2 demonstration labels are shifted from positive/negative to favourable/unfavourable.

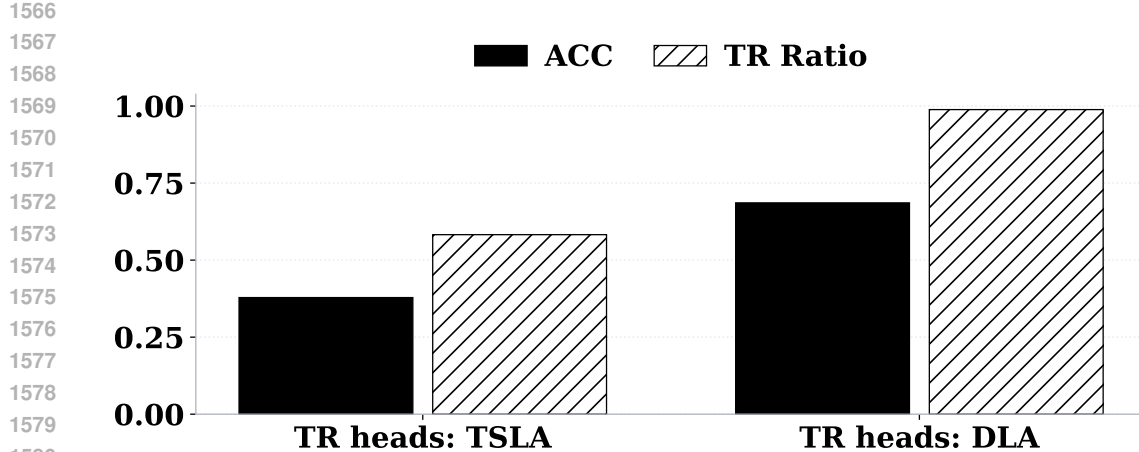


Figure 30: Results on Yi-34B: Effects of ablating top 10% TR heads identified using TSLA or DLA when the SST-2 demonstration labels are shifted from positive/negative to favourable/unfavourable.

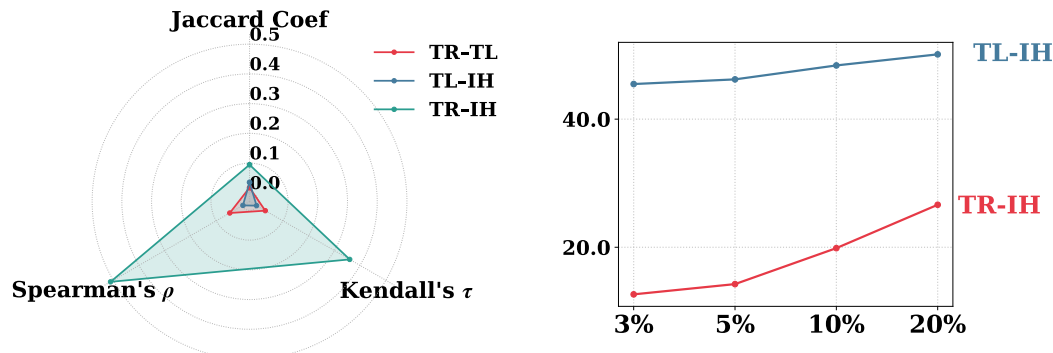


Figure 31: Results of overlap, correlation, and consistency analysis of attention head types averaged across datasets on Llama3.1-8B.

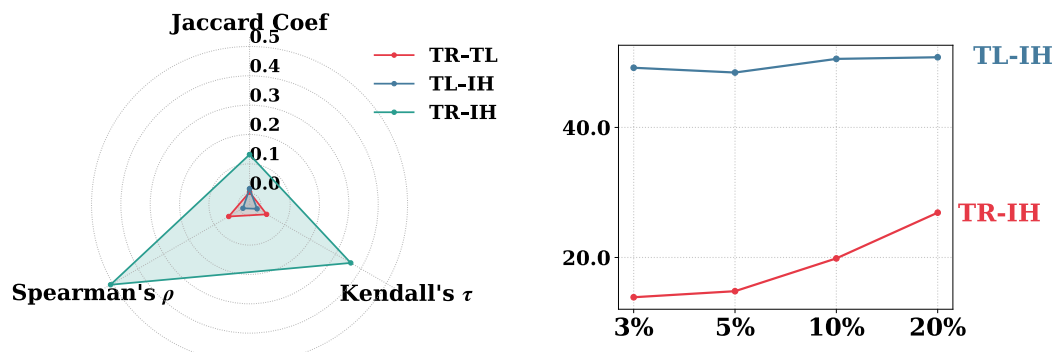


Figure 32: Results of overlap, correlation, and consistency analysis of attention head types averaged across datasets on Llama3.2-3B.

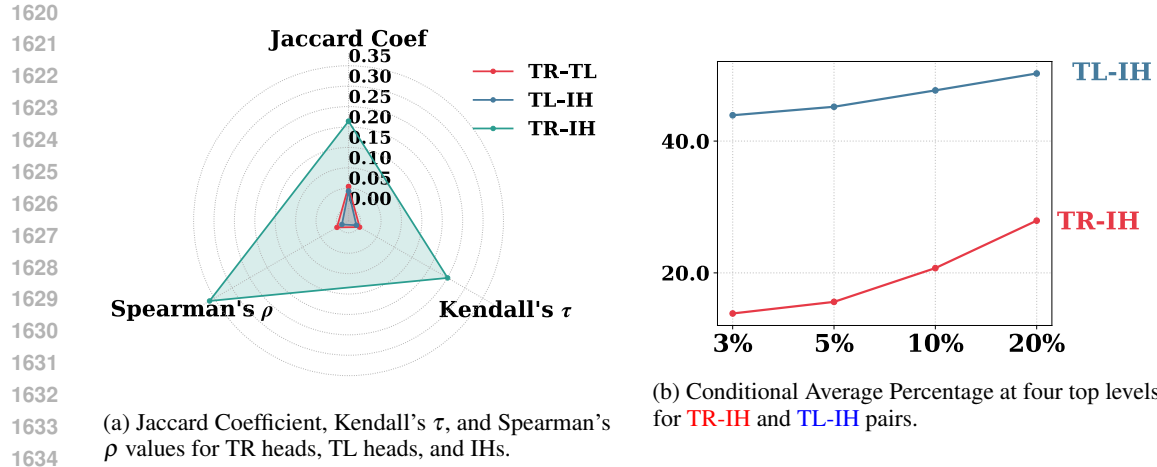
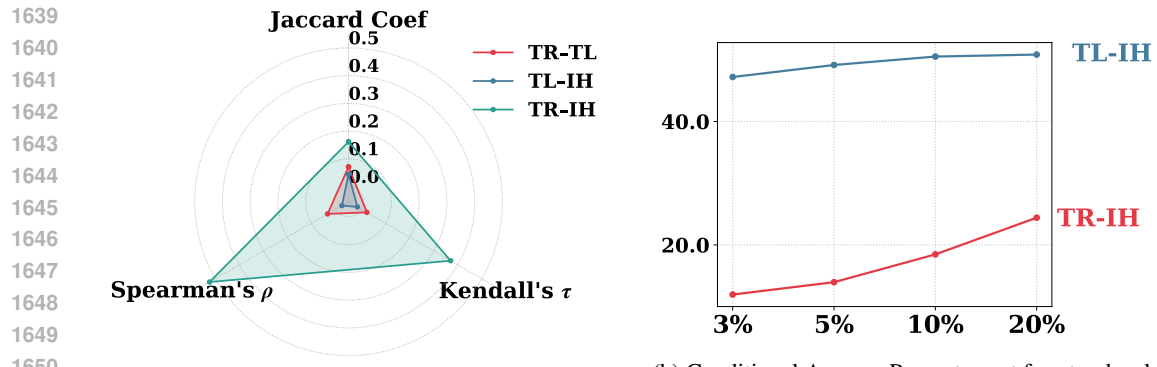
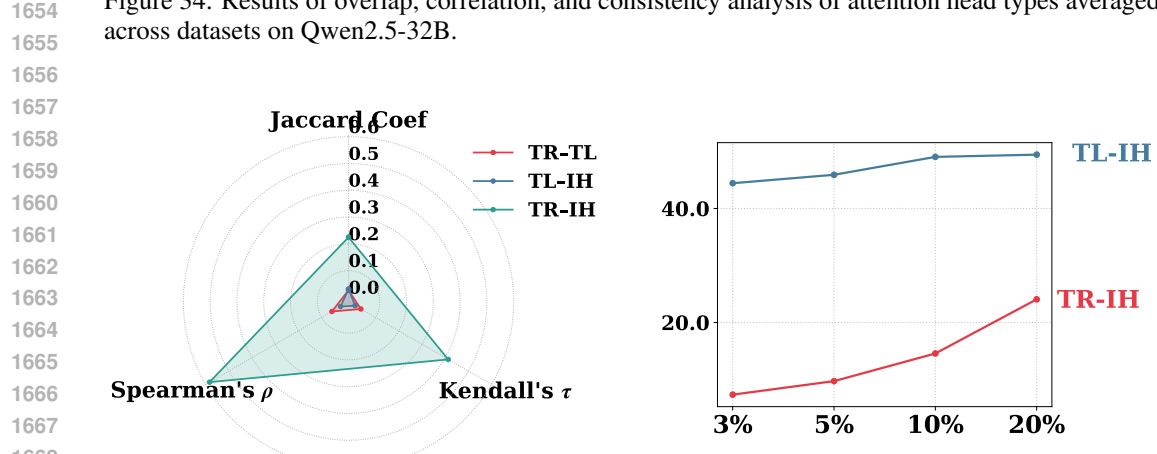


Figure 33: Results of overlap, correlation, and consistency analysis of attention head types averaged across datasets on Qwen2-7B.



(a) Jaccard Coefficient, Kendall's  $\tau$ , and Spearman's  $\rho$  values for TR-IH and TL-IH pairs.



(a) Jaccard Coefficient, Kendall's  $\tau$ , and Spearman's  $\rho$  values for TR heads, TL heads, and IHs.

Figure 35: Results of overlap, correlation, and consistency analysis of attention head types averaged across datasets on Yi-34B.

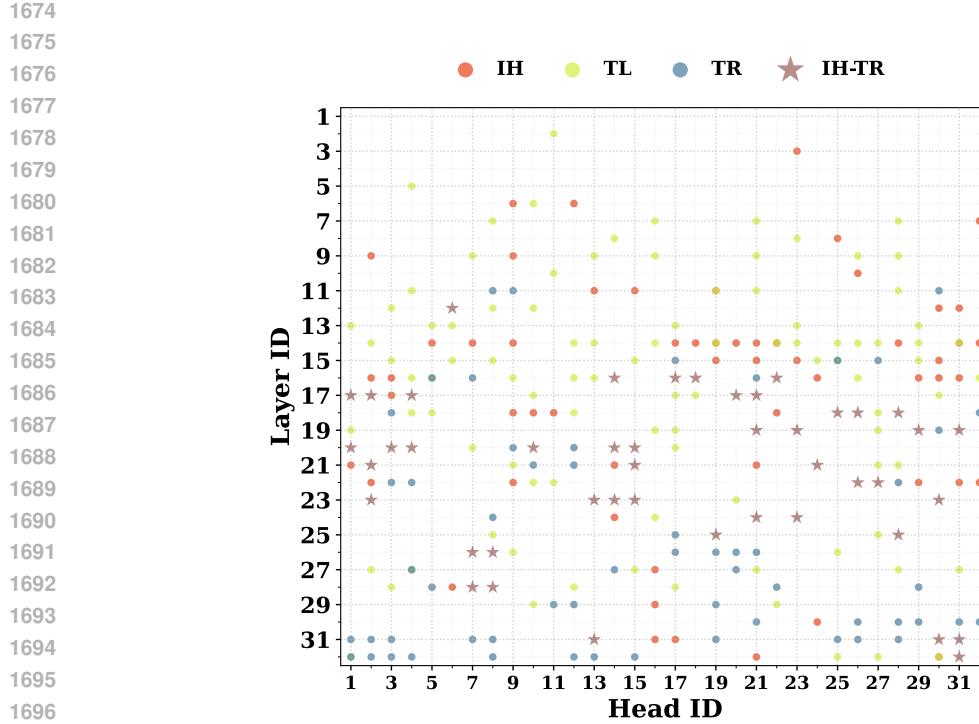


Figure 36: Distribution of the top 10% TR heads, TL heads, and IHs across layers for the SST-2 dataset on Llama3.1-8B.

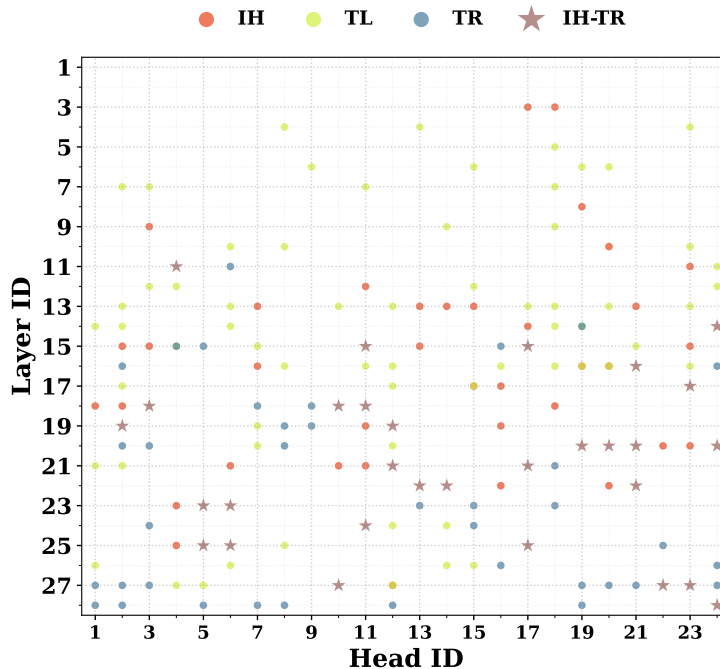


Figure 37: Distribution of the top 10% TR heads, TL heads, and IHs across layers for the SST-2 dataset on Llama3.2-3B.

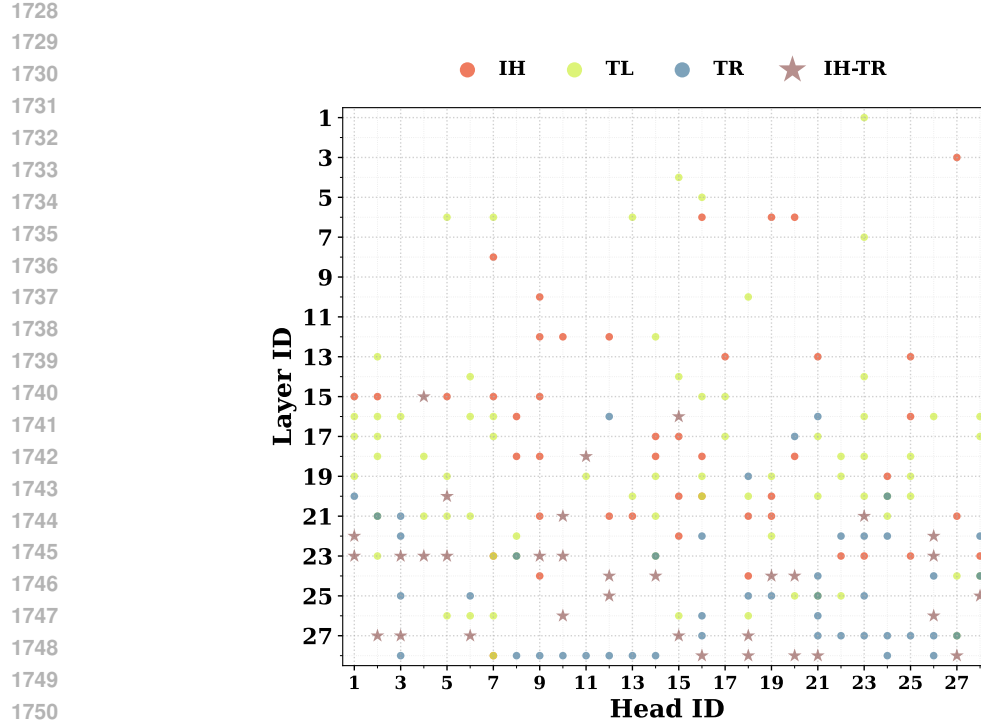


Figure 38: Distribution of the top 10% TR heads, TL heads, and IHs across layers for the SST-2 dataset on Qwen2-7B.

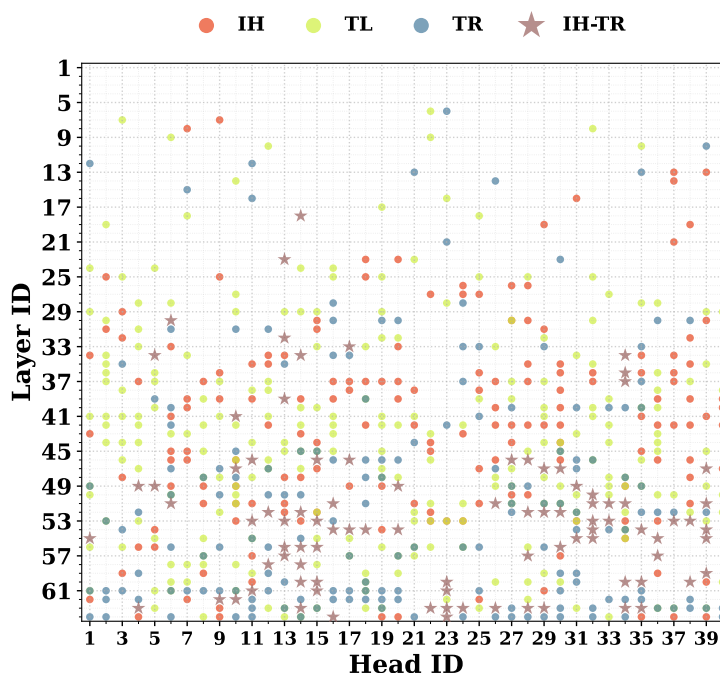


Figure 39: Distribution of the top 10% TR heads, TL heads, and IHs across layers for the SST-2 dataset on Qwen2.5-32B.

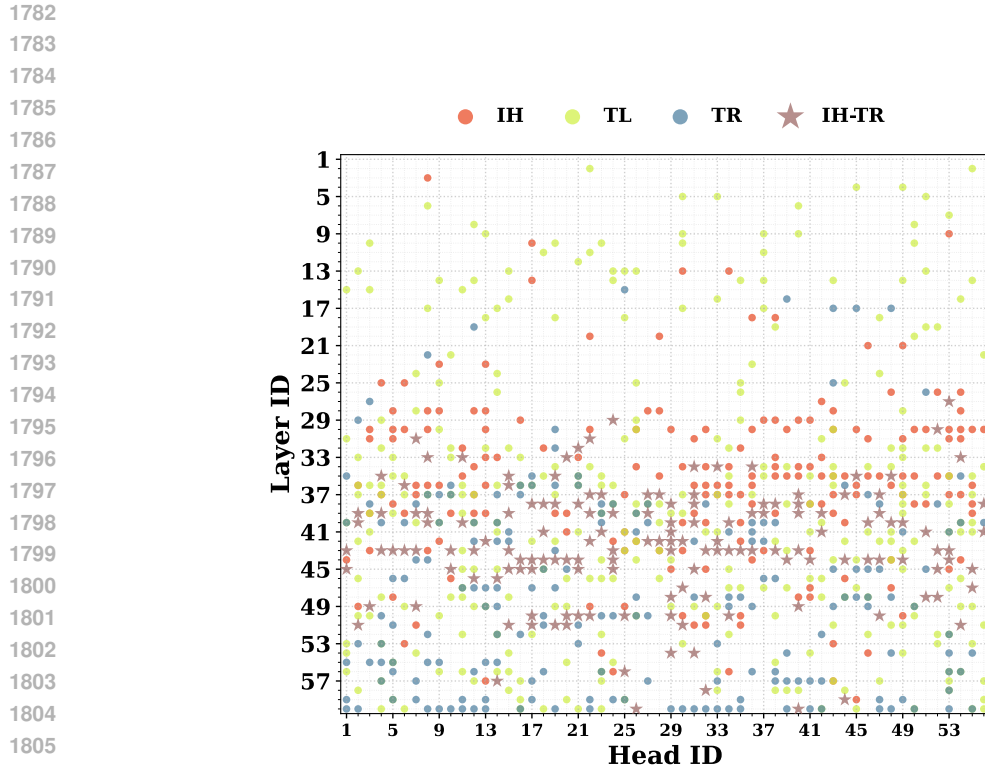


Figure 40: Distribution of the top 10% TR heads, TL heads, and IHs across layers for the SST-2 dataset on Yi-34B.

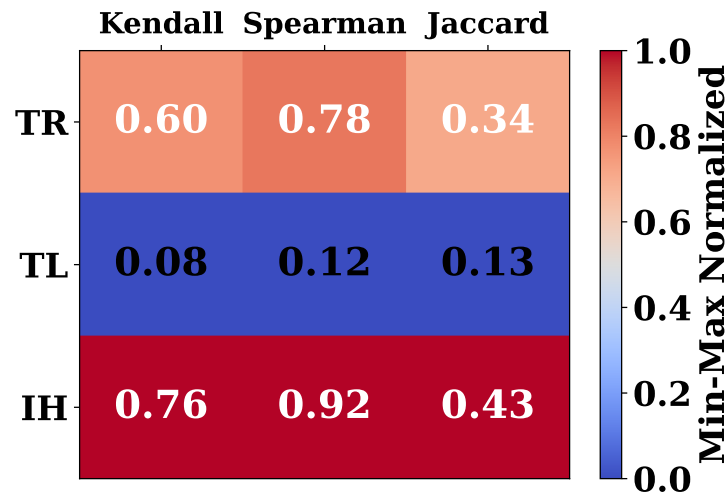


Figure 41: Overlap and correlation of the TR heads, TL heads, and IHs across datasets on Llama3.1-8B.

1836

1837

1838

1839

1840

1841

1842

1843

1844

1845

1846

1847

1848

1849

1850

1851

1852

1853

1854

1855

1856

1857

Figure 42: Overlap and correlation of the TR heads, TL heads, and IHs across datasets on Llama3.2-3B.

1859

1860

1861

1862

1863

1864

1865

1866

1867

1868

1869

1870

1871

1872

1873

1874

1875

1876

1877

1878

1879

1880

1881

1882

1883

1884

1885

1886

1887

1888

1889

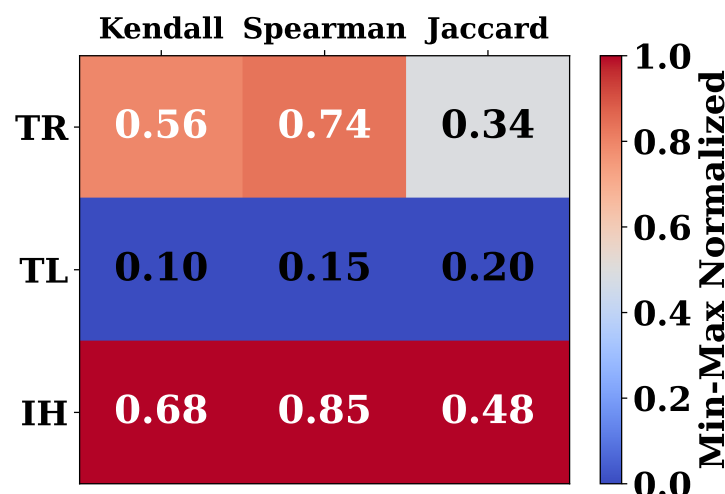
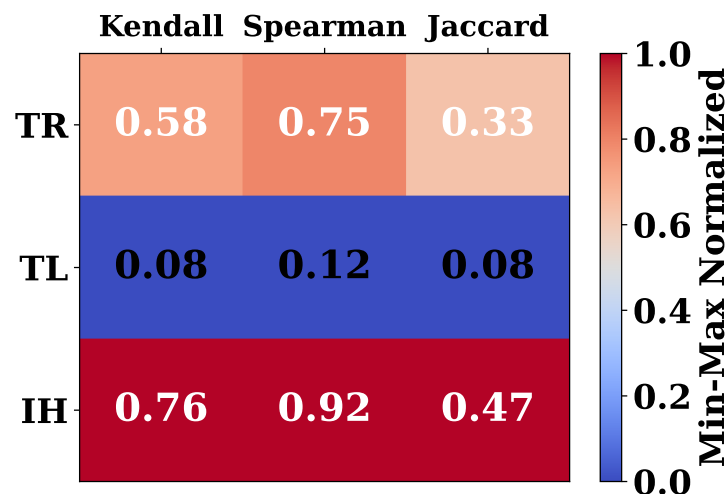


Figure 43: Overlap and correlation of the TR heads, TL heads, and IHs across datasets on Qwen2-7B.

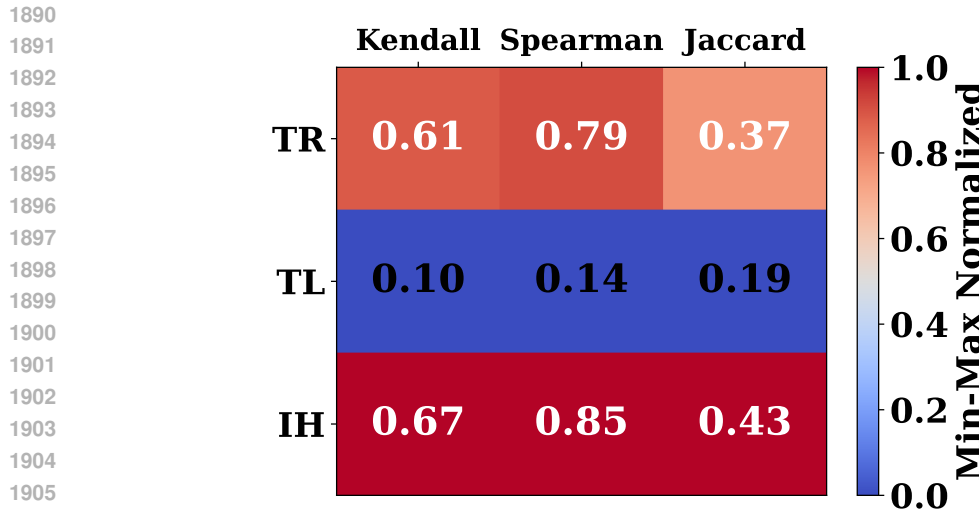


Figure 44: Overlap and correlation of the TR heads, TL heads, and IHs across datasets on Qwen2.5-32B.

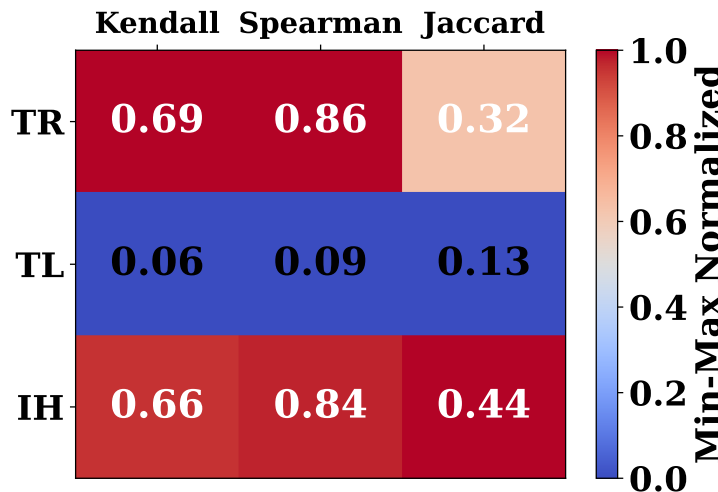


Figure 45: Overlap and correlation of the TR heads, TL heads, and IHs across datasets on Yi-34B.

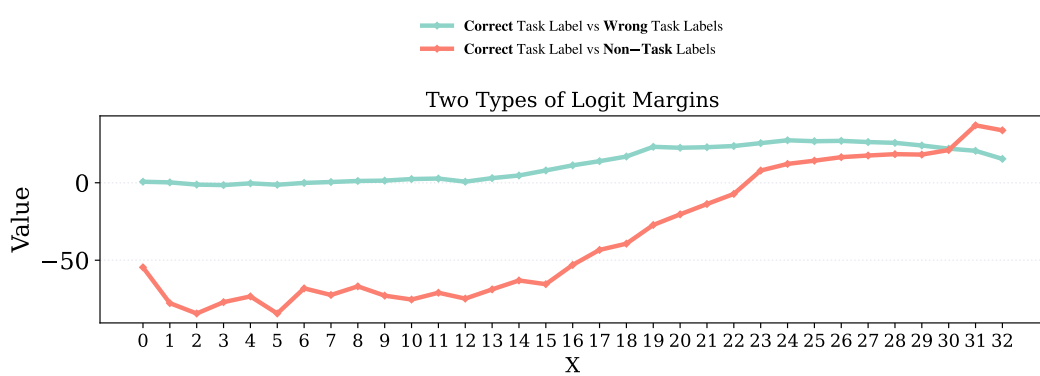


Figure 46: Dynamics of logit margin between 1) correct and incorrect task labels and 2) task labels and task-irrelevant labels across layers on Llama3-8B.

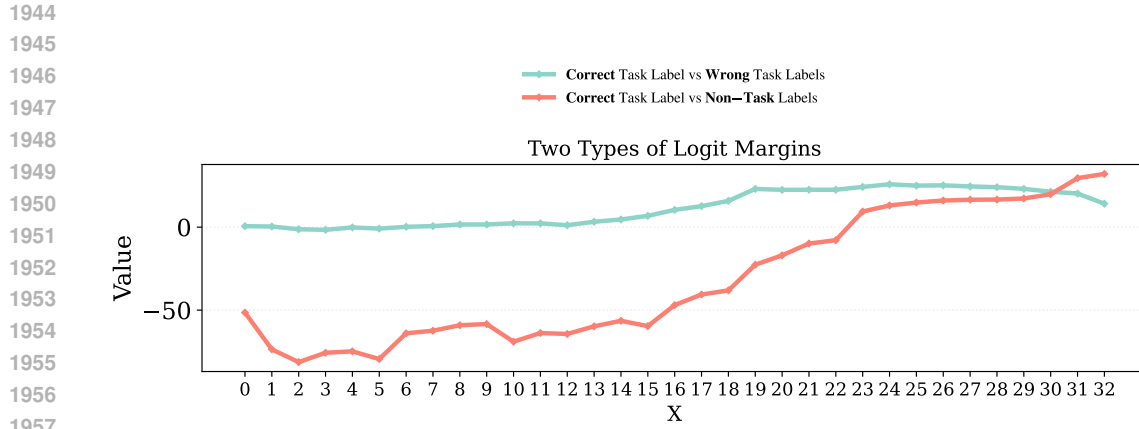


Figure 47: Dynamics of logit margin between 1) correct and incorrect task labels and 2) task labels and task-irrelevant labels across layers on Llama3.1-8B.

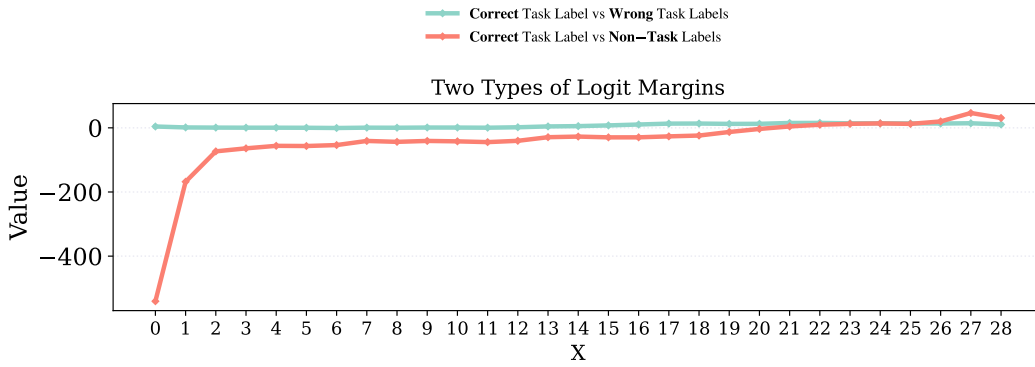


Figure 48: Dynamics of logit margin between 1) correct and incorrect task labels and 2) task labels and task-irrelevant labels across layers on Llama3.2-3B.

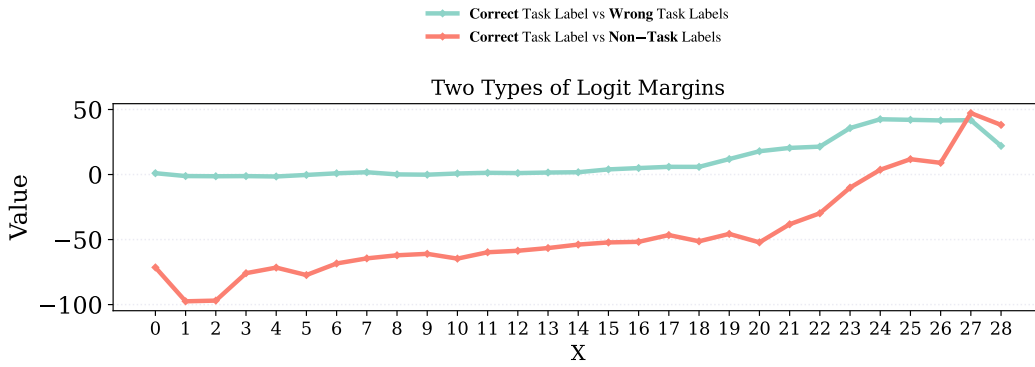


Figure 49: Dynamics of logit margin between 1) correct and incorrect task labels and 2) task labels and task-irrelevant labels across layers on Qwen2-7B.

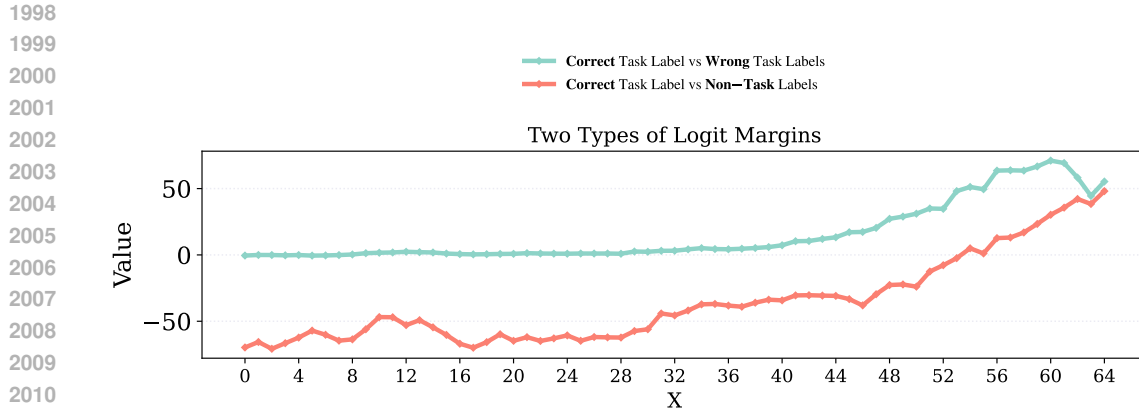


Figure 50: Dynamics of logit margin between 1) correct and incorrect task labels and 2) task labels and task-irrelevant labels across layers on Qwen2.5-32B.

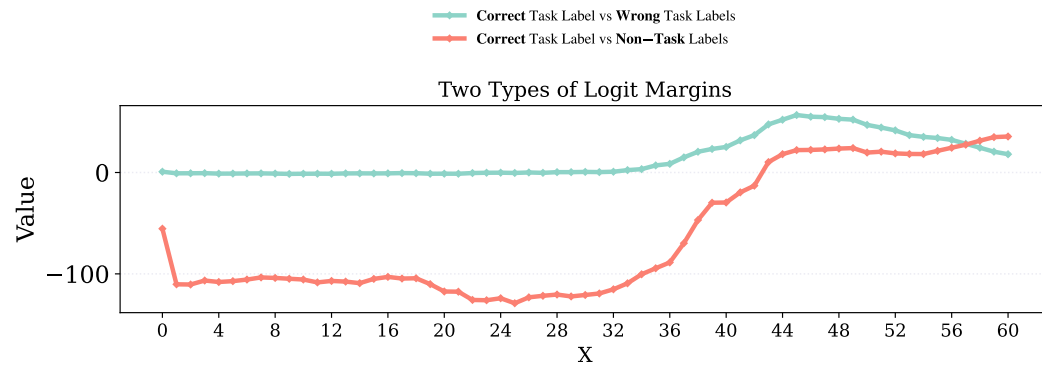


Figure 51: Dynamics of logit margin between 1) correct and incorrect task labels and 2) task labels and task-irrelevant labels across layers on Yi-34B.

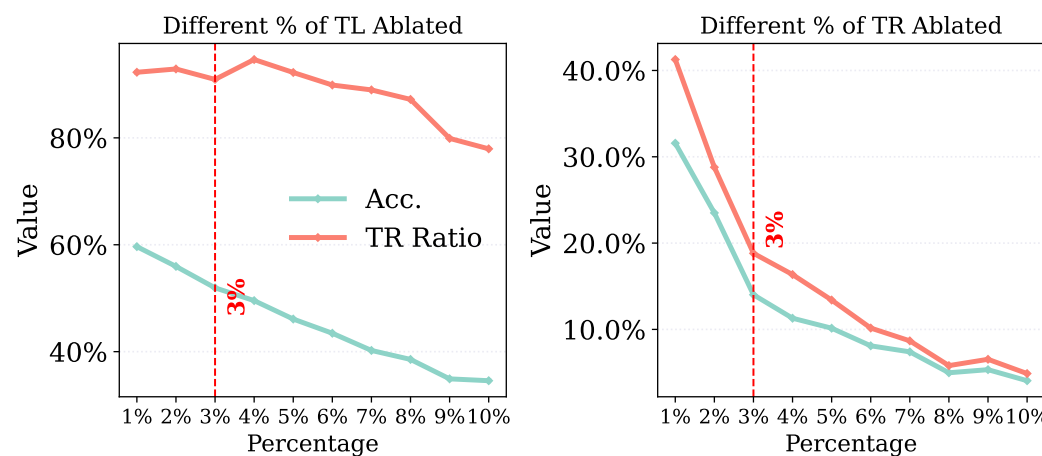


Figure 52: Dataset average accuracy and TR ratio resulted from ablating TL and TR heads at top percentage levels from 1% to 10%.

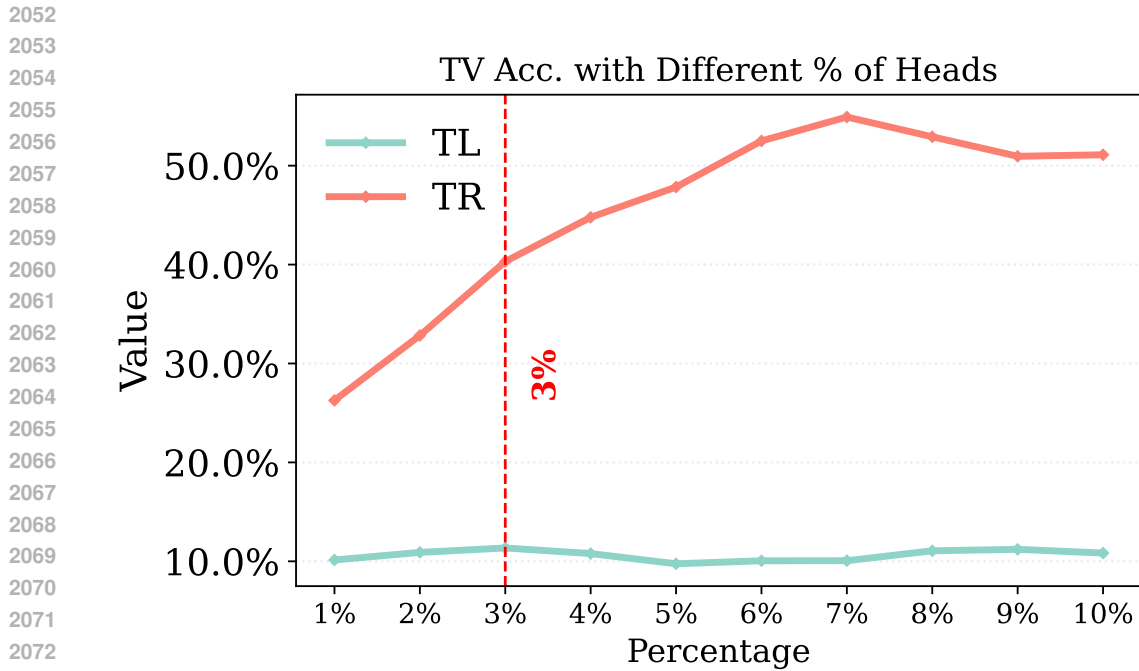


Figure 53: Dataset average accuracy and TR ratio resulted from using the outputs TL and TR heads at top percentage levels from 1% to 10% as task vectors.

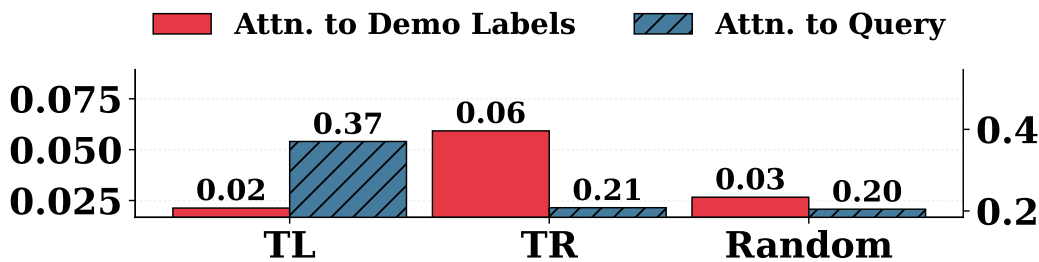


Figure 54: Dataset average cumulative attention weights assigned by the top TL, TR, and random heads of Llama3.1-8B to the demonstration labels and query tokens.

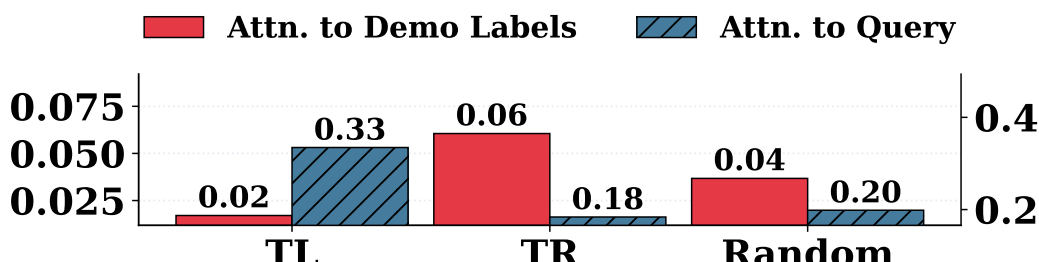


Figure 55: Dataset average cumulative attention weights assigned by the top TL, TR, and random heads of Llama3.2-3B to the demonstration labels and query tokens.

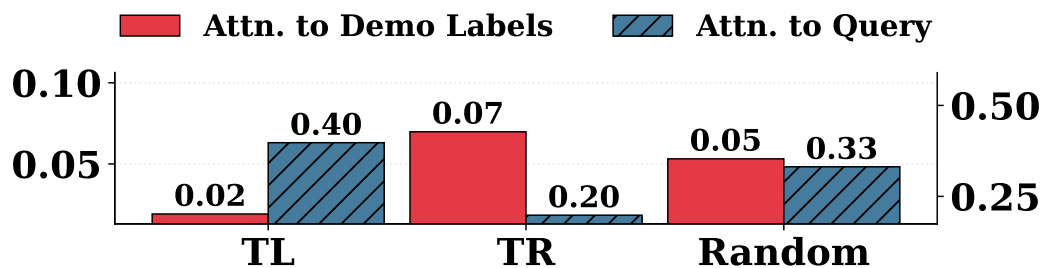


Figure 56: Dataset average cumulative attention weights assigned by the top TL, TR, and random heads of Qwen2-7B to the demonstration labels and query tokens.

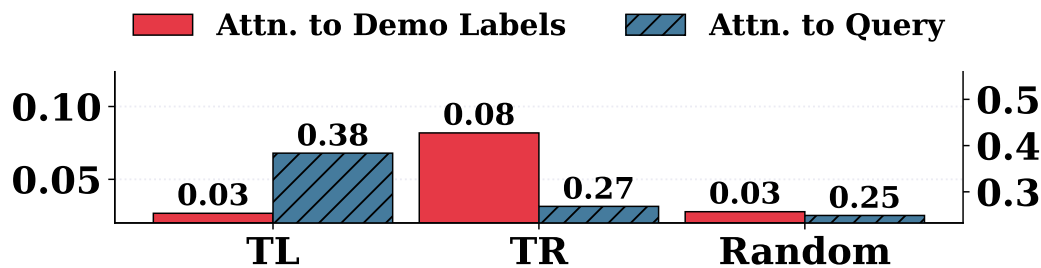


Figure 57: Dataset average cumulative attention weights assigned by the top TL, TR, and random heads of Qwen2.5-32B to the demonstration labels and query tokens.

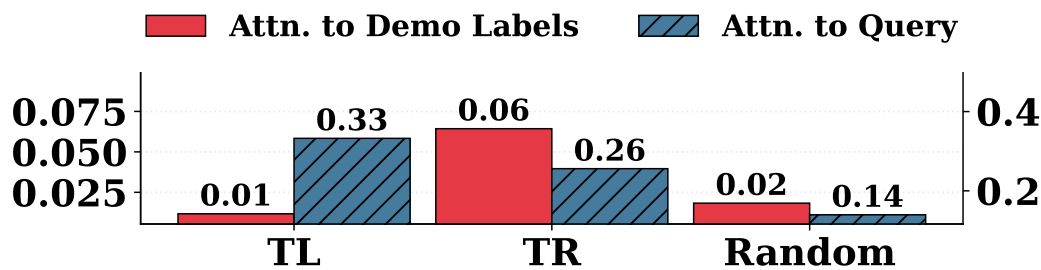


Figure 58: Dataset average cumulative attention weights assigned by the top TL, TR, and random heads of Yi-34B to the demonstration labels and query tokens.

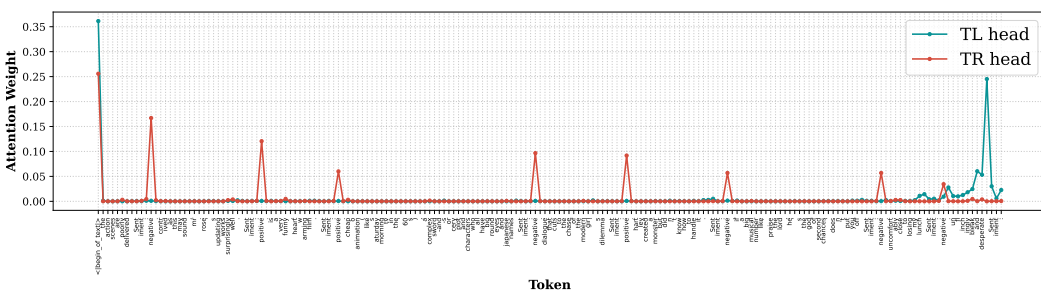


Figure 59: Attention distributions of the top-1 Llama3-8B TL and TR heads on SST-2 over the ICL prompt formed using the second test query of SST-2.

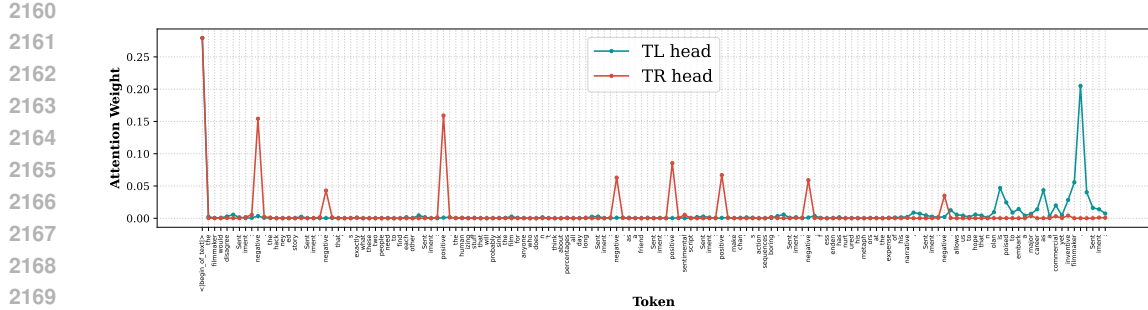


Figure 60: Attention distributions of the top-1 Llama3-8B TL and TR heads on SST-2 over the ICL prompt formed using the test query of SST-2.

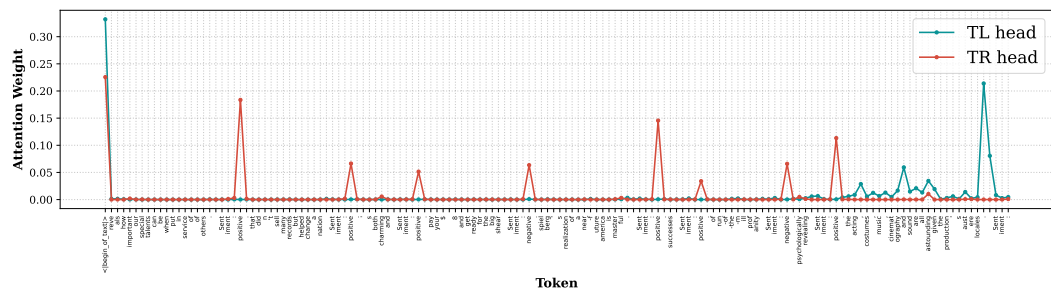


Figure 61: Attention distributions of the top-1 Llama3-8B TL and TR heads on SST-2 over the ICL prompt formed using the fourth test query of SST-2.

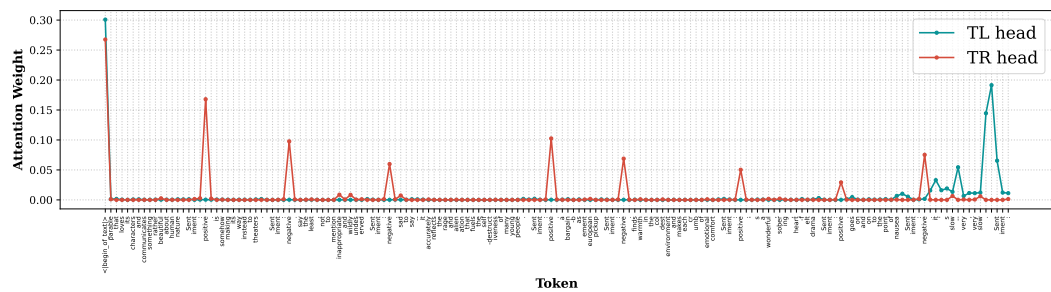


Figure 62: Attention distributions of the top-1 Llama3-8B TL and TR heads on SST-2 over the ICL prompt formed using the fifth test query of SST-2.

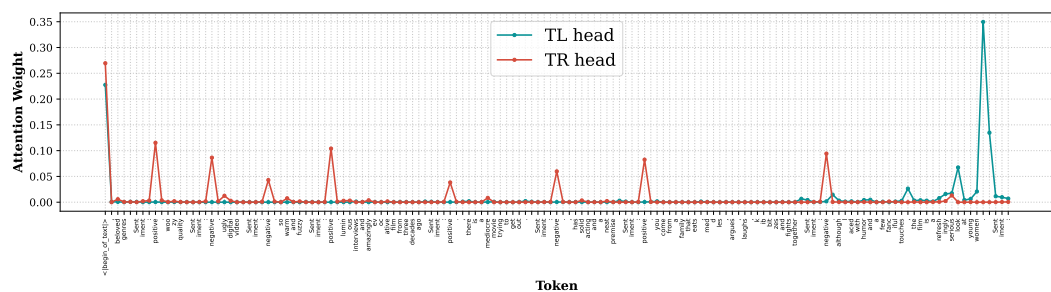


Figure 63: Attention distributions of the top-1 Llama3-8B TL and TR heads on SST-2 over the ICL prompt formed using the sixth test query of SST-2.

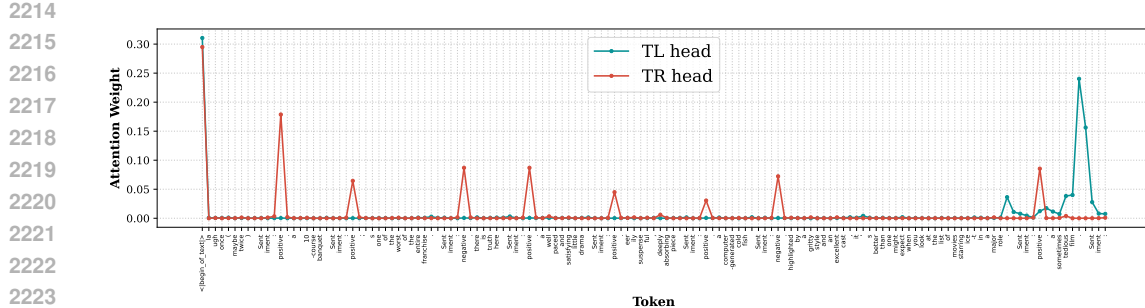


Figure 64: Attention distributions of the top-1 Llama3-8B TL and TR heads on SST-2 over the ICL prompt formed using the seventh test query of SST-2.

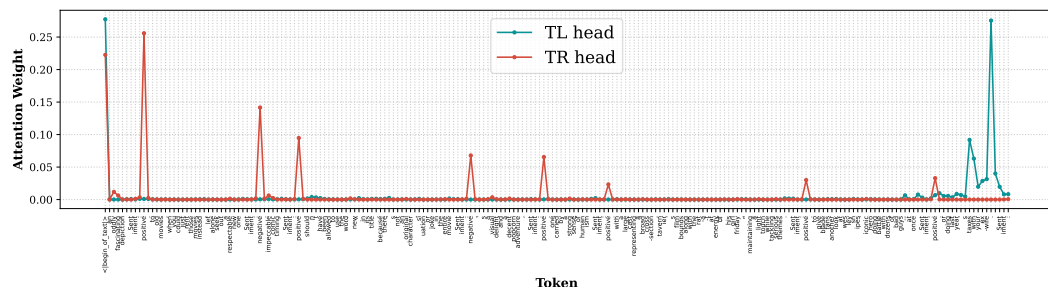


Figure 65: Attention distributions of the top-1 Llama3-8B TL and TR heads on SST-2 over the ICL prompt formed using the eighth test query of SST-2.

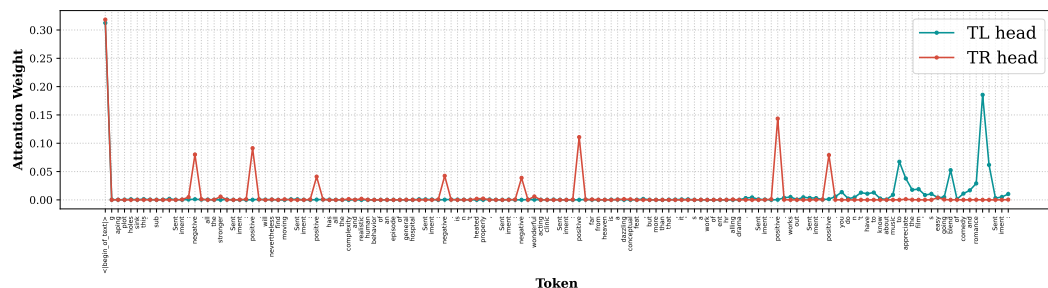


Figure 66: Attention distributions of the top-1 Llama3-8B TL and TR heads on SST-2 over the ICL prompt formed using the ninth test query of SST-2.

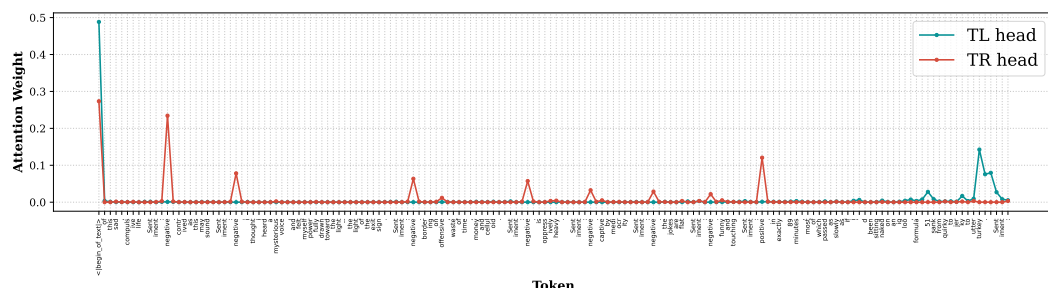


Figure 67: Attention distributions of the top-1 Llama3-8B TL and TR heads on SST-2 over the ICL prompt formed using the tenth test query of SST-2.

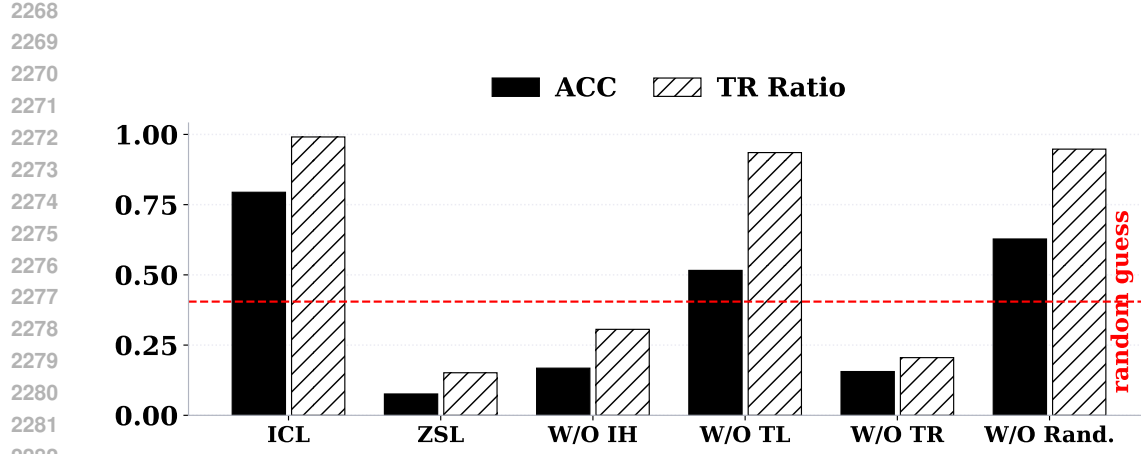


Figure 68: Effects of ablating the top 3% of TR, TL, and IH heads across datasets on Llama3.1-8B.

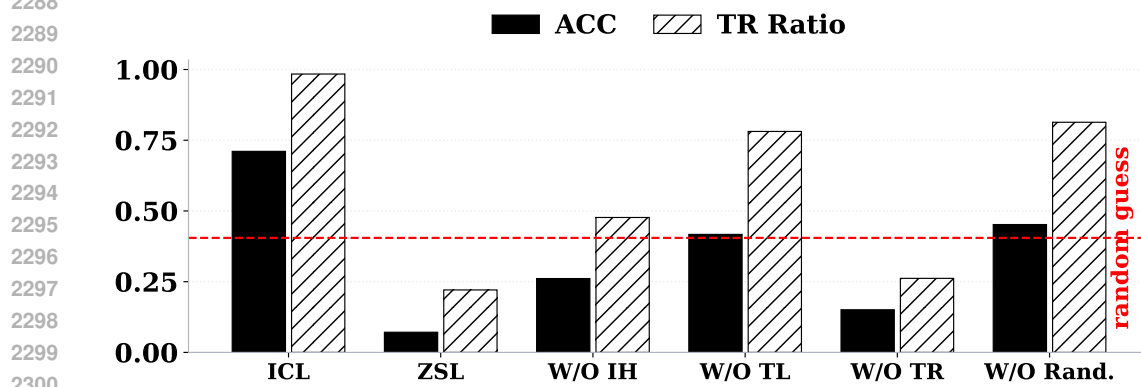


Figure 69: Effects of ablating the top 3% of TR, TL, and IH heads across datasets on Llama3.2-3B.

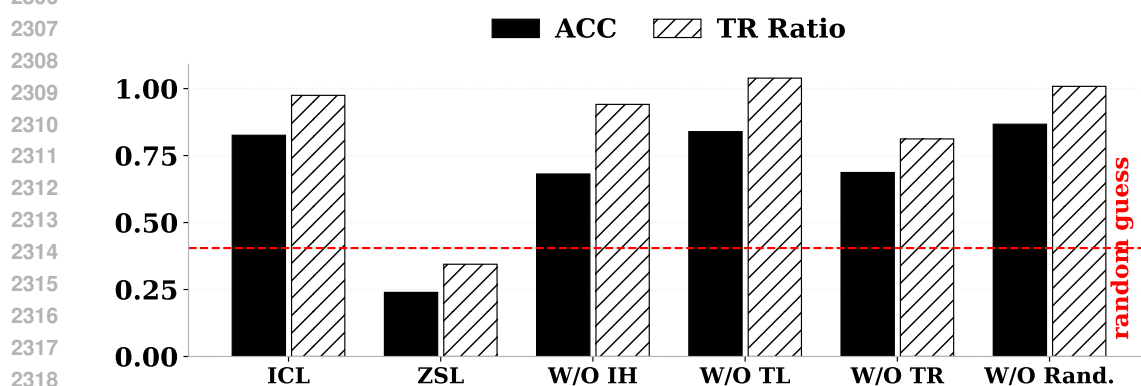


Figure 70: Effects of ablating the top 3% of TR, TL, and IH heads across datasets on Qwen2-7B.

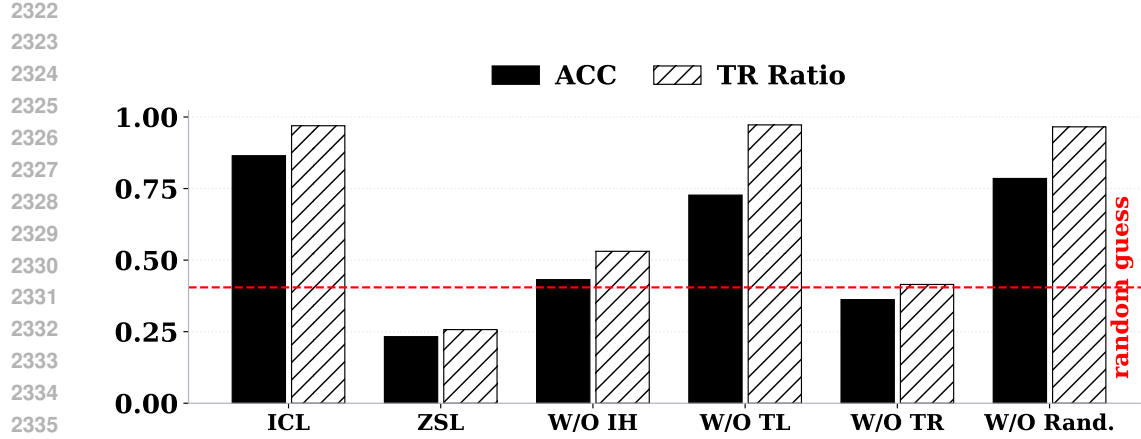


Figure 71: Effects of ablating the top 3% of TR, TL, and IH heads across datasets on Qwen2.5-32B.

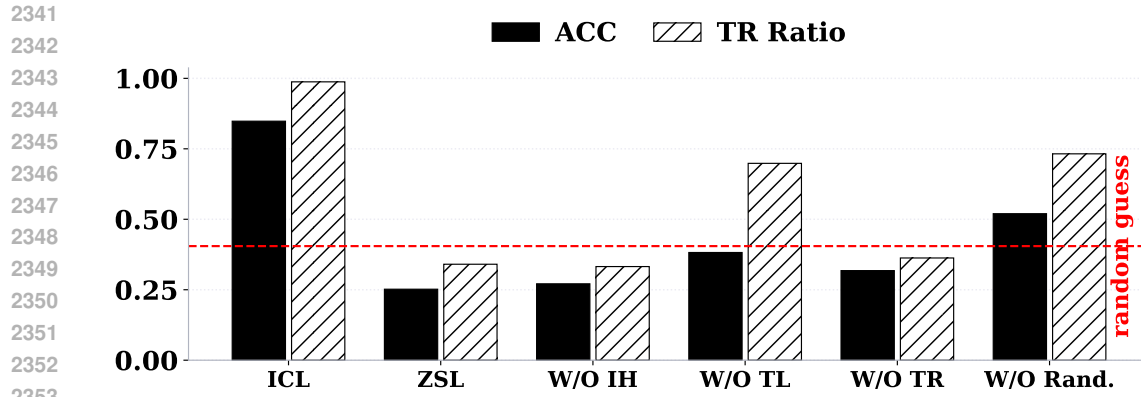


Figure 72: Effects of ablating the top 3% of TR, TL, and IH heads across datasets on Yi-34B.

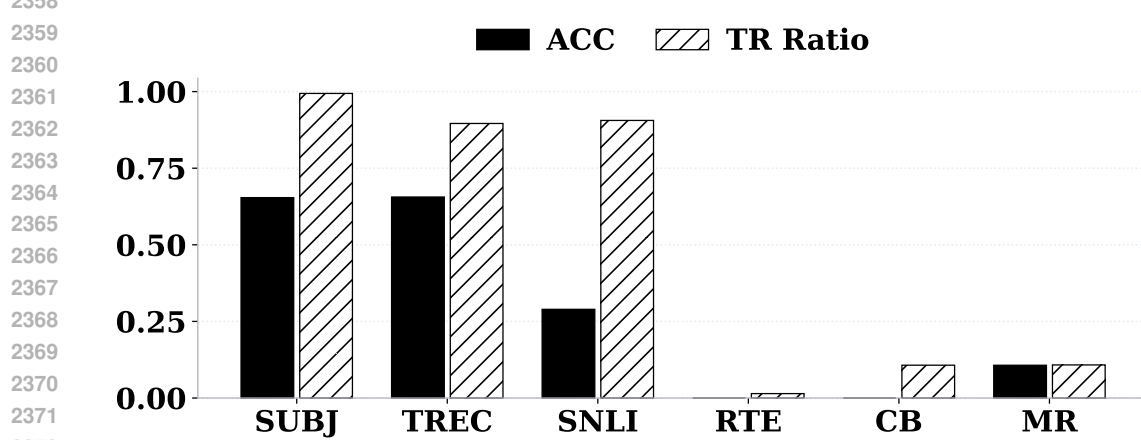


Figure 73: Effects of ablating TR heads identified on SST-2 when transferred to other datasets using Llama3-8B.

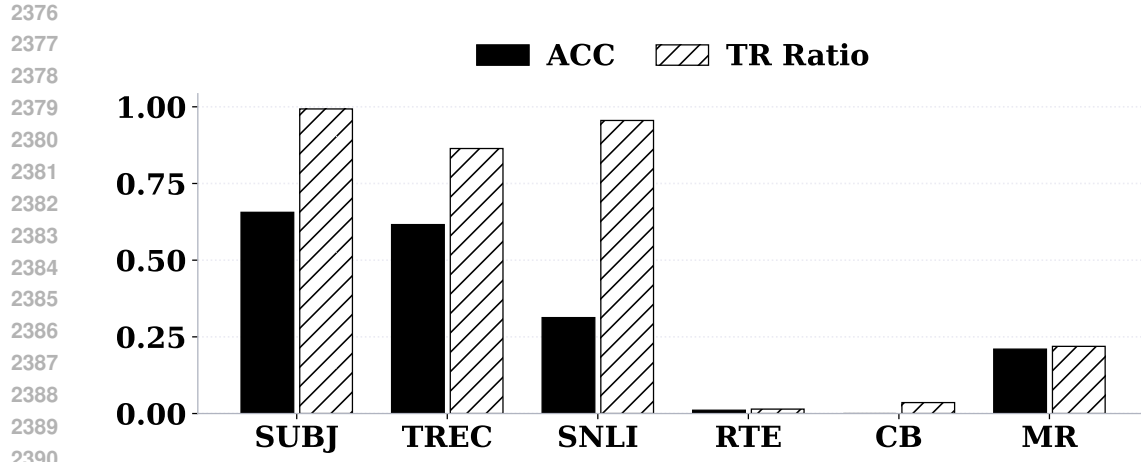


Figure 74: Effects of ablating TR heads identified on SST-2 when transferred to other datasets using Llama3.1-8B.

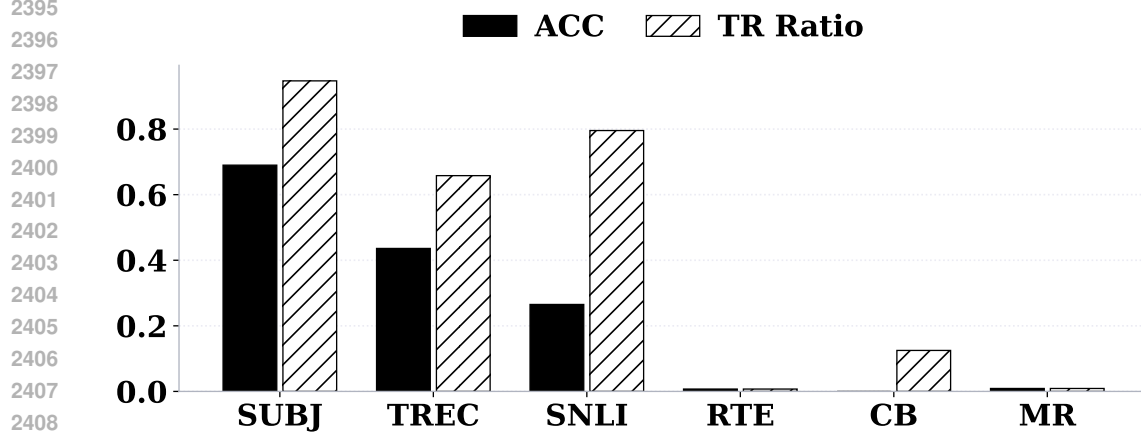


Figure 75: Effects of ablating TR heads identified on SST-2 when transferred to other datasets using Llama3.2-3B.

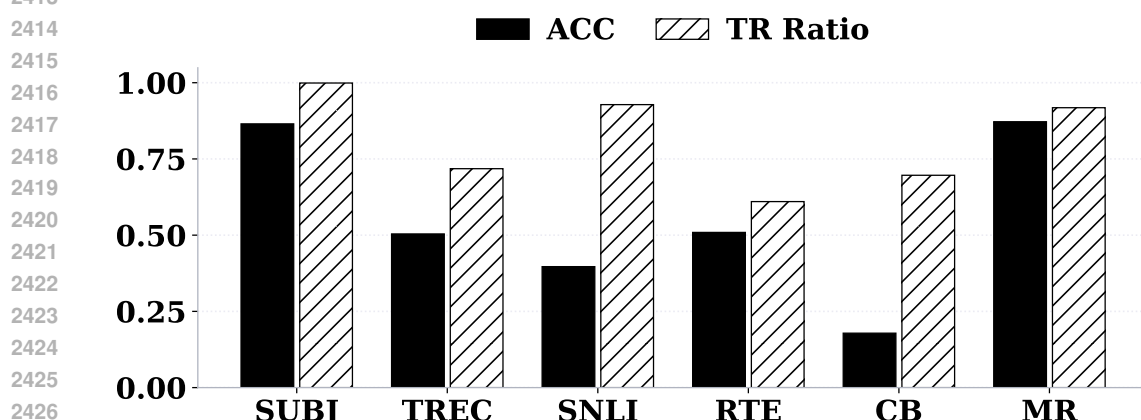


Figure 76: Effects of ablating TR heads identified on SST-2 when transferred to other datasets using Qwen2-7B.

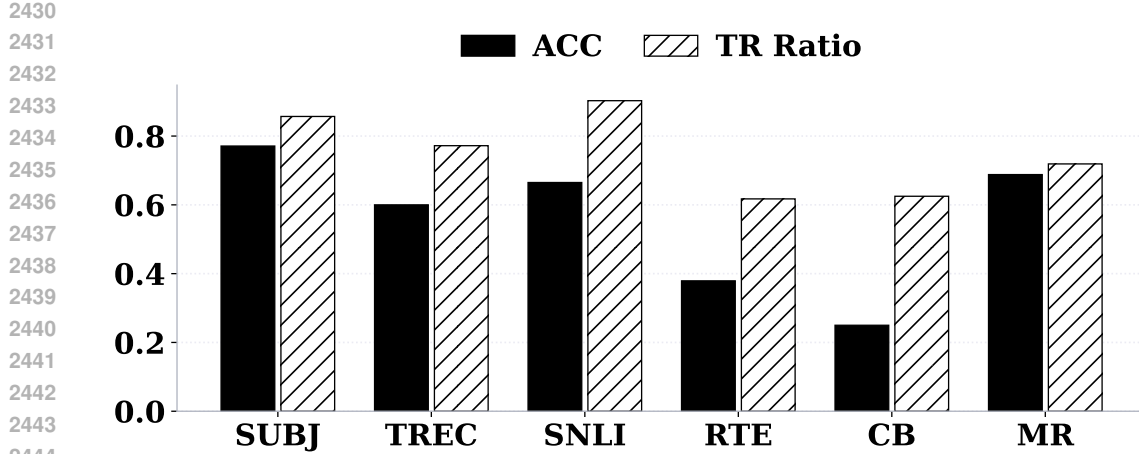


Figure 77: Effects of ablating TR heads identified on SST-2 when transferred to other datasets using Qwen2.5-32B.

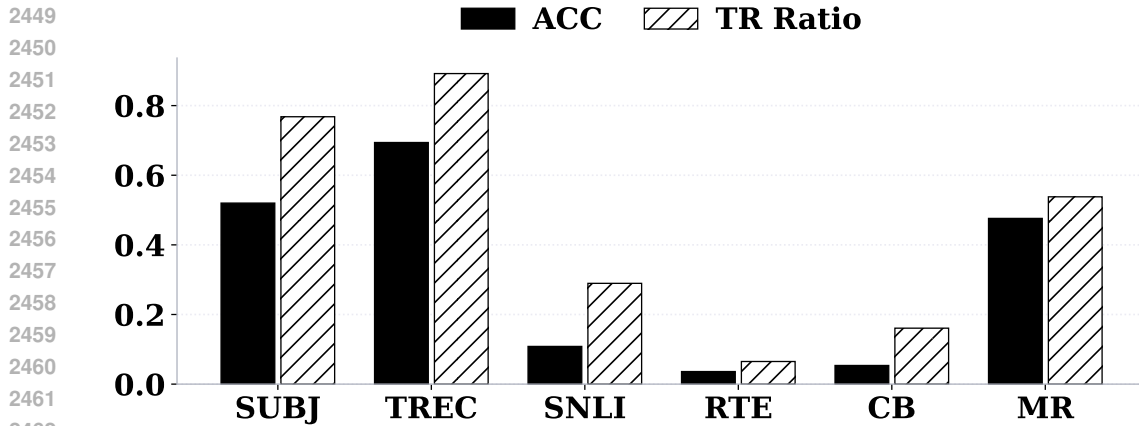


Figure 78: Effects of ablating TR heads identified on SST-2 when transferred to other datasets using Yi-34B.



Figure 79: Effects of ablating TR and TL heads under perturbed ICL inputs on Llama3.1-8B.

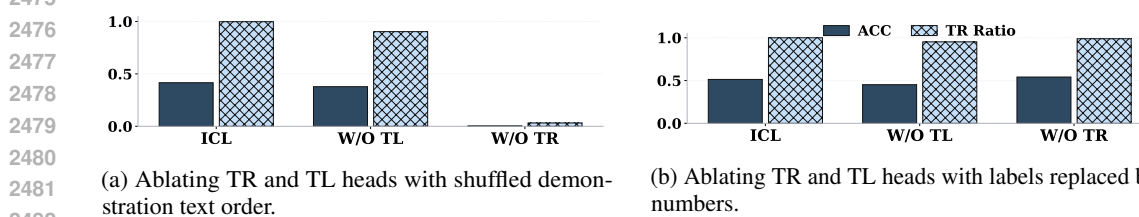
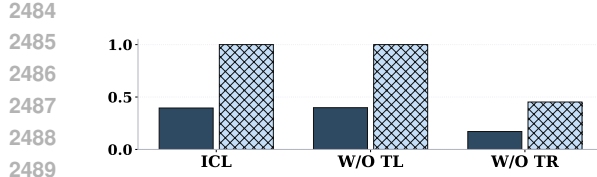
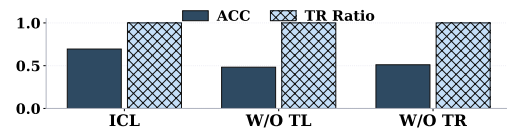


Figure 80: Effects of ablating TR and TL heads under perturbed ICL inputs on Llama3.2-3B.

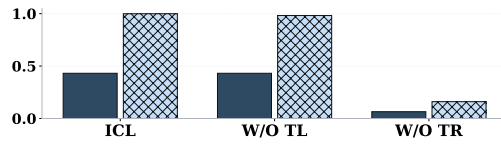


(a) Ablating TR and TL heads with shuffled demonstration text order.

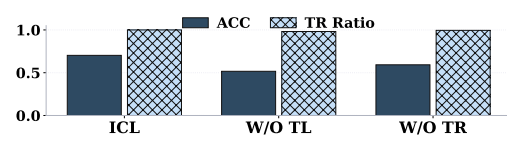


(b) Ablating TR and TL heads with labels replaced by numbers.

Figure 81: Effects of ablating TR and TL heads under perturbed ICL inputs on Qwen2-7B.

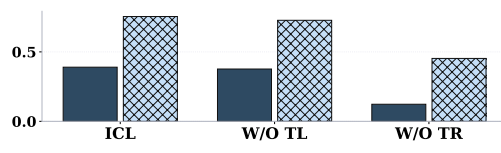


(a) Ablating TR and TL heads with shuffled demonstration text order.

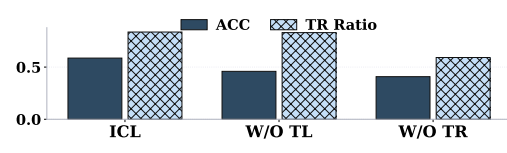


(b) Ablating TR and TL heads with labels replaced by numbers.

Figure 82: Effects of ablating TR and TL heads under perturbed ICL inputs on Qwen2.5-32B.



(a) Ablating TR and TL heads with shuffled demonstration text order.



(b) Ablating TR and TL heads with labels replaced by numbers.

Figure 83: Effects of ablating TR and TL heads under perturbed ICL inputs on Yi-34B.

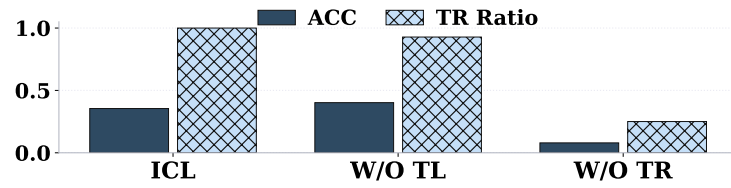


Figure 84: Effects of ablating TR and TL heads on Llama3-8B when demonstration labels are flipped.

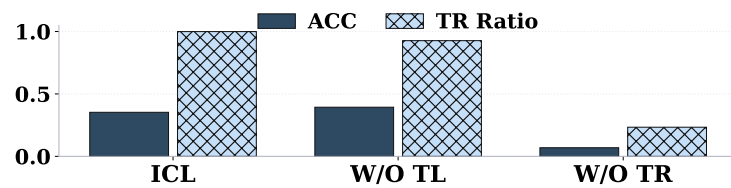


Figure 85: Effects of ablating TR and TL heads on Llama3.1-8B when demonstration labels are flipped.

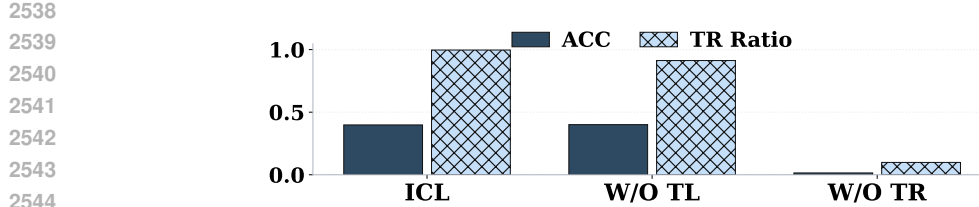


Figure 86: Effects of ablating TR and TL heads on Llama3.2-3B when demonstration labels are flipped.

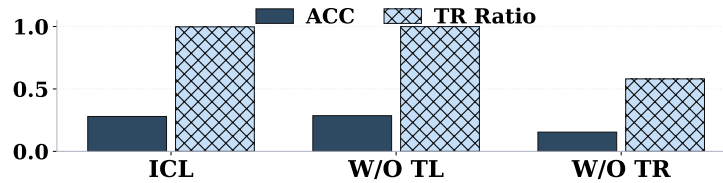


Figure 87: Effects of ablating TR and TL heads on Qwen2-7B when demonstration labels are flipped.

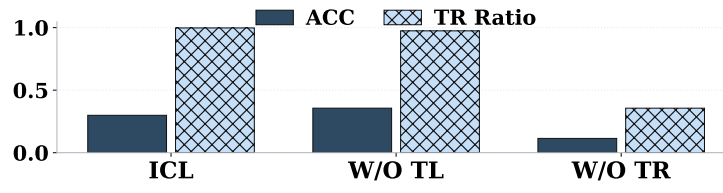


Figure 88: Effects of ablating TR and TL heads on Qwen2.5-32B when demonstration labels are flipped.

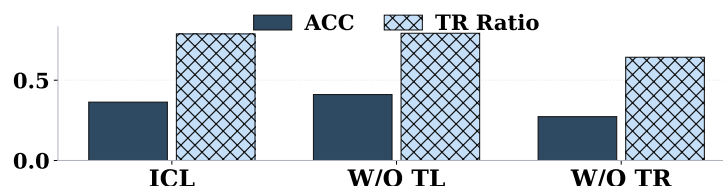


Figure 89: Effects of ablating TR and TL heads on Yi-34B when demonstration labels are flipped.

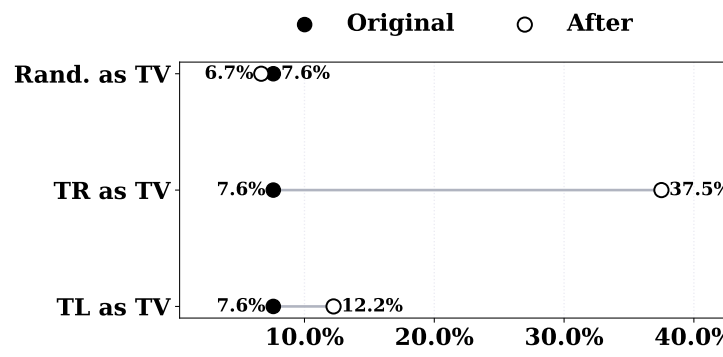


Figure 90: Steering zero-shot hidden states of Llama3.1-8B using task vectors from TR, TL, or random heads.

2592

2593

2594

2595

2596

2597

2598

2599

2600

2601

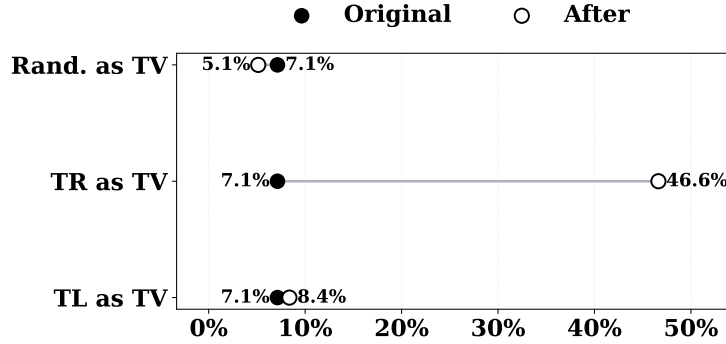
2602

2603

2604

2605

2606 Figure 91: Steering zero-shot hidden states of Llama3.2-3B using task vectors from TR, TL, or  
 2607 random heads.



2608

2609

2610

2611

2612

2613

2614

2615

2616

2617

2618

2619

2620

2621

2622

2623

2624

2625

2626

2627

2628

2629

2630

2631

2632

2633

2634

2635

2636

2637

2638

2639

2640

2641

2642

2643

2644

2645

Figure 91: Steering zero-shot hidden states of Llama3.2-3B using task vectors from TR, TL, or random heads.

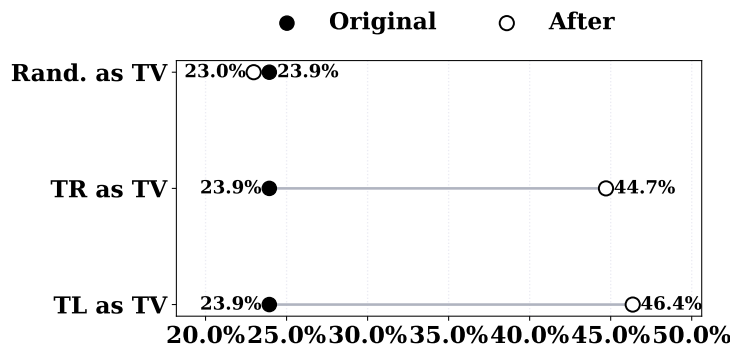


Figure 92: Steering zero-shot hidden states of Qwen2-7B using task vectors from TR, TL, or random heads.

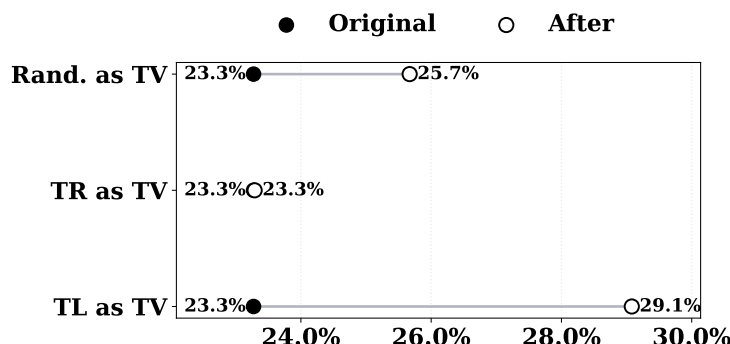


Figure 93: Steering zero-shot hidden states of Qwen2.5-32B using task vectors from TR, TL, or random heads.

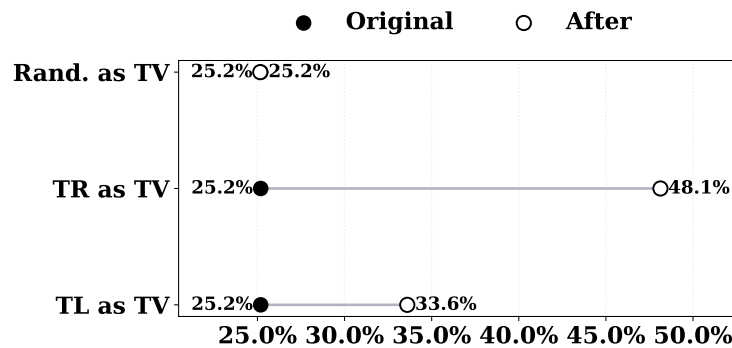


Figure 94: Steering zero-shot hidden states of Yi-34B using task vectors from TR, TL, or random heads.

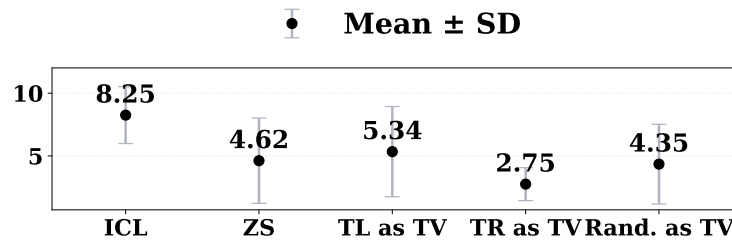


Figure 95: Mean and standard deviation of review ratings with Llama3.1-8B when task vectors from different head types are applied.

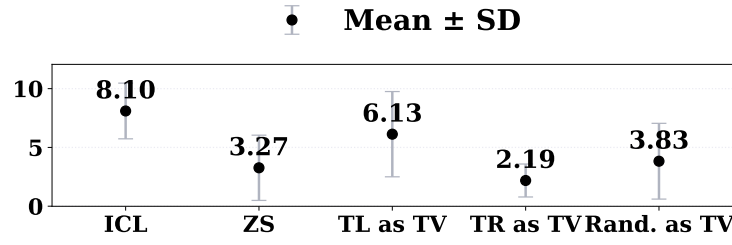


Figure 96: Mean and standard deviation of review ratings with Llama3.2-3B when task vectors from different head types are applied.

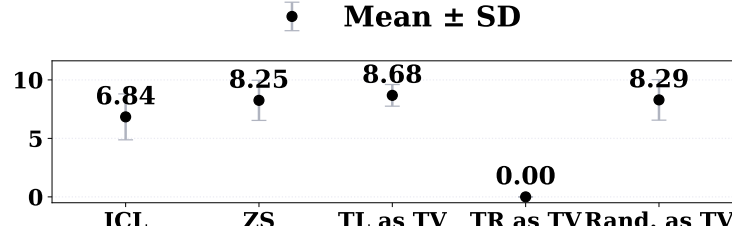
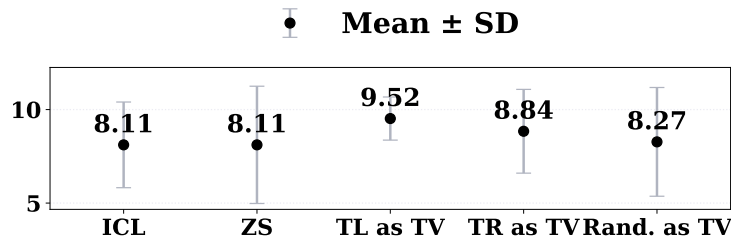


Figure 97: Mean and standard deviation of review ratings with Qwen2-7B when task vectors from different head types are applied.



2710  
2711  
Figure 98: Mean and standard deviation of review ratings with Qwen2.5-32B when task vectors from  
2712  
2713  
2714  
2715  
2716  
2717  
2718  
2719  
2720  
2721  
2722  
2723  
2724  
2725  
2726  
2727  
2728  
2729  
2730  
2731  
2732  
2733  
2734  
2735  
2736  
2737  
2738  
2739  
2740  
2741  
2742  
2743  
2744  
2745  
2746  
2747  
2748  
2749  
2750  
2751  
2752  
2753

Figure 98: Mean and standard deviation of review ratings with Qwen2.5-32B when task vectors from different head types are applied.

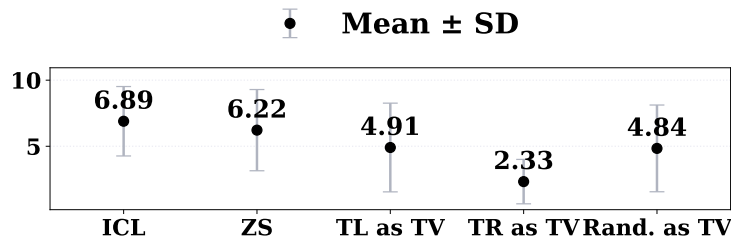


Figure 99: Mean and standard deviation of review ratings with Yi-34B when task vectors from different head types are applied.

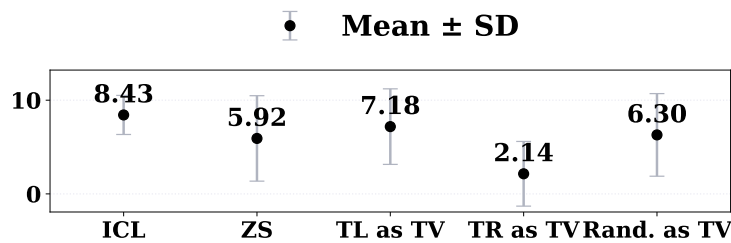


Figure 100: Mean and standard deviation of the ratings of book reviews generated using Llama3-8B when task vectors from different head types identified on the SubjQA dataset are applied.

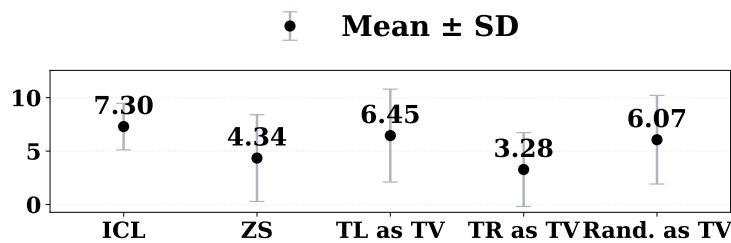
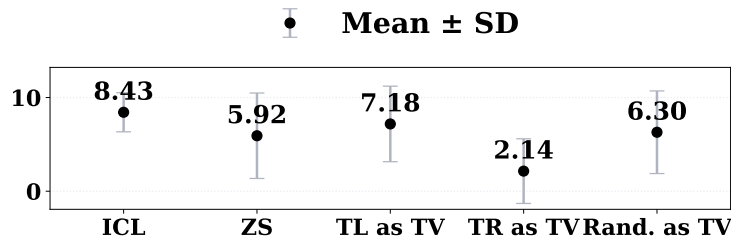
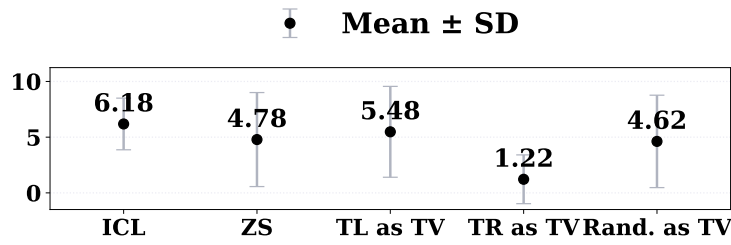


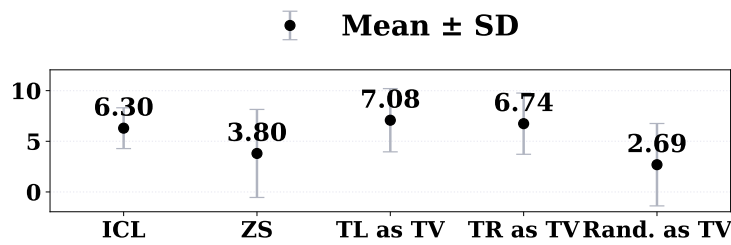
Figure 101: Mean and standard deviation of the ratings of book reviews generated using Llama3.1-8B when task vectors from different head types identified on the SubjQA dataset are applied.



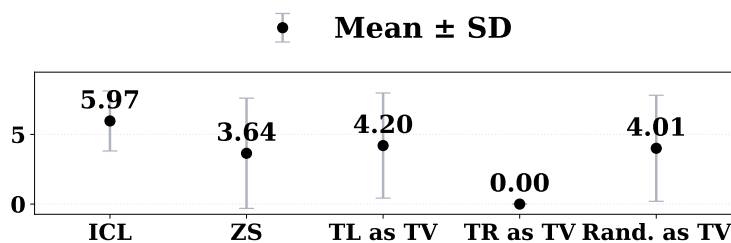
2764  
2765                    Figure 102: Mean and standard deviation of the ratings of book reviews generated using Llama3.2-3B  
2766                    when task vectors from different head types identified on the SubjQA dataset are applied.  
2767  
2768  
2769  
2770



2778  
2779                    Figure 103: Mean and standard deviation of the ratings of book reviews generated using Qwen2-7B  
2780                    when task vectors from different head types identified on the SubjQA dataset are applied.  
2781  
2782  
2783  
2784



2794  
2795  
2796  
2797                    Figure 104: Mean and standard deviation of the ratings of book reviews generated using Qwen2.5-32B  
2798                    when task vectors from different head types identified on the SubjQA dataset are applied.  
2799  
2800  
2801  
2802  
2803  
2804  
2805



2806  
2807                    Figure 105: Mean and standard deviation of the ratings of book reviews generated using Yi-34B  
2808                    when task vectors from different head types identified on the SubjQA dataset are applied.  
2809

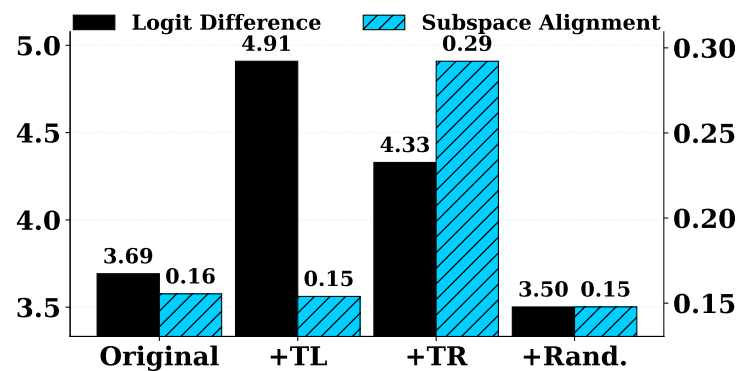


Figure 106: Geometric effects of TR and TL head outputs on hidden states in Llama3.1-8B.

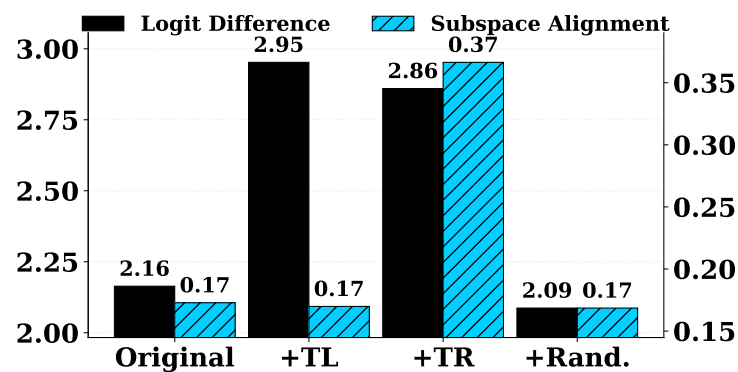


Figure 107: Geometric effects of TR and TL head outputs on hidden states in Llama3.2-3B.

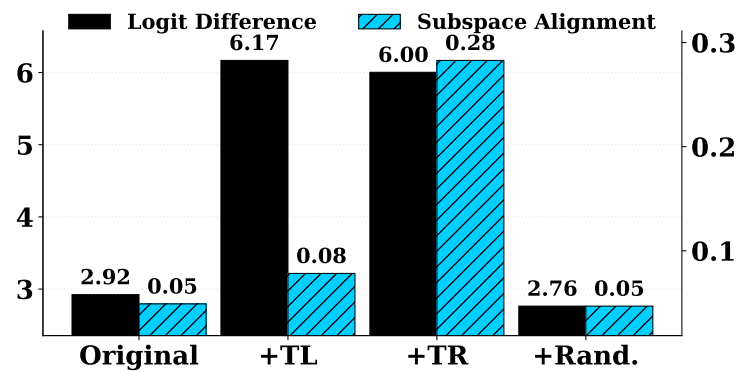


Figure 108: Geometric effects of TR and TL head outputs on hidden states in Qwen2-7B.

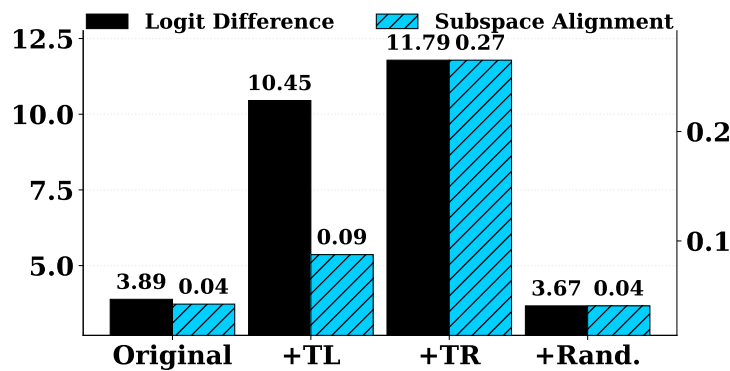


Figure 109: Geometric effects of TR and TL head outputs on hidden states in Qwen2.5-32B.

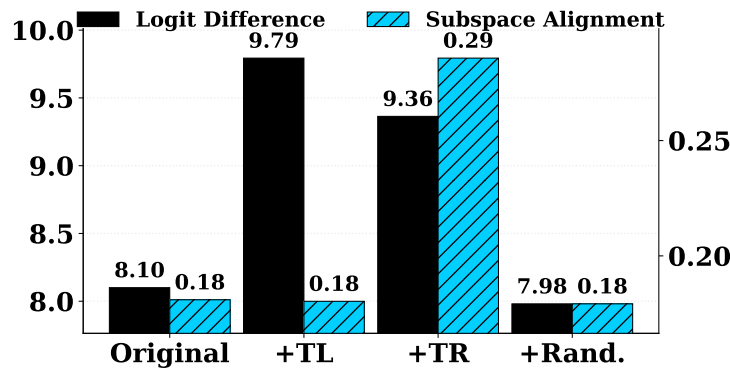


Figure 110: Geometric effects of TR and TL head outputs on hidden states in Yi-34B.

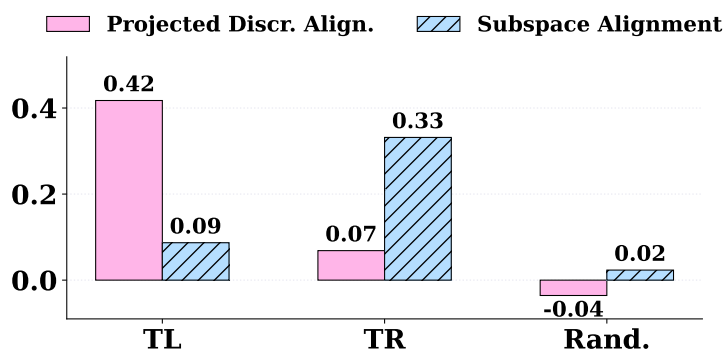


Figure 111: Impact of TL and TR head outputs on hidden states w.r.t. task subspace in Llama3.1-8B.

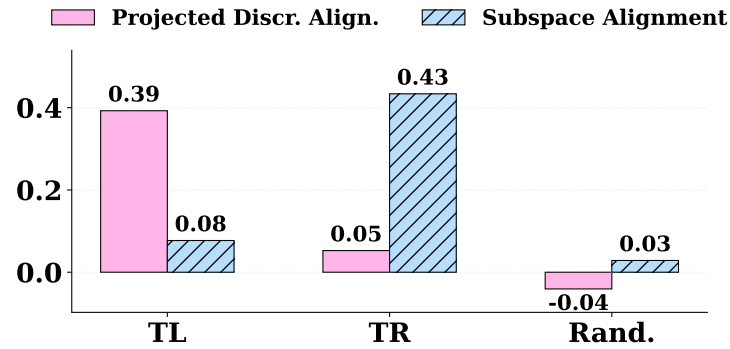


Figure 112: Impact of TL and TR head outputs on hidden states w.r.t. task subspace in Llama3.2-3B.

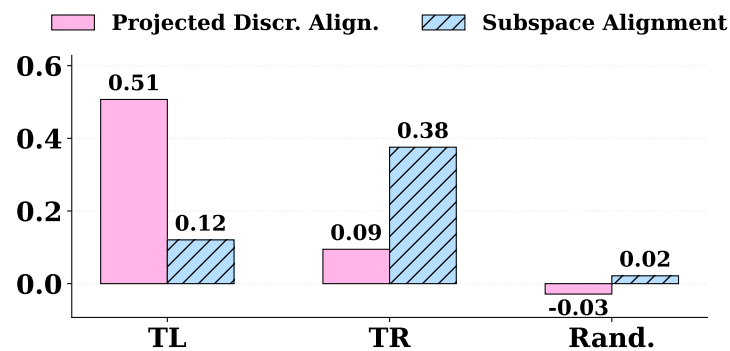


Figure 113: Impact of TL and TR head outputs on hidden states w.r.t. task subspace in Qwen2-7B.

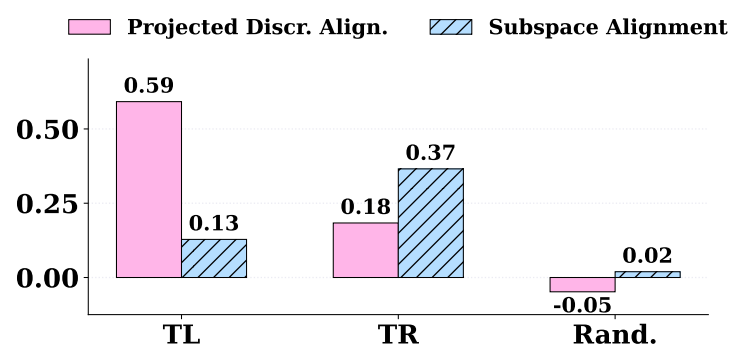


Figure 114: Impact of TL and TR head outputs on hidden states w.r.t. task subspace in Qwen2.5-32B.

2970  
2971 Table 4: Jaccard coefficient and Spearman’s  $\rho$  for TL and TR scores across tasks.  
2972  
2973

	TL Task 1&2	TR Task 1&2
Jaccard coefficient	0.1860	<b>0.3421</b>
Spearman’s $\rho$	0.2980	<b>0.8365</b>

	Llama3-8B	Llama3.1-8B	Llama3.2-3B	Qwen2-7B	Qwen2.5B	Yi-34B
	$1.96 \times 10^{-4}$	$1.96 \times 10^{-4}$	$7.63 \times 10^{-6}$	$7.63 \times 10^{-6}$	$7.63 \times 10^{-6}$	$6.28 \times 10^{-4}$

2981  
2982 Table 5: Statistical significance of the difference between the norms of token unembeddings projected  
2983 to different subspaces across models.  
2984

	TL heads mean layer	IHs mean layer	TR heads mean layer	TL < IHs?	IHs < TR heads?
0.03	16.89	16.69	26.22	0.84985	5.6052e-45
0.05	16.94	16.74	25.08	0.80371	0.0000e+00
0.10	16.75	16.88	23.27	0.59518	0.0000e+00

2985  
2986 Table 6: Mean layer index of TL heads, IHs, and TR heads across datasets on Llama3-8B, with  
2987 p-values for distribution differences.  
2988

	TL heads mean layer	IHs mean layer	TR heads mean layer	TL < IHs?	IHs < TR heads?
0.03	16.85	16.67	26.07	0.71998	8.4078e-45
0.05	16.36	16.77	25.33	0.22671	0.0000e+00
0.10	16.12	16.79	23.25	0.049241	0.0000e+00

2989  
2990 Table 7: Mean layer index of TL heads, IHs, and TR heads across datasets on Llama3.1-8B, with  
2991 p-values for distribution differences.  
2992

	TL heads mean layer	IHs mean layer	TR heads mean layer	TL < IHs?	IHs < TR heads?
0.03	14.51	15.69	23.04	0.040803	1.3459e-26
0.05	14.25	15.78	22.59	0.0024930	3.0489e-35
0.10	14.38	15.75	20.96	0.00044495	1.0738e-36

3000  
3001 Table 8: Mean layer index of TL heads, IHs, and TR heads across datasets on Llama3.2-3B, with  
3002 p-values for distribution differences.  
3003

	TL heads mean layer	IHs mean layer	TR heads mean layer	TL < IHs?	IHs < TR heads?
0.03	19.06	18.57	24.87	0.31254	2.6148e-28
0.05	18.01	18.62	24.64	0.37007	1.7432e-42
0.10	16.22	18.97	23.38	2.4055e-09	1.8049e-41

3004  
3005 Table 9: Mean layer index of TL heads, IHs, and TR heads across datasets on Qwen2-7B, with  
3006 p-values for distribution differences.  
3007

	TL heads mean layer	IHs mean layer	TR heads mean layer	TL < IHs?	IHs < TR heads?
0.03	46.26	44.08	56.80	0.0012338	0.0000e+00
0.05	43.19	44.53	54.89	0.35802	0.0000e+00
0.10	39.42	45.11	51.36	1.7597e-20	0.0000e+00

3008  
3009 Table 10: Mean layer index of TL heads, IHs, and TR heads across datasets on Qwen2.5-32B, with  
3010 p-values for distribution differences.  
3011

	TL heads mean layer	IHs mean layer	TR heads mean layer	TL < IHs?	IHs < TR heads?
0.03	36.64	38.16	47.21	0.071766	0.0000e+00
0.05	35.57	38.20	46.90	0.0011017	0.0000e+00
0.10	34.09	38.25	45.20	1.0199e-12	0.0000e+00

Table 11: Mean layer index of TL heads, IHs, and TR heads across datasets on Yi-34B, with p-values for distribution differences.

Setting	Generated Review
ICL	Poignant character arcs explore relatable themes with depth. Cinematic score heightens emotional impact of pivotal scenes. Timely social commentary addresses important issues with nuance. Strong performances deliver believable emotions and connection.
ZS	1. What is the purpose of this review? 2. What is the author's purpose? 3. How do you know? 4. What is the audience? 5. How do you know?
TL as TV	The movie was very entertaining. I enjoyed the movie and the characters. It was a great movie to watch. I would recommend it to others. It was a very entertaining movie.
TR as TV	Write a positive review for a movie. The positive review should be within 30 words.
Random as TV	Thank you for the positive review. It is always nice to hear when someone enjoyed the film. I am glad that you enjoyed the film and that you took the time to write a review.

Table 12: Sample reviews generated under different settings with Llama3-8B.

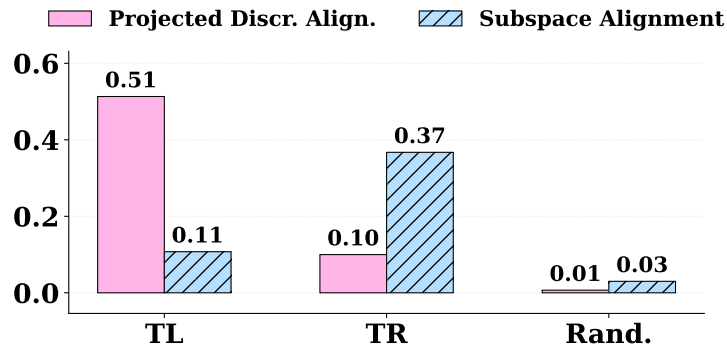
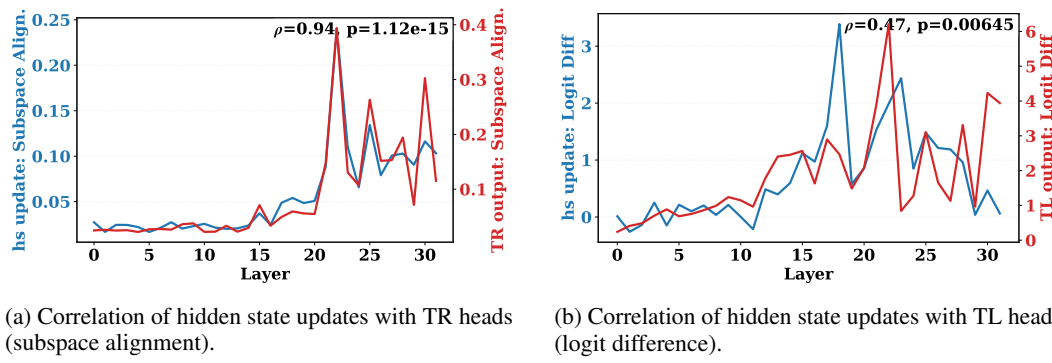


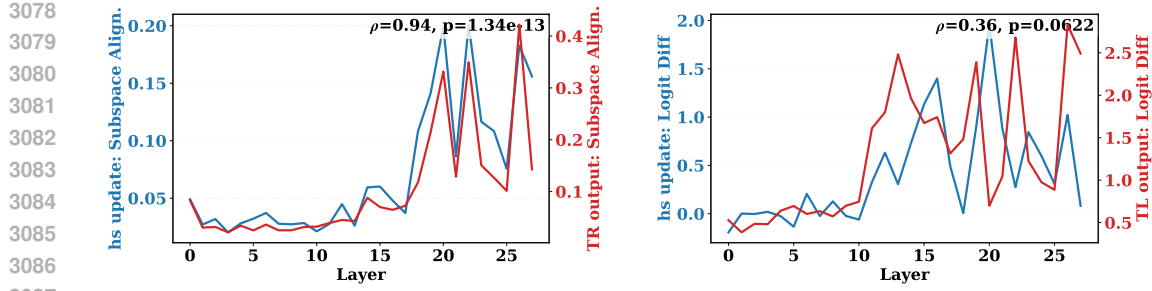
Figure 115: Impact of TL and TR head outputs on hidden states w.r.t. task subspace in Yi-34B.



(a) Correlation of hidden state updates with TR heads (subspace alignment).

(b) Correlation of hidden state updates with TL heads (logit difference).

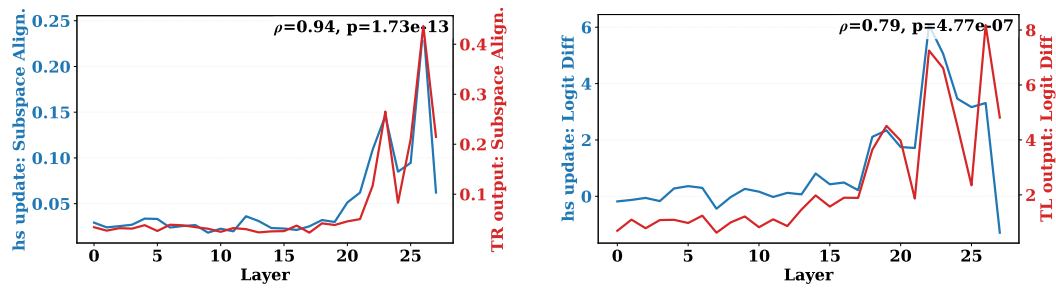
Figure 116: Layerwise correlation of TR and TL head effects on Llama3.1-8B.



(a) Correlation of hidden state updates with TR heads (subspace alignment).

(b) Correlation of hidden state updates with TL heads (logit difference).

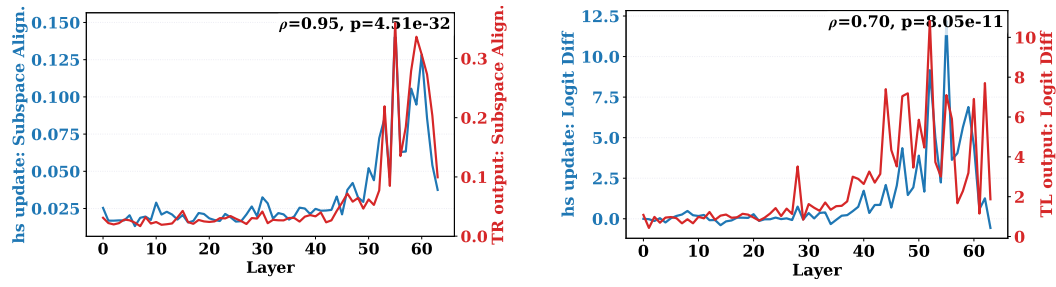
Figure 117: Layerwise correlation of TR and TL head effects on Llama3.2-3B.



(a) Correlation of hidden state updates with TR heads (subspace alignment).

(b) Correlation of hidden state updates with TL heads (logit difference).

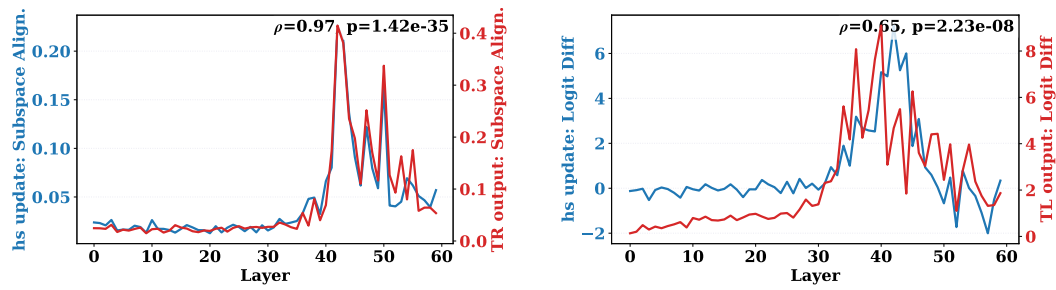
Figure 118: Layerwise correlation of TR and TL head effects on Qwen2-7B.



(a) Correlation of hidden state updates with TR heads (subspace alignment).

(b) Correlation of hidden state updates with TL heads (logit difference).

Figure 119: Layerwise correlation of TR and TL head effects on Qwen2.5-32B.



(a) Correlation of hidden state updates with TR heads (subspace alignment).

(b) Correlation of hidden state updates with TL heads (logit difference).

Figure 120: Layerwise correlation of TR and TL head effects on Yi-34B.

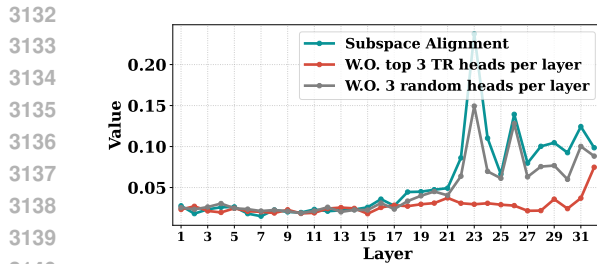


Figure 121: Layerwise ablation of TR and TL heads (top 3 per layer) in Llama3-8B.

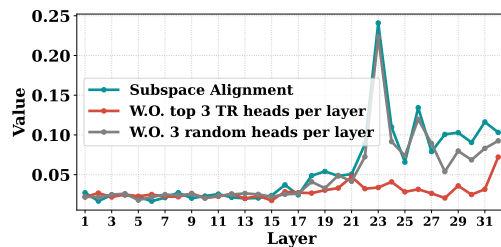


Figure 122: Layerwise ablation of TR and TL heads (top 3 per layer) in Llama3.1-8B.

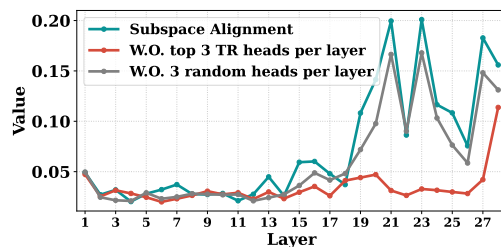
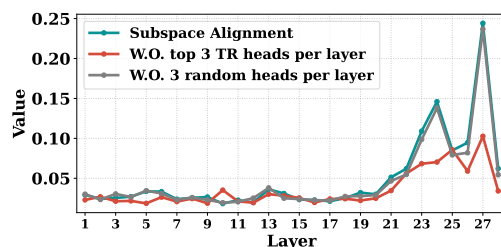


Figure 123: Layerwise ablation of TR and TL heads (top 3 per layer) in Llama3.2-3B.



3186  
 3187  
 3188  
 3189  
 3190  
 3191  
 3192  
 3193  
 3194  
 3195  
 3196  
 3197  
 3198  
 3199  
 3200  
 3201  
 3202  
 3203  
 3204  
 3205  
 3206  
 3207  
 3208  
 3209  
 3210  
 3211  
 3212  
 3213  
 3214  
 3215  
 3216  
 3217  
 3218  
 3219  
 3220  
 3221  
 3222  
 3223  
 3224  
 3225  
 3226  
 3227  
 3228  
 3229  
 3230  
 3231  
 3232  
 3233  
 3234  
 3235  
 3236  
 3237  
 3238  
 3239

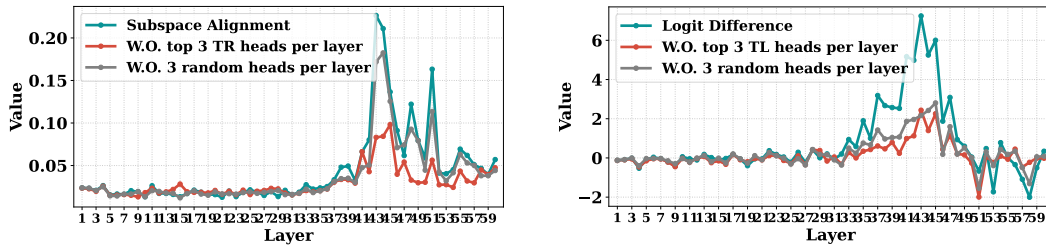


Figure 126: Layerwise ablation of TR and TL heads (top 3 per layer) in Yi-34B.